



UNIVERSITY OF TRENTO - Italy
International PhD Program in Biomolecular Sciences
Centre for Integrative Biology (CIBIO)
XXIXth Cycle

Cellular mimics within lipid vesicles and in thermal out-of-equilibrium chambers

Tutor

Prof. Sheref S. MANSY

CIBIO - University of Trento


Ph.D. Thesis of

Noël YEH MARTIN

CIBIO - University of Trento

Academic Year 2017 - 2018

I, Noël Yeh Martín, declare that this PhD thesis entitled “Cellular mimics in lipid vesicles and in thermal out-of-equilibrium chambers” is my own work and the use of all material from other sources have been properly and fully acknowledge.



NOEL YEH MARTIN

ABSTRACT

The absence of clear criteria to recognize life and evaluate attempts at building a cell from component parts has slowed progress towards the construction of cellular mimics that fully display the properties of natural living cells. In the first part of this PhD thesis, a method to objectively quantify progress is proposed. In the second part of the thesis, preliminary results are shown and discussed for the construction of out-of-equilibrium cellular mimics generated by thermal gradients that do not rely on compartments made from lipid membranes.

THESIS SUMMARY AND CONTRIBUTION

It is generally accepted that cellular components alone, such as DNA, proteins or lipids, are non-living. However, somehow when combined in the right way the result of their cooperation is referred to as living. To date, no one has been able to assemble a living cell from component parts. Part of the problem is that without a satisfactory definition of life, it is difficult to recognize progress in reaching the goal of synthesizing an artificial living cell. In the first chapter, this topic is discussed. For the first time, cellular mimics (also called artificial cells) were built that were able to chemically communicate with natural cells by sensing and sending information in the form of small chemical molecules. This technology permitted the implementation of a type of cellular imitation game where natural cells could test the life-like behaviour of the artificial cells by assessing how well the artificial systems were able to communicate. Since chemical communication leads to changes in gene expression, we proposed a more direct and unbiased way to quantify the life-likeness of the artificial cells by analysing the response of the natural cells through RNA sequencing analysis. The transcriptome of *Vibrio fischeri* was analysed and compared when the bacteria were in the presence of functional artificial cells that could communicate or nonfunctional artificial cells that could not. The analysis revealed that functional artificial cells better deceived *V. fischeri* than nonfunctional artificial cells, since functional artificial cells affected the gene expression of *V. fischeri* more closely to other *V. fischeri* than to nonfunctional artificial cells. Furthermore, artificial cells were constructed that sensed *V. fischeri* and in response degraded a quorum molecule of the pathogen *P. aeruginosa*, laying the foundation for future therapeutic applications.

The construction of cellular mimics has relied thus far on the compartmentalization of biological molecules within lipid membranes or synthetic amphiphiles that self-assemble into cell-like structures. Compartmentalization provides a way to confine the cell-like components in a defined space separated from the environment. In the second chapter, thermal gradients are used as another mechanism for the accumulation of biomolecules in confined spaces that does not depend on a physical

barrier to define the compartment. Preliminary experiments are presented showing the accumulation of the components of transcription and translation machinery from an *E. coli* cell extract inside of a thermophoretic chamber subjected to a thermal gradient.

Chapter 1:

This chapter was adapted from the article “Two-way chemical communication between artificial and natural cells” published in ACS Central Science in 2017. Experiments were conceived by Sheref Mansy, Roberta Lentini and Noël Yeh Martín (co-first co-author). I performed all the experiments presented in this chapter except for the RNA-seq analysis, which was performed by Luca Belmonte and Michele Forlin. Roberta Lentini performed the experiments shown in Supplementary Figures 1 and 6. I conducted experiments presented in Figure 6 and Figure 18 in parallel with Roberta Lentini. Plasmid names starting with “RLxxx” were cloned by Roberta Lentini. Plasmid MC002 was cloned by Michele Cornella. The chapter has been completely rewritten with respect to the aforementioned manuscript except for the RNA sequencing analysis part in the material and method section that has been copied from the manuscript. Furthermore, figures have been modified and complemented with further data and details.

Chapter 2:

The project presented in (chapter 2) is a collaboration between the laboratories of Sheref Mansy (Univeristy of Trento) and Dieter Braun (Ludwig Maximilians Universität, LMU-Munich) with the invaluable help of Christof Mast (LMU-Munich). Christof Mast conceived, designed and built the experimental setup used for the thermal accumulation experiments and developed with LabVIEW a software that controls the setup and another software to analyze the data. I implemented a working protocol to make a homemade *E. coli* cell extract and cloned genetic constructs for the thermal accumulation experiments. I learnt the different procedures to build the thermophoretic chambers and participated in the accumulation experiments under the supervision of Christof Mast.

Other contributions:

- I participated in the writing of a review article entitled “Communicating artificial cells” published in *Current Opinion in Chemical Biology* in 2016.
- I provided data during the revision of the article entitled “Cell-free translation is more variable than transcription” published in *ACS Synthetic Biology* in 2017. In particular, I contributed to Figure 4 (main text), Supplementary Figure S8, S12 and S21. Experiments were conducted in parallel with Giuliano Berloff to provide evidence that translation is more variable than transcription in a homemade *E. coli* cell extract.
- I am currently exploring experimental conditions to assess whether transition metal ions could have templated amino acid polymerization in the absence of enzymes. For this reason, I am investigating the stability of peptide-metal complexes under different conditions. Obtained preliminary data are shown in Appendix.

CONTENTS

ABSTRACT	3
THESIS SUMMARY AND CONTRIBUTION.....	4
CHAPTER 1: A Turing test-like approach to guide progress towards the construction of artificial cellular life.....	9
INTRODUCTION.....	11
Synthetic minimal cells	10
Cellular mimics	11
The imitation game.....	14
Cellular Imitation game.....	14
RESULTS.....	18
Sensing quorum molecules in vitro.....	18
Artificial cells can sense <i>Vibrio fischeri</i> quorum molecules.....	20
Artificial cells can synthesize N-(3-oxo-hexanoyl)-L-homoserine lactone.....	22
Two-way chemical communication between artificial and <i>V. fischeri</i> cells.....	24
Artificial cells can sense <i>Vibrio fischeri</i> and disrupt <i>P. aeruginosa</i> quorum sensing .	38
SUPPLEMENTARY FIGURES	44
SUPPLEMENTARY TABLES.....	50
MATERIAL AND METHODS.....	51
Bacterial strains and media	51
Colony forming unit assay	51
Preparation of liposomes.....	52
In vitro transcription-translation reactions	52
Artificial sensing cells	53
Artificial sender cells.....	54
Cellular Imitation game.....	54
RNAseq analysis	55
Quenching <i>P. aeruginosa</i>	56
Biofilm disruption	57
Vesicle stability.....	58
The effect of cholesterol on chemical communication.....	58
SUMMARY	59
DISCUSSION AND FUTURE PERSPECTIVES	60
Considerations on the artificial lipid membrane composition.....	60

Considerations on the RNA-seq data interpretation	61
Consideration on the cellular imitation game	62
Improving artificial cells for chemical communication with <i>V. fischeri</i>	63
CHAPTER 2: Cellular mimics inside non-equilibrium, open thermophoretic chambers.	64
INTRODUCTION	65
Cell membranes	65
Thermophoresis	65
Cellular mimics in out-of-equilibrium conditions	67
RESULTS	69
Cell-free extract	69
Thermophoretic chamber	70
Setup	73
Thermal accumulation experiments	74
SUPPLEMENTARY FIGURES	81
SUPPLEMENTARY TABLES	84
<i>E. coli</i> homemade cell extract	85
Cutting the geometry of the thermophoretic chamber	86
Thickness measurement of the thermophoretic chamber	87
Temperature measurement inside the thermophoretic chamber	87
Labview software for data acquisition analysis	88
Finite element simulations	88
Previous thermophoretic chambers	88
SUMMARY	90
DISCUSSION AND PERSPECTIVES	91
CONCLUSIONS	94
APPENDIX	96
REFERENCES	105

Chapter 1: A Turing test-like approach to guide progress towards the construction of artificial cellular life

This chapter is adapted from:

Two-Way Chemical Communication between Artificial and Natural Cells

Roberta Lentini,[‡] **Noël Yeh Martín**,[‡] Michele Forlin, Luca Belmonte, Jason Fontana, Michele Cornella, Laura Martini, Sabrina Tamburini, William E. Bentley, Olivier Jousson, and Sheref S. Mansy

ACS Cent. Sci. 3, 117–123, 2017. DOI: 10.1021

[‡]These authors contributed equally to the work.

INTRODUCTION

Despite the impressive progress of science and technology, building a living cell from scratch remains a great challenge. Scientists working in this direction encounter the following problems. First, our incomplete understanding of cellular complexity limits what can be built in the laboratory that can mimic or fully display the properties of living cells. Second, there is neither a satisfactory definition of life nor are there well-defined criteria to differentiate living from non-living systems (1). Consequently, any attempts at building living cells from their component parts have relied on subjective evaluations of progress. To avoid the problems related to the current subjective definitions of life, we instead decided to develop an objective measure of progress towards the construction of artificial cellular life without relying on a definition of life.

Synthetic minimal cells

Extant cells gradually became complex systems over billions of years of evolution. Thus, it is not surprising that the Mycoplasmas, known as the simplest culturable and free-living cells, contain hundreds of genes. Among the Mycoplasmas, *Mycoplasma genitalium* is to date the free living natural bacterium that possesses the smallest genome with 580 kilobase pairs and approximately 500 genes (2). However, *M. genitalium* is still a remarkably complex organism that can be used as an experimental platform to identify the minimum set of components needed to sustain life as we know it. Following this line of research, the Craig Venter team developed and improved over the years different tools and methods for the in vitro construction and transplantation of synthetic minimal genomes (2–5). After identifying the genes that were not essential under ideal laboratory conditions by means of improved mutagenesis techniques, the team impressively succeed in chemically synthesizing a minimal version of the 531 kb genome of *Mycoplasma mycoides* with a total of 473 genes. The minimized genome was functional and controlled the recipient cells after transplantation (6). The resulting new synthetic cell named JCVI-syn3.0 contained a smaller genome than *M. genitalium* and was capable of autonomous growth under controlled conditions. JCVI-syn3.0 is to date the best approximation of a minimal living cell that has been partially built in a

laboratory. Creating synthetic, simplified versions of natural genomes can be one strategy to discover the minimum set of essential parts to create and sustain living cells similar to life as we know it. However, the abovementioned minimal genome depended on the transcription and translation machinery and other cytoplasmic components of a pre-existing cell. In addition, JCVI-syn3.0 cells needed 149 genes of unknown function to live. In this regard, the minimization approach taken by Venter et al did not provide complete knowledge on how cells work nor on how to assemble the needed set of components in a way to build a cell from scratch.

Cellular mimics

The identification and individual characterization of the molecules of a cell are not enough to understand how a cell manages to persist as a living entity over time. Instead, it is important to delineate how the individual molecules interact and cooperate to give rise to a living cell. Such an endeavor exploits a learning by building methodology more akin to that of engineering while also accepting the complexity that is often described by systems biology/chemistry. Current attempts at building living cells are quite primitive, essentially placing DNA and transcription-translation machinery within lipid vesicles in a way that mimics a predefined feature of some target cell. Although many simpler versions that only contain purified proteins within lipid vesicles are still being built, most modern attempts at building artificial cells rely on either cell extracts or purified RNA and protein components to mediate the transcription and translation reactions needed to generate the desired phenotype. Cell extracts from *E. coli* are commercially available, and well developed protocols are available to produce functioning extracts in-house (7, 8). Alternatively, each purified component of the translation machinery from *E. coli*, i.e. the PURE system (9, 10), can be similarly bought commercially or generated in the laboratory (11). The differences between the extract and purified systems is that the extract is cheaper and provides more robust activity, whereas the PURE system is much more tractable in terms of understanding the role of every single component of the assembled cellular mimic and lacks endogenous nuclease activity. To date, the maximum genetic complexity that has been expressed inside of phospholipid vesicle compartments is a six gene circuit using a homemade *E. coli* cell-free extract (12). The total synthesis of the T4

bacteriophage from its 169 kbp genome has also been recently achieved by the same group using a similar *E. coli* extract (13). With further development, this technology could be used to program artificial cells with more complex genetic circuits or even with complete genomes to potentially mimic increasingly complex biological functions.

To mimic the cellular compartment, artificial cells are typically assembled within lipid defined structures, usually made of phospholipids. However, a variety of other unnatural compartmentalization possibilities also exist. Examples include synthetic compartments made of protein-polymer conjugates (proteinosomes), inorganic nanoparticles (colloidosomes), amphiphilic block copolymers (polymersomes) or membrane-free compartments (coacervates) (14). In the past years, several groups have reported simplified reconstitutions of the spatial organization of cells inside polymeric vesicles (15) and phospholipid vesicles (16). Such spatially organized artificial cells are able to mediate cascading reactions through the cooperation of different sub-compartments that resemble cellular organelles. These artificial systems provide advantages and disadvantages. These new types of compartments, for example, may provide new functionalities that are not easily implemented with biological molecules. However, the nonbiological molecules that compose the compartment may not be compatible with the needed biological machinery.

One of the more active areas of research is the development of mechanisms to divide vesicles into daughter vesicles. Several groups have reported the first steps of division by reconstituting minimal *E. coli* division machinery inside of lipid vesicles (17, 18). It is also possible to divide artificial cells without proteins. For example, DNA replication by PCR was shown to induce vesicle division in a highly contrived chemical system (19). Replication and division are also of main interest from an origin of life perspective. In this case, artificial systems are built from prebiotically plausible molecules. The main goal is to construct a simple chemical system capable of replicating its genetic material without the need of proteins and that grows and divides to eventually start evolving. Intense research is conducted to discover plausible ways of achieving those aspects. For example, fatty acid vesicles upon the addition of fatty acid micelles convert into unstable filament-like structures that divide into daughter vesicles after mild agitation (20). Other groups focus on RNA enzymes capable of self-replication (21, 22) or on non-enzymatic RNA polymerization (23).

An often neglected but essential property of life is communication. Living organisms actively communicate to adapt to the environment by sensing and responding to different molecules. Some examples of chemical communication between similar or different types of artificial cells have been recently reported (24, 25). Interestingly, in a recent paper the Ces group showed the construction of hybrids cells composed of a living cell encapsulated in an artificial cell compartment. Both parts were shown to chemically cooperate to produce a fluorescent molecule (26). Some artificial cells have also been shown to elicit a response in natural cells. For example, Gardner et al constructed an artificial cell that produced molecules via the autocatalytic formose reaction that elicited a luminescent response from natural cells (27). In recent work, phospholipid vesicles encapsulating the PURE system were capable of synthesizing and releasing a small natural molecule that activated a reporter gene inside *P. aeruginosa* (28).

In previous work from our laboratory, artificial cells were built that could act as chemical translators expanding the ability of natural cells to respond to chemicals that the natural cells could not naturally sense (29). In this case, artificial cells were engineered to sense a molecule, not recognized by bacteria, and in turn release a molecule that induced the activation of a reporter gene in *E. coli* cells. Cellular mimics provide a better understanding of the essential processes, mechanisms and functions of living cells. Importantly, this technology with further development could also lead to therapeutic and industrial applications. However, if the goal is to build a complex system displaying the properties of life, none of the described systems help in evaluating progress in that direction. Without well-defined benchmarks that can be objectively satisfied for a system to be considered alive, efforts at building cellular mimics with the purpose of building a living cell will be evaluated with a certain degree of subjectivity.

The imitation game

Scientists and engineers in the field of artificial intelligence encountered 70 years ago similar problems. Creating a machine that “thinks” or that displays some sort of “intelligence” was challenging in the absence of an agreed-upon definition of the terms “thought” and “intelligence”. To bypass that issue, the mathematician Alan Turing suggested the “imitation game” in his seminal paper “Computing machinery and intelligence” (30). The game is set in a way that a human and a computer communicate through text-based digital communication. Both are physically separated to avoid direct recognition. The role of the human is to interrogate, while the computer tries to deceive the human into thinking that communication takes place with another human. The computer passes the test if the human is not capable of distinguishing the computer’s responses from the responses of a human. By replacing the question “Can machines think?” with “Can computers deceive a human into thinking that the computer is another person?” Alan Turing provided an alternative method to assess progress in building machines that display intelligence. Such an imitation game, later known as the Turing test, did not give a definition of “thought” but nevertheless paved the way for progress in artificial intelligence.

Cellular Imitation game

Similarly, to bypass the problems associated with a lack of a definition of “life”, Cronin and colleagues proposed that a type of cellular imitation game could be used to guide the construction of cellular mimics (31). As mentioned earlier, living cells chemically communicate with one another and with their environment. If artificial cells can be built that perceive the molecules secreted from living cells and in response synthesize the same or similar chemical messages that can go back to the natural cells, then it should be possible to evaluate the performance of the artificial cell by observing or analyzing the response of natural cells. As in the case of the Turing test where the human evaluates the “intelligence” of a computer by textual communication, in the cellular version of the game, the natural cell evaluates the “life-like behavior” of the artificial system by chemical communication. Artificial cells that sense and produce chemical

molecules that engage in two-way chemical communication with natural cells had not been constructed by the time we started to implement the cellular imitation game and has not to date been achieved by other laboratories. To the best of our knowledge the closest example found in the literature consists of water-in-oil droplets encapsulating an *E. coli* cell extract and DNA engineered to express proteins that either sense or synthesize a biological molecule naturally produced by a luminescent bacterium. Chemical communication happened between artificial sender cells and engineered *E. coli* cells carrying a fluorescent reporter gene or between artificial sensor cells and producer engineered *E. coli* cells (32). This experimental setting required, however, the use of genetically modified natural cells to assess whether one-way communication was taking place. In other words, communication was forced to happen in a specific and programmed way, and only in one direction.

To develop a cellular version of the Turing test, intact natural cells were needed that could also evaluate in a natural and unbiased manner the communication process. Bacteria were desirable to fill the role, because bacteria are much simpler than eukaryotic cells, thus facilitating the construction of the cellular mimics. Additionally, bacterial chemical communication is well characterized. Bacteria speak to each other by sensing and sending messages in the form of small chemical molecules called autoinducers that diffuse through membranes and activate specific genes involved in the production of luminescence and/or biofilms, depending on the bacterial species. This chemical language is also known as quorum sensing (QS), and QS is used to coordinate the behavior of bacteria in a cell density dependent manner (33). One of the best-known quorum sensing pathways is that of *Vibrio fischeri*. *V. fischeri* are typically found living in symbiosis with squid or fish species and use QS to coordinate the production of light (34). To communicate, *V. fischeri* use an amphipathic molecule composed of a homoserine lactone ring and an oxygen containing six carbon atoms oxidized acyl chain. More specifically, this homoserine lactone is N-(3-oxohexanoyl)-L-homoserine lactone (hereafter referred to as 3OC6 HSL) (Figure 1). The synthesis of 3OC6 HSL is catalyzed by the LuxI enzyme, using as substrates S-adenosylmethionine (SAM) and 3-oxohexanoyl acyl chains (35). The genes involved in the production of light (*lux* genes) are six, and the genes all belong to the *lux* operon (*luxICDABEG*), which also contains the *luxI* gene. The activation of these genes occurs via the transcriptional activator protein LuxR that in the presence of 3OC6 HSL

binds to a consensus binding site within the promoter region called the lux box and hereafter referred to as plux (Figure 2).

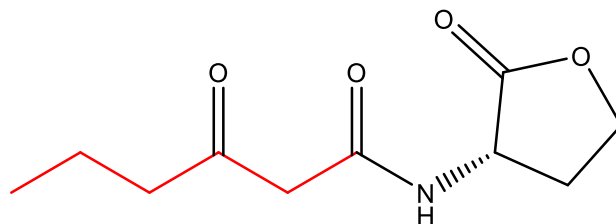


Figure 1. Chemical structure of the *V. fischeri* quorum molecule N-(3-oxohexanoyl)-L-homoserine lactone. This amphipathic quorum molecule is composed of a homoserine lactone ring and a 6-carbon oxidized acyl chain, highlighted in red.

V. fischeri seemed to be a perfect candidate to play the role of the natural cell in the cellular imitation game. Reconstituting a simplified and minimal version of one of the QS pathways of *V. fischeri* would require only two genes, *luxR* and *luxI*. Moreover, the amphipathic nature of the homoserine lactone allowed for the simple diffusion of the chemical signal through a phospholipid based artificial compartment without the need of any membrane protein system. Importantly, since this QS mechanism leads to the production of light, communication could be easily assessed by measuring the luminescence coming from the bacteria. And more importantly, since chemical communication in this case leads to changes in gene expression, next generation sequencing technologies could be used to quantify the extent of communication allowing for a more objective way to evaluate the extent of mimicry or life-likeness of the artificial cell. It is a more objective and unbiased method because the performance of the artificial system is directly evaluated by the natural cell and not by an observer.

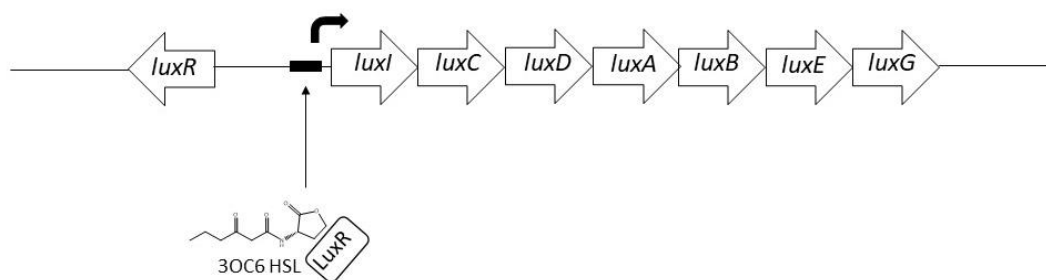


Figure 2. Schematic representation of the activation of the lux genes in *V. fischeri*. The LuxR-3OC6 HSL complex binds the lux box consensus sequence (black rectangle) and activates the transcription of the lux operon.

To pass the cellular version of the imitation game, artificial cells need to speak the same chemical language as natural cells. For this purpose, to participate in the game artificial cells need to be equipped with DNA coding for the genes necessary to perceive and produce homoserine lactone, transcription and translation machinery that allows for the intended communication, and a compartment that is compatible with the release of the homoserine lactone. To avoid the problems associated with a lack of a definition of life, the artificial cells were assessed for their ability to communicate with *Vibrio fischeri* in a way that mimicked natural *Vibrio fischeri* (Figure 3).

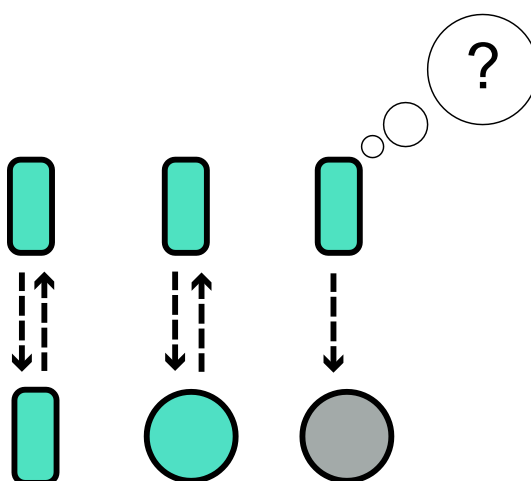


Figure 3. Schematic representation of the cellular imitation game implemented in this work. Artificial cells (circles) and *V. fischeri* cells (teal rectangles) are engaged in two-way chemical communication. Artificial cells capable of sensing and producing 3OC6 HSL (teal circle) are expected to better deceive *V. fischeri* cells than artificial cells that are not capable of communicating (grey circle).

RESULTS

To construct artificial cells that can chemically communicate with natural cells, simplified versions of the quorum sensing pathway of the Gram-negative bacterium *Vibrio fischeri* were reconstituted and tested for activity. Chemical communication in this case, as previously described, depends on the production, release and sensing of a small chemical molecule termed N-3-(oxo-hexanoyl) homoserine lactone (3OC6 HSL).

Sensing quorum molecules in vitro

The first thing was to assemble genetic constructs that could confer upon the artificial cells the ability to sense the quorum molecules produced and released by *V. fischeri*. For this purpose, the DNA construct (BBa_T9002) from the registry of standard biological parts perfectly matched our needs. The genetic construct encoded the wild type LuxR receptor under the pTet constitutive promoter. Importantly, the genetic construct also contained the gene coding for the fluorescent protein GFPmut3b under the plux inducible transcriptional regulator binding site. In this way, since LuxR has been shown to act as a transcriptional activator upon the binding of 3OC 6HSL, the ability to sense 3OC6 HSL could be easily monitored by fluorescence. A commercial *E. coli* cell extract provided the transcription-translation machinery needed to test the function of the DNA construct. GFPmut3b was 4-fold more expressed in the presence of 10 μ M of commercial 3OC6 HSL than in the absence of this quorum signal (Figure 4).

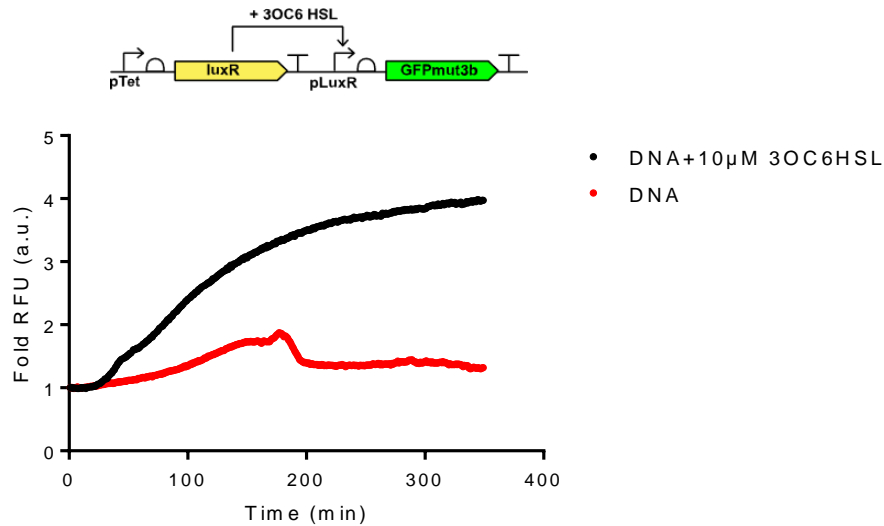


Figure 4. Sensing 3OC6 HSL in vitro. Top: schematic representation of the genetic parts of the quorum sensor DNA (BBa_T9902) extracted from the registry of biological standard parts. Bottom: GFPmut3b expression from in vitro transcription-translation reaction in the presence or absence of 10 μ M of commercial 3OC6 HSL was monitored over 6 h by fluorescence spectroscopy. $n = 1$ representative experiment.

Interestingly, N-octanoyl-L-homoserine lactone (C8 HSL), another quorum molecule produced by *V. fischeri* with an eight carbon atoms oxidized acyl chain, can also bind the LuxR transcriptional activator, but such an interaction leads to a weaker activation of gene expression in vivo compared to 3OC6 HSL (36). However, a higher affinity mutant version of the protein for both homoserine lactones (T33A S116A S135I LuxR, hereafter referred to as LuxR*) has been reported (37). This LuxR mutant when tested in in vitro transcription-translation reactions, activated GFPmut3b cell-free expression 7-fold in the presence of C8 HSL and 6-fold in the presence of 3OC6 HSL with respect to the control sample where the homoserine lactones were not added (Supplementary Figure 1 and Supplementary Table 1). Moreover, (T33A,M65R,S116A,S135I LuxR, hereafter referred to as M65R*) was only responsive to C8 HSL, as reported in the same study (37) (Supplementary Figure 1 and Supplementary Table 1).

Artificial cells can sense *Vibrio fischeri* quorum molecules

Next, to assess whether the synthetic sensing mechanism of the artificial cells was able to respond to the natural quorum molecules of *V. fischeri*, the supernatant of a *V. fischeri* culture at high cell density was added to a suspension of 1:2 POPC (1-palmitoyl-2-oleoyl-glycero-3-phosphocholine):cholesterol liposomes encapsulating commercial *E. coli* cell extract that expressed constitutively wild type or mutant versions of LuxR. POPC is a phospholipid molecule composed of a choline head group and two acyl chains of 16 and 18 carbon atoms (Figure 5). In this case, the genetic constructs encoded firefly luciferase instead of GFPmut3b (Table 1).

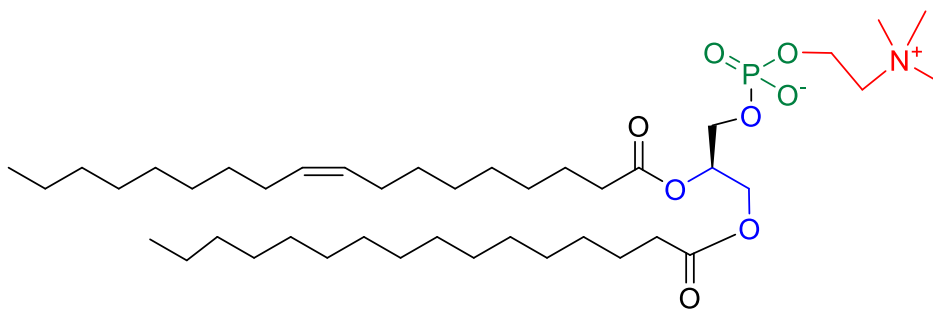


Figure 5. Chemical structure of 1-palmitoyl-2-oleoyl-*sn*-glycero-3-phosphocholine (POPC). POPC is a phospholipid composed of a choline head group (highlighted in red), a phosphate group (highlighted in green), glycerol (highlighted in blue) and two acyl chains of 16 (palmitoyl) and 18 (oleoyl) carbon atoms.

After 4 h of incubation at 30 °C, artificial cells were disrupted with triton x-100 and the substrate of the firefly luciferase (luciferin) was added to the solution. 69-, 19-, and 8-fold more luminescence was observed for artificial cells expressing LuxR, LuxR*, and M65R LuxR*, respectively, in response to the supernatant of *V. fischeri* than in the absence of the supernatant (Figure 6). Here, the supernatant of a *V. fischeri* culture was used to distinguish the luminescence produced by the artificial cells from the natural luminescence coming from the bacterium itself. The data indicate the ability of artificial cells to sense molecules secreted from *V. fischeri*.

Plasmid name	Vector	Insert	Function
RL082A	pSB1A3	pTet- <i>luxR</i> - plux-fireflyluciferase	C6 sensing
RL093A	pSB1A3	pTet-(T33A,S116,M135I) <i>luxR</i> - plux-fireflyluciferase	C6/C8 sensing
RL094A	pSB1A3	pTet-(T33A,R65M,S116,M135I) <i>luxR</i> - plux-fireflyluciferase	C8 sensing

Table 1. list of genetic constructs used for sensing *V. fischeri* quorum molecules inside of artificial cells.

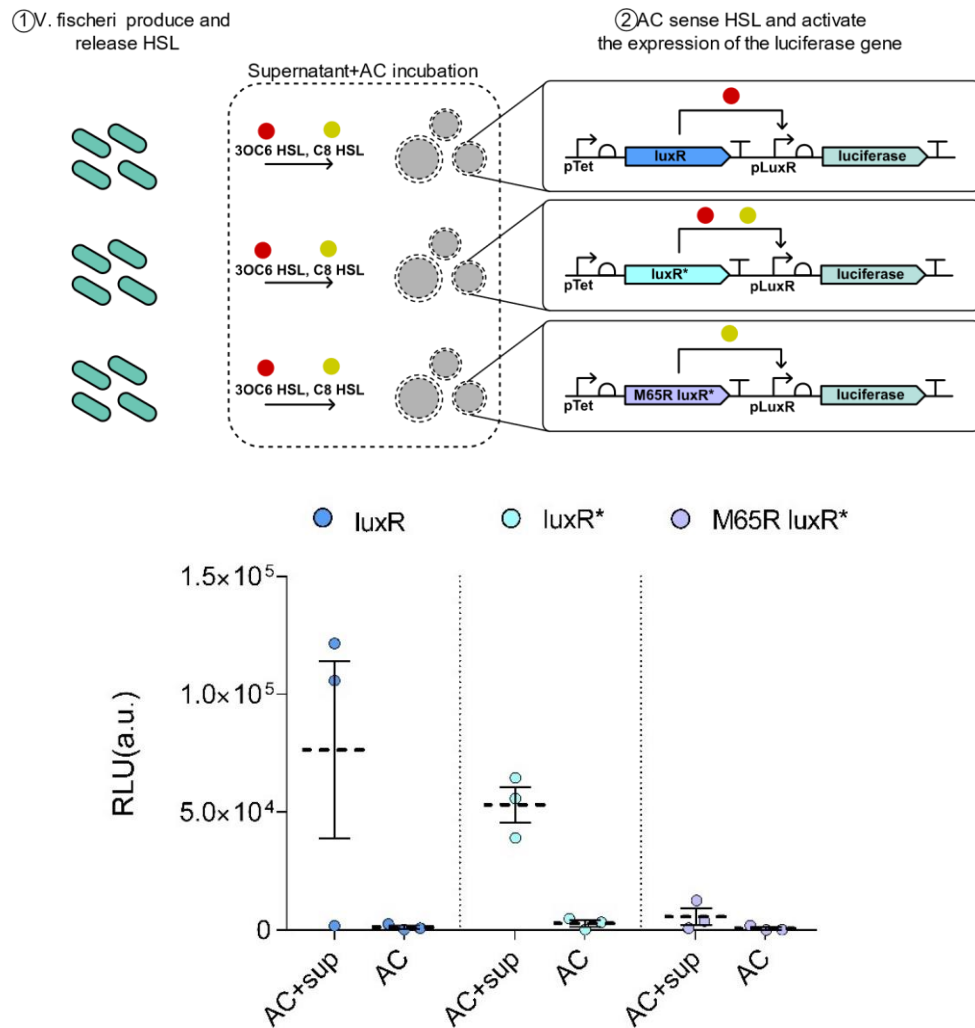


Figure 6. Artificial cells can sense quorum molecules released by *Vibrio fischeri*. Top: Schematic representation of the experimental setting. *V. fischeri* (teal, oblong) release quorum molecules that are sensed by artificial cells (gray circles). Artificial cells (AC) expressing either LuxR or LuxR* and in contact with the supernatant of *V. fischeri* (+sup) were able to sense the presence of homoserine lactones and in turn express the encoded firefly luciferase gene in a greater extent than artificial cells encoding M65R luxR*. Negative control reactions were the artificial cells encapsulating the same genetic constructs in the absence of the supernatant from *V. fischeri*. Dotted lines in the graph represent the mean of $n=3$ independent experiments, dashed lines indicate the mean and error bars correspond to the standard error of the mean (SEM). RLU (relative luminescence units). a.u. (arbitrary units).

Artificial cells can synthesize N-(3-oxo-hexanoyl)-L-homoserine lactone

The next step was to demonstrate that artificial cells can also produce and release quorum molecules to *V. fischeri*. The synthesis of 3OC6 HSL in *V. fischeri* cells is catalyzed by the LuxI enzyme as described earlier. Interestingly, mutant versions of LuxI obtained by error-prone PCR in directed evolution experiments have been reported to produce higher amounts of 3OC6 HSL with respect to the wild type enzyme when tested in *E. coli* (38). To confer upon the artificial cells the ability to synthesize 3OC6 HSL and to test for the best activity, genetic constructs encoding wild type or mutant versions of *luxI* synthase were cloned under a T7 constitutive promoter (Table 2). DNA coding for wild type *luxI*, E34G E63G *LuxI* (hereafter referred to as *LuxI***), and E34G E40G E63G *LuxI* (hereafter referred to as *LuxI**) and the transcription–translation machinery provided by a commercial *E. coli* extract were placed directly inside of liposomes to ensure that the synthesized quorum molecule could escape the artificial cell membranes. Liposomes were incubated with *V. fischeri* for 3 h at 30 °C. The luminescence per colony forming unit data indicated that liposomes expressing the three different versions of the LuxI enzyme were capable of inducing a greater luminescent response from *V. fischeri* than liposomes without DNA. This indicated that artificial cells successfully produced and released 3OC6 HSL (Figure 7). The bulk luminescence levels of *V. fischeri* over 3 h of incubation were similar, independent of the LuxI version expressed inside the artificial cells. (Supplementary Figure 2). This suggests that the different mutations in the *luxI* sequence did not sufficiently alter the kinetics of the synthesis of 3OC6 HSL, at least not under the employed experimental conditions. Since the artificial cells could not divide, the colony forming units only reflected the number of viable *V. fischeri* cells (Supplementary Figure 2). Sample controls for this experiment were diluted and undiluted samples of *V. fischeri*, *V. fischeri* cultured with liposomes encapsulating only LBS and *V. fischeri* diluted with 100 nM 3OC6 HSL.

Plasmid name	Vector	Insert	Function
MC002A	pET21b	pT7-luxI	C6 sending
NY015A	pET21b	pT7- E63GluxI	C6 sending
NY018A	pET21b	pT7- (E34G,R40G,E63G) luxI	C6 sending
NY019A	pET21b	pT7- (E34G,E63G) luxI	C6 sending

Table 2. list of the genetic constructs coding for wild type or mutant versions of the LuxI synthase.

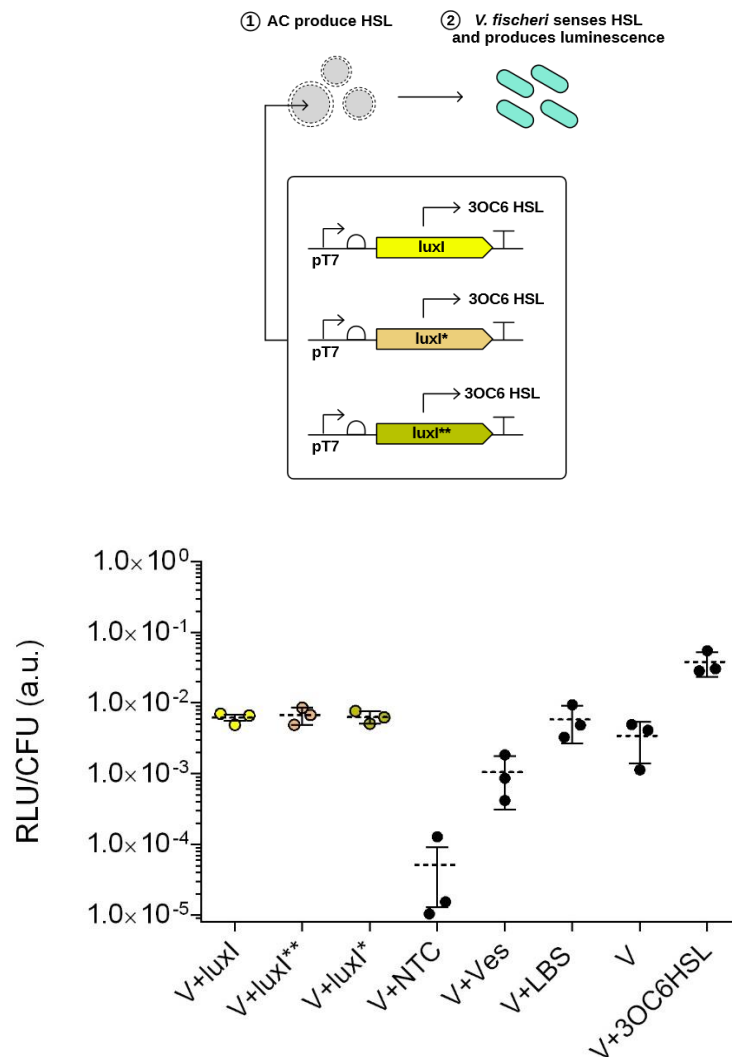


Figure 7. Artificial cells can produce *Vibrio fischeri* N-(3-oxo-hexanoyl)-L-homoserine lactone. Top: schematic diagram of the experimental setting. Artificial cells encapsulating and expressing three different versions of the LuxI synthase produce 3OC6 HSL, which diffuses towards *V. fischeri* cells and activates the production of luminescence. Bottom: Artificial cells expressing luxI, luxI* and luxI** successfully induced the production of bioluminescence in *V. fischeri*. Sample controls (black dots) were *V. fischeri* with: artificial cells without DNA (NTC); 1:2 POPC:cholesterol vesicles encapsulating LBS (Ves); LBS=Bacteria liquid medium (LBS); *Vibrio fischeri* non-diluted culture (V); or supplemented with 100nM of commercial N-(3-oxohexanoyl)-L-homoserine lactone (V+3OC6 HSL). Y-axis is in log scale. Dotted lines correspond to the mean of n=3 independent experiments; error bars indicate the standard error of the mean (SEM). RLU/CFU, relative luminescence units/per colony forming unit per milliliter.

Two-way chemical communication between artificial and *V. fischeri* cells

Chemical communication requires the ability to both sense and send information in the form of molecules. After showing that the artificial cells were capable of sensing and sending quorum signaling molecules, the final step was to build artificial cells that could combine both parts to chemically communicate directly with *Vibrio fischeri*. First, to confirm that the homoserine lactones produced by a low-density *V. fischeri* culture were sufficient to activate the production of LuxI synthase inside artificial cells, *E. coli* transformed with the BBa_T9002 genetic construct were incubated with the supernatant of *V. fischeri* at $OD_{600\text{ nm}} = 0.25$. The number of cells expressing GFPmut3b was assessed by flow cytometry (Supplementary Figure 3) and was similar to the number of cells expressing the same genetic construct in the presence of 10 nM 3OC6 HSL. Then, four different genetic constructs that included the wild type or mutant versions of the LuxR transcriptional activator and LuxI synthase were initially tested for activity (Table 3 and Supplementary Figure 4).

Plasmid name	Vector	Insert	Function	
			Sensing	Sending
RL078A	pSB1A3	pTet- <i>luxR</i> - <i>plux</i> - <i>luxI</i>	C6	C6
NY009A	pSB1A3	pTet-(T33A,S116,M135I) <i>luxR</i> - <i>plux</i> - <i>luxI</i>	C6/C8	C6
NY013A	pSB1A3	pTet-(T33A,S116,M135I) <i>luxR</i> - <i>plux</i> - (E34G,R40G,E63G) <i>luxI</i>	C6/C8	C6
NY014A	pSB1A3	pTet- <i>luxR</i> - <i>plux</i> -(E34G,R40G,E63G) <i>luxI</i>	C6	C6
RL081A	pSB1A3	pTet- <i>luxR</i> - <i>plux</i> -T7polimerase	C6	T7pol

Table 3. Genetic constructs tested for the cellular imitation game experiments.

Artificial cells were added to a *V. fischeri* culture at $OD_{600\text{ nm}} = 0.2-0.3$ exhibiting low luminescence and incubated for 3 h at 30 °C. The artificial cells containing DNA encoding *luxR** and *luxI** were the only artificial cells that induced a detectable luminescent response per colony forming unit (CFU) and, therefore, were the only artificial cells capable of chemically communicating with *V. fischeri* (Supplementary Figure 4). To confirm that artificial cells could withstand the presence of *V. fischeri*, the

stability of the artificial cells was assessed by a calcein leakage assay (Supplementary Figure 5). 80 mM of the calcein dye was added to 1:2 POPC: cholesterol liposomes encapsulating the same DNA and components required for optimal chemical communication. Liposomes were incubated with *V. fischeri* at $OD_{600\text{ nm}} = 0.28$ for 3 h at 30 °C. At this concentration, the fluorescence of calcein was low due to self-quenching. Upon the breakage of the liposomes, calcein would be released, thus giving rise to increased fluorescence. The calcein signal remained low and constant over the 3 h of incubation, indicating that the artificial cells were stable in the presence of *V. fischeri*. After identifying the optimal genetic construct that conferred upon the artificial cells the ability to sense and synthesize 3OC6 HSL and confirming that the artificial cells could withstand the presence of *V. fischeri* and that the supernatant of a low-density *V. fischeri* culture contains enough homoserine lactones to activate the expression of *luxI*, the next step was to setup a type of cellular imitation game to assess how well the artificial cells were able to communicate. For this purpose, artificial cells carrying DNA coding for *luxR** and *luxI** (hereafter referred as to functional artificial cells) or carrying RL081A (Table 3) coding for *luxR** and T7 RNA polymerase (hereafter referred as to nonfunctional artificial cells) were constructed. Nonfunctional artificial cells were able to sense 3OC6 HSL but were not capable of synthesizing the quorum molecule in response. Nonfunctional artificial cells were used as negative controls for the two-way communication experiments. The experiments also included an undiluted culture of *V. fischeri* as a positive control for chemical communication. Artificial cells encapsulating LBS (hereafter referred as to empty artificial cells) and cultures of *V. fischeri* diluted with LBS with or without 100 nM 3OC6 HSL were additional used as controls. The luminescence per single cell induced by functional artificial cells was similar to the luminescence levels of the undiluted *V. fischeri* culture (Figure 8). Both luminescence values were considerably higher than the luminescence induced by nonfunctional artificial cells.

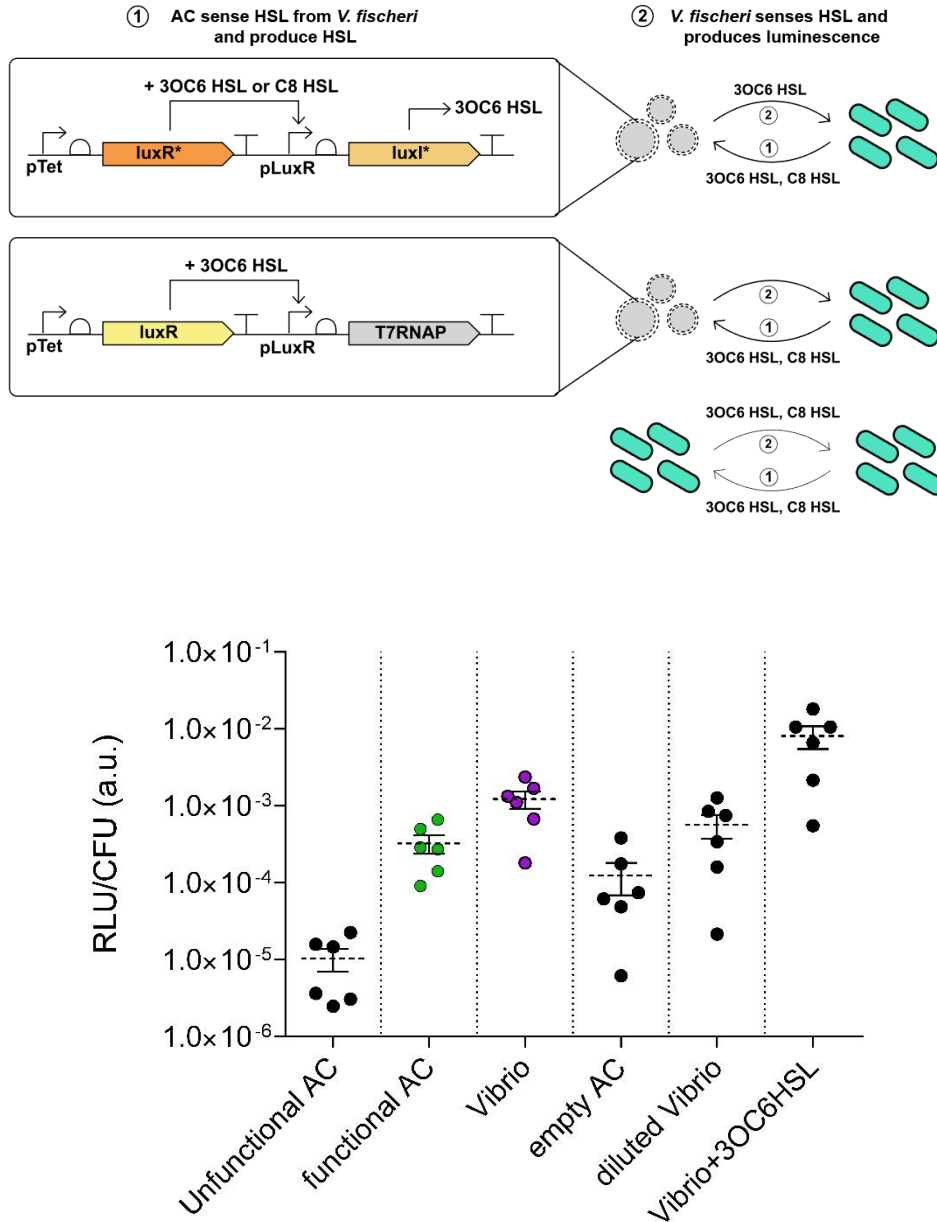


Figure 8. Luminescence of *V. fischeri* induced by functional and nonfunctional artificial cells. Top: schematic representation of the experimental setting for two-way chemical communication between artificial cells and *V. fischeri*. Functional artificial cells sense both 3OC6 HSL and C8 HSL and respond by synthesizing and releasing 3OC6 HSL. Nonfunctional artificial cells sense 3OC6 HSL and respond by synthesizing T7 RNA polymerase. *V. fischeri* sense and synthesize both 3OC6 HSL and C8 HSL. Bottom: Similar luminescence response per single cell was induced by functional artificial cells and *V. fischeri*. (AC) Artificial cell. Sample controls were: (Vibrio) non-diluted culture, (Empty AC) Artificial cells encapsulating LBS, (diluted Vibrio) *V. fischeri* culture diluted 1:1 (volume ratio) with LBS and (Vibrio+3OC6 HSL) *V. fischeri* diluted culture with LBS supplemented with 100nM commercial 3-oxo-hexanoyl-homoserine lactone. Dotted lines represent the mean of $n=6$ independent experiments, error bars correspond to the standard error of the mean (SEM). (RLU/CFU) relative luminescence units per colony forming units per milliliter. (a.u.) arbitrary units. Y-axis is in log₁₀ scale.

The luminescence data was confirmed by RT-qPCR (Figure 9), which showed that the expression of *luxA* and *luxB*, two lux genes coding for the two subunits of *V. fischeri* luciferase, was similarly upregulated 5-fold both for communication mediated by artificial cells and for natural *V. fischeri*-*V. fischeri* communication corresponding to the undiluted culture sample. *luxA* and *luxB* were previously reported to be upregulated by 3OC6 HSL (34).

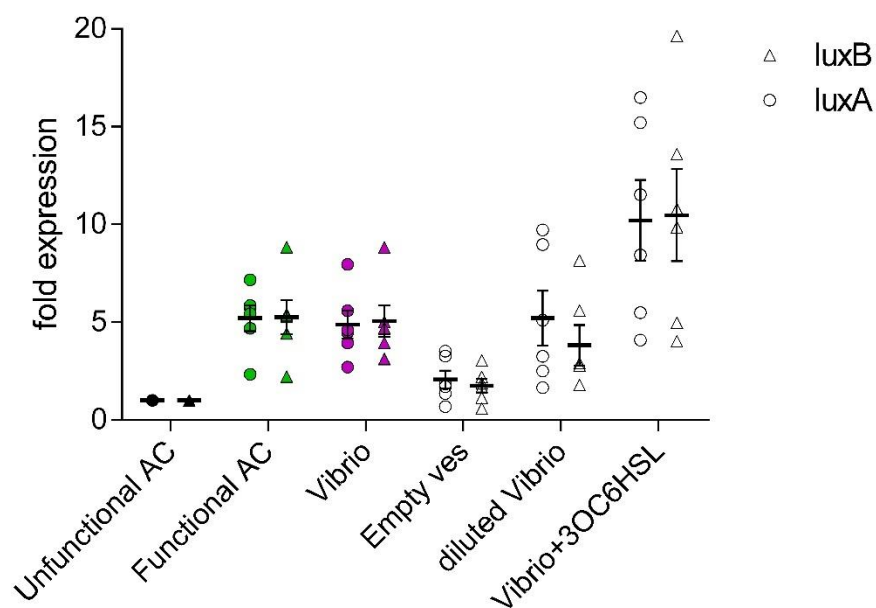


Figure 9. Transcription activation of the *V. fischeri* luciferase subunit genes in the presence of functional and nonfunctional artificial cells. Shown is the fold expression of *luxA* and *luxB* (assessed by RT-qPCR) normalized to the negative control (*V. fischeri* in the presence of nonfunctional artificial cells). Sample controls were: (*Vibrio*) non-diluted culture, (*Empty AC*) Artificial cells encapsulating LBS, (*diluted Vibrio*) *V. fischeri* culture diluted 1:1 (volume ratio) with LBS and (*Vibrio+3OC6 HSL*) *V. fischeri* diluted culture with LBS supplemented with 100 nM commercial 3-oxo-hexanoyl-homoserine lactone. Solid lines indicate the mean of n=6 independent experiments, error bars correspond to the standard error of the mean (SEM).

RNA-seq can be used to quantify the extent to which artificial cells mimic natural cells. Although the luminescence and RT-qPCR data showed that the artificial cells behaved to some extent as natural *V. fischeri*, such data were not enough to determine the extent of mimicry. To more quantitatively assess the performance of the artificial cells, the gene expression profile of natural cells in response to the activity of artificial cells was evaluated. The six experiments of the cellular imitation game were subjected to

RNA-sequencing analysis. Incubation of *V. fischeri* with nonfunctional artificial cells gave 175 differently expressed coding sequences with respect to the *V. fischeri*-*V. fischeri* communicating sample (Tables 4 and 5). The same experiment in the presence of functional artificial cells containing DNA encoding *luxR** and *luxI** instead gave 107 differently expressed coding sequences with respect to the *V. fischeri*-*V. fischeri* communicating sample (Tables 4 and 6), meaning that the functional artificial cells better mimicked the influence of natural *V. fischeri* on *V. fischeri* than nonfunctional artificial cells. Although the RNA sequencing analysis, after false discovery rate (FDR) adjusted p value >0.05, did not identify statistically significant differences in the expression of the lux operon in response to functional and nonfunctional artificial cells, the average increase in the number of reads from the six RNA-seq samples (Figure 10) was similar to the activation measured by RT-qPCR (Figure 9). The lux genes did not significantly differ in expression between samples due to the great variability among the six experiments (Figure 9). To better visualize the difference in transcript levels, the fragments per kilobase of transcript per million mapped reads (FPKM) values for the lux genes for the six individual experiments were plotted for the two comparisons and clearly revealed that the expression over the entire lux operon, except for *luxI* and *luxR*, was more similar between natural *V. fischeri* and functional artificial cells than with nonfunctional artificial cells (Figure 11 and 12).

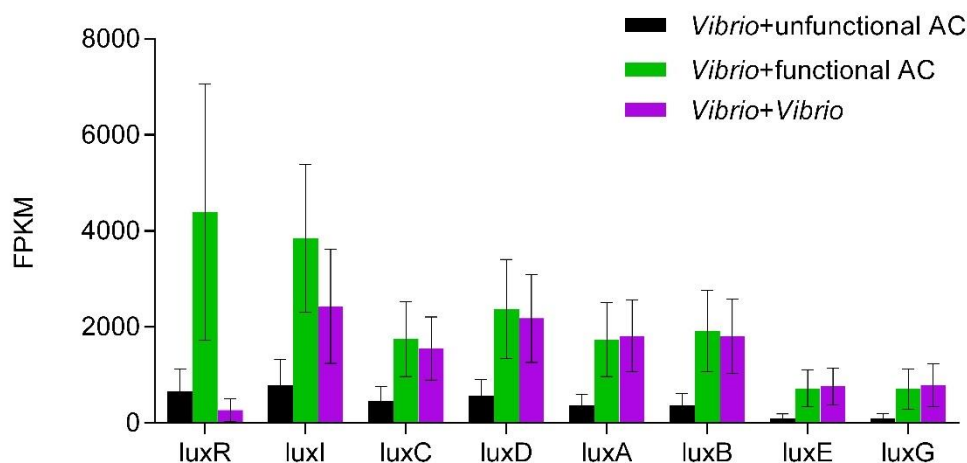


Figure 10. Transcript levels of the lux operon genes from *V. fischeri* in contact with *V. fischeri*, functional and nonfunctional artificial cells. Error bars indicates the standard error of the man (SEM) of n=6 independent experiments. FPKM (Fragments per kilobase of transcript per million mapped reads).

The interpretation of the *luxI* and *luxR* data was more difficult and should not be considered due to the impossibility to discriminate between the in vivo or artificially transcribed RNA transcripts since total RNA was extracted from the same sample pool containing both artificial and natural cells. Both genes were expressed in *V. fischeri* and functional artificial cells and *luxR* transcripts were also present in nonfunctional artificial cells.

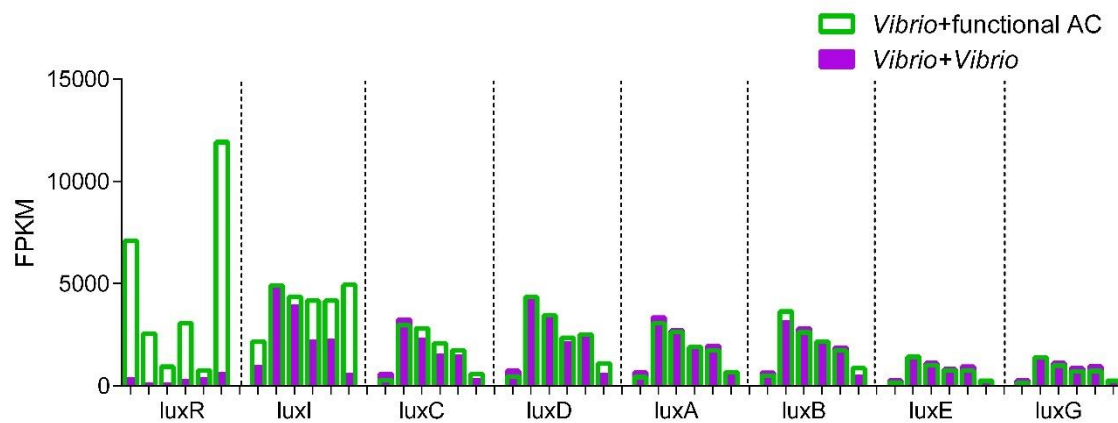


Figure 11. Transcript levels of the lux operon genes from sample comparisons (*Vibrio fischeri* + *Vibrio fischeri* vs *Vibrio fischeri* + functional AC). Shown are the FPKM of 6 individual replicates. FPKM (Fragments per kilobase of transcript per million mapped reads).

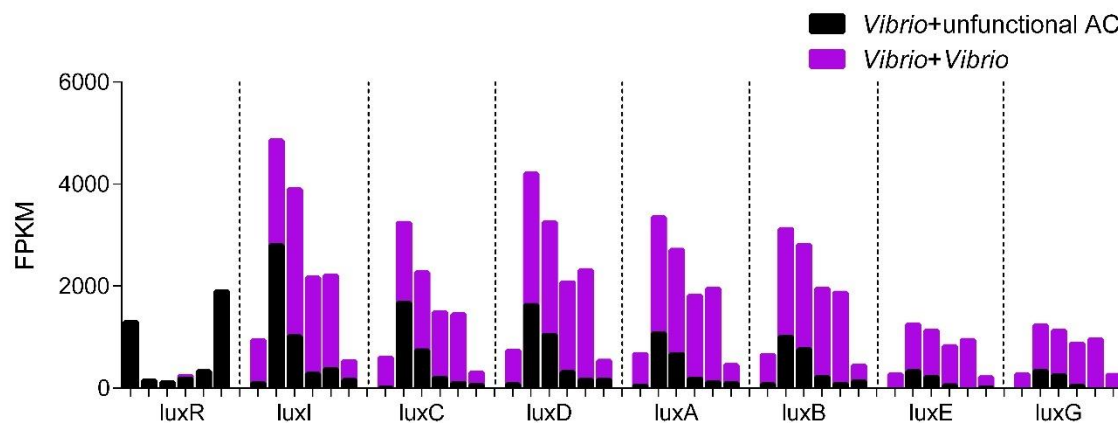


Figure 12. Transcript levels of the lux operon genes from sample comparisons (*Vibrio fischeri* + *Vibrio fischeri* vs *Vibrio fischeri* + nonfunctional AC). Shown are the FPKM of 6 individual replicates. FPKM (Fragments per kilobase of transcript per million mapped reads).

Furthermore, a correlation between the gene expression profile of *V. fischeri* in response to functional and nonfunctional artificial cells showed that six of the seven genes of the lux operon fell off the correlation trend (Figure 13) suggesting that the critical difference between the two types of artificial cells was their effect on quorum signaling, as expected.

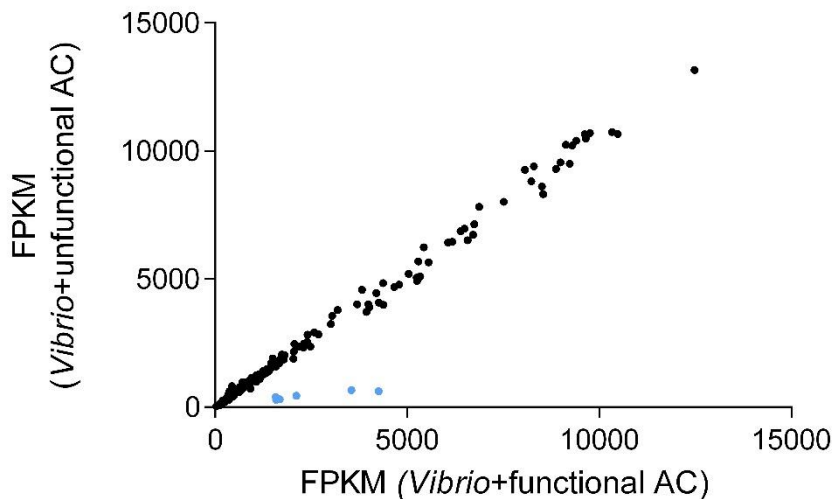


Figure 13. Correlation plot of *V. fischeri* gene expression in response to functional and nonfunctional artificial cells. *V. fischeri* was highly correlated, $r = 0.99$. Blue dots indicate the genes falling off the correlation trend, including six out of the seven genes of the lux operon. FPKM (Fragments per kilobase of transcript per million mapped reads).

The data were then plotted in a way to visualize how much more *Vibrio*-like were functional artificial cells with respect to nonfunctional artificial cells (Figure 14). Here we considered the coding sequences all over the *Vibrio fischeri* genome, independently of whether the coding sequences were statistically differently expressed or not. The average FPKM values obtained per coding sequence from the six replicate experiments for both comparisons were subtracted. In comparison 1, average FPKM values of the sample (bacteria in presence of functional artificial cells) were subtracted from the average FPKM values of the sample (bacteria in presence of same bacteria). The same was done for comparison 2 (bacteria in contact with nonfunctional artificial cells) compared with (bacteria in presence of bacteria). The plot showed that the overall distribution of the computed FPKM values for each coding sequence of *V. fischeri* in the presence of functional artificial cells (green area) was closer to 0 than the distribution of the coding sequences of *V. fischeri* in the presence of nonfunctional

artificial cells (black area). Therefore, functional artificial cells were more *V. fischeri*-like than nonfunctional artificial cells (Figure 14).

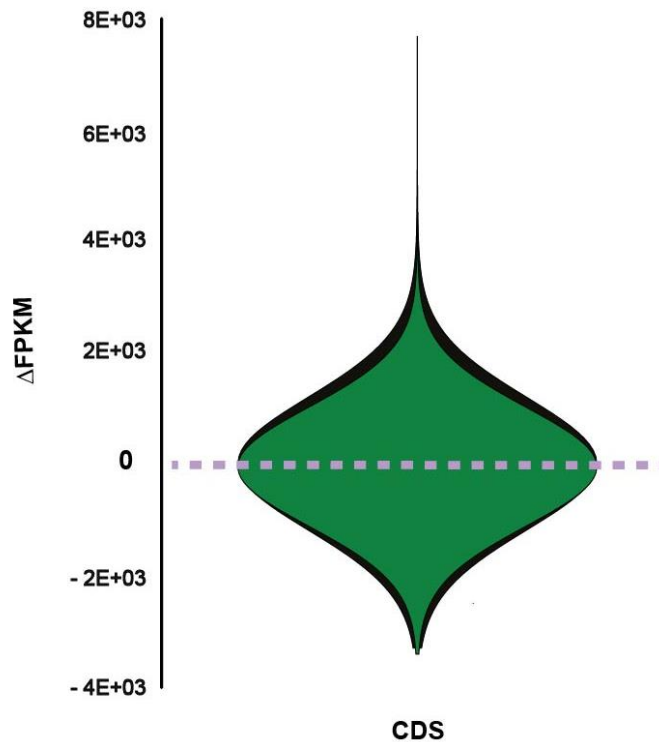


Figure 14. *V. fischeri* transcriptome correlation. Distribution of the difference in FPKM per coding sequence between comparison 1 (*V. fischeri* with functional artificial cells) compared to (*V.fischeri-V.fischeri*) (green) and *V. fischeri-V. fischeri* with *V. fischeri*- nonfunctional artificial cells (black). FPKM (fragments per kilobase of transcript per million mapped reads), CDS (Coding DNA Sequences). Purple dotted line indicates the *V. fischeri* reference coding DNA sequences distribution.

From the obtained RNA-seq data, we proposed a way to calculate how *V. fischeri*-like the artificial cells were. The nonfunctional artificial cells changed the expression of 175 coding sequences differently than *V. fischeri*. Instead, an artificial cell that would have functioned identically to *V. fischeri* would not have induced any differences in gene expression. If we assume that nonfunctional artificial cells were 0% *V. fischeri*-like, then any reduction in the number of differences in gene expression would increase the degree of likeness of the artificial cell to *V. fischeri*. This calculation would indicate that the functional artificial cells in our case were 39% more *V. fischeri*-like than nonfunctional artificial cells ($[(175 - 107)/175] \times 100$). This value is clearly an overestimation because only two genes, *luxR** and *luxI** were genetically encoded

inside the functional artificial cells. The remaining components came from an *E. coli* cell extract that was used to provide the transcription and translation machinery. The percentage of reduced genomes dedicated to gene expression is similar to the 39% lifelike value calculated here. For example, 41% of the synthetically produced, reduced *Mycoplasma mycoides* genome (i.e., JCVI-syn3.0) is necessary for gene expression (6). In other words, the data only make sense when put into the context of the entire genetic system required to support the synthesis of RNA, protein, and the products of protein enzymes, in this case quorum molecules. That is, it is more accurate to say that if the artificial cells used here were completely genetically encoded, then these artificial cells would be 39% more *V. fischeri*-like than nonfunctional artificial cells, according to the described cellular imitation game.

Table 4. 81 differently expressed genes commonly found in both *V. fischeri* in presence of functional and nonfunctional artificial cells

identifiers	Protein names
VFMJ11_0124	50S ribosomal protein L28
VFMJ11_2503	Acetyl-coenzyme A synthetase
VFMJ11_2417	Acetylglutamate kinase
VFMJ11_2396	Acetylnornithine aminotransferase
VFMJ11_2240	Acriflavin resistance plasma membrane protein
VFMJ11_0310	Adenylyl-sulfate kinase
VFMJ11_0599	Amino-acid acetyltransferase
VFMJ11_2164	Amino-acid carrier protein AlsT
VFMJ11_0730	Antibiotic biosynthesis monooxygenase
VFMJ11_2395	Arginine N-succinyltransferase
VFMJ11_2415	Argininosuccinate lyase
VFMJ11_2416	Argininosuccinate synthase
VFMJ11_A0831	BfdA
VFMJ11_2512	Bifunctional purine biosynthesis protein PurH
VFMJ11_2516	CBS-domain containing protein
VFMJ11_2501	Cyclic nucleotide binding protein
VFMJ11_2028	Cysteine synthase
VFMJ11_2330	Cytochrome b
VFMJ11_2643	Dipeptide transport system permease protein DppB
VFMJ11_2642	Dipeptide transport system permease protein DppC
VFMJ11_2644	Dipeptide-binding protein
VFM11_0634	Fe-S protein assembly co-chaperone HscB
VFMJ11_A0502	Formimidoylglutamase
VFMJ11_2645	Glutathione import ATP-binding protein GsiA
VFMJ11_2605	Hydrolase
VFMJ11_0262	Immunogenic protein
VFMJ11_0628	Inositol-1-monophosphatase
VFMJ11_A0804	Lipoprotein, putative
VFMJ11_0601	Membrane-bound lytic murein transglycosylase A
VFMJ11_2421	Methylenetetrahydrofolate reductase
VFMJ11_2418	N-acetyl-gamma-glutamyl-phosphate reductase
VFMJ11_2394	N-succinylglutamate 5-semialdehyde dehydrogenase
VFMJ11_2241	Periplasmic component of efflux system
VFMJ11_0299	Phosphoadenosine phosphosulfate reductase
VFMJ11_0204	Phosphoribulokinase 1
VFMJ11_2409	Pili assembly protein PilM
VFMJ11_2406	Pilus expression protein
VFMJ11_2377	Probable HTH-type transcriptional regulator LeuO
VFMJ11_2526	Regulatory protein CsgD
VFMJ11_2279	RNA polymerase-binding transcription factor DksA
VFMJ11_0308	Sulfate adenylyltransferase subunit 1
VFMJ11_0307	Sulfate adenylyltransferase subunit 2

VFMJ11_0297	Sulfite reductase [NADPH] flavoprotein alpha-component
VFMJ11_0298	Sulfite reductase [NADPH] hemoprotein beta-component
VFMJ11_0602	ThiF family protein
VFMJ11_0261	Transporter
VFMJ11_0309	Transporter, divalent anion:sodium symporter family
VFMJ11_2508	tRNA-dihydrouridine synthase
VFMJ11_2495	Two-component response regulator
VFMJ11_A0807	Type VI secretion protein, family
VFMJ11_A0824	Type VI secretion-associated protein, family
VFMJ11_0199	Uncharacterized protein
VFMJ11_0660	Uncharacterized protein
VFMJ11_2393	Uncharacterized protein
VFMJ11_2496	UPF0056 inner membrane protein
VFMJ11_0300	VcgC
VFMJ11_0306	2',3'-cyclic-nucleotide 2'-phosphodiesterase
VFMJ11_0304	Acetyltransferase
VFMJ11_2293	Acetyltransferase component of pyruvate dehydrogenase complex
VFMJ11_2475	Anaerobic C4-dicarboxylate transporter
VFMJ11_2474	Aspartate ammonia-lyase (Aspartase)
VFMJ11_2158	Catalase
VFMJ11_2157	CytC
VFMJ11_2413	Dihydrolipoamide dehydrogenase
VFMJ11_1700	Formate acetyltransferase
VFMJ11_A0425	Formate/nitrite transporter family protein
VFMJ11_2456	Fumarate reductase flavoprotein subunit
VFMJ11_2458	Fumarate reductase subunit C
VFMJ11_2459	Fumarate reductase subunit D
VFMJ11_2412	Hybrid peroxiredoxin hyPrx5
VFMJ11_1621	L-asparaginase 2
VFMJ11_2391	OsmC/Ohr family protein
VFMJ11_2620	suppressor for copper-sensitivity A
VFMJ11_2294	Pyruvate dehydrogenase E1 component
VFMJ11_2370	Pyruvate kinase
VFMJ11_2160	Superoxide dismutase [Cu-Zn]
VFMJ11_2156	Uncharacterized protein
VFMJ11_2155	Uncharacterized protein
VFMJ11_2045	Uncharacterized protein
VFMJ11_2581	Uncharacterized protein
VFMJ11_0691	Urea amidohydrolase subunit alpha

Upregulated genes are highlighted in red, blue instead indicate the downregulated genes

Table 5. List of 94 differently expressed coding sequences found in *V. fischeri* in presence of nonfunctional artificial cells

Gene identifier	Protein names
VFMJ11_0421	A/G-specific adenine glycosylase
VFMJ11_A0118	ABC transporter ATP-binding protein
VFMJ11_2112	Accessory colonization factor AcfA
VFMJ11_2691	Acetolactate synthase
VFMJ11_0599	Amino-acid acetyltransferase
VFMJ11_2215	Amino-acid carrier protein AlST
VFMJ11_2151	Amylo-1,6-glucosidase
VFMJ11_2131	Chaperone protein DnaK
VFMJ11_0587	Chromate transport protein
VFMJ11_2558	Conserved domain protein
VFMJ11_0007	Cystine transport system permease protein
VFMJ11_0008	Cystine-binding protein
VFMJ11_0074	Cytochrome c4
VFMJ11_2651	Cytochrome c5
VFMJ11_2502	DNA polymerase III subunit epsilon
VFMJ11_2509	DNA-binding protein Fis
VFMJ11_0656	Endoribonuclease L-PSP
VFMJ11_1979	Flagellar hook-length control protein
VFMJ11_2184	Flagellin
VFMJ11_2280	Glutamyl-Q tRNA(Asp) synthetase
VFMJ11_1267	GTP cyclohydrolase-2
VFMJ11_2169	Homoserine O-succinyltransferase
VFMJ11_0006	L-cystine import ATP-binding protein
VFMJ11_0535	Long-chain-fatty-acid--CoA ligase
VFMJ11_2154	Magnesium transporter
VFMJ11_2147	Maltose transport system permease protein MalF
VFMJ11_2148	Maltose transport system permease protein MalG
VFMJ11_2146	Maltose/maltodextrin-binding protein
VFMJ11_2149	Multiple sugar-binding transport ATP-binding protein
VFMJ11_2668	N5-carboxyaminoimidazole ribonucleotide mutase
VFMJ11_2669	N5-carboxyaminoimidazole ribonucleotide synthase
VFMJ11_2152	Neopullulanase
VFMJ11_0475	OmpU, outer membrane protein
VFMJ11_0397	Ornithine carbamoyltransferase
VFMJ11_0033	Phosphomethylpyrimidine synthase
VFMJ11_2063	Phosphoribosylformylglycinamide cyclo-ligase
VFMJ11_2064	Phosphoribosylglycinamide formyltransferase
VFMJ11_2218	Putative Hemerythrin HHE cation binding domain
VFMJ11_0004	Ribonuclease P protein component
VFMJ11_2173	RNA polymerase sigma factor RpoS (Sigma-38)
VFMJ11_0439	S-adenosylmethionine synthase
VFMJ11_2104	S-adenosylmethionine:tRNA ribosyltransferase-isomerase

VFMJ11_A0825	Serine-threonine protein kinase
VFMJ11_0460	Sodium-dependent phosphate transporter
VFMJ11_2430	Sodium-type polar flagellar protein (MotX)
VFMJ11_0453	Transcriptional regulator
VFMJ11_A0866	Transcriptional regulator (LysR family)
VFMJ11_0043	Transporter (metabolite exporter family)
VFMJ11_0057	Uncharacterized protein
VFMJ11_2150	Uncharacterized protein
VFMJ11_2217	Uncharacterized protein
VFMJ11_2204	Uncharacterized protein
VFMJ11_0150	Uncharacterized protein
VFMJ11_0345	Uncharacterized protein
VFMJ11_0376	Uncharacterized protein
VFMJ11_0498	Uncharacterized protein
VFMJ11_1786	UPF0260 protein VFMJ11_1786
VFMJ11_0151	WbfD protein
VFMJ11_0114	Xanthine permease
VFMJ11_0023	3-ketoacyl-CoA thiolase
VFMJ11_2105	Acetoin utilization AcuB protein
VFMJ11_2067	Acyl-coenzyme a dehydrogenase
VFMJ11_2170	Anaerobic C4-dicarboxylate transporter
VFMJ11_0395	Aspartate carbamoyltransferase regulatory chain
VFMJ11_2221	Autonomous glycol radical cofactor
VFMJ11_0506	Deoxyribose-phosphate aldolase
VFMJ11_A0108	Ferredoxin-type protein NapF
VFMJ11_A0177	Formate acetyltransferase
VFMJ11_0070	Glycerol-3-phosphate transporter
VFMJ11_A0597	Integral membrane protein
VFMJ11_2657	Ketol-acid reductoisomerase
VFMJ11_0452	Lysine-tRNA ligase
VFMJ11_1732	Methyl-accepting chemotaxis protein
VFMJ11_0357	MshA, mannose-sensitive haemagglutinin
VFMJ11_0018	NADH dehydrogenase subunit ii-related protein
VFMJ11_0504	Nucleoside permease
VFMJ11_2109	Peroxiredoxin-2
VFMJ11_0508	Phosphopentomutase
VFMJ11_0022	Protein YhdH
VFMJ11_0509	Purine nucleoside phosphorylase DeoD-type
VFMJ11_0685	Putative N-acetylmannosamine kinase
VFMJ11_0019	Sulfurtransferase TusA homolog
VFMJ11_1508	Tetratricopeptide repeat family protein
VFMJ11_0507	Thymidine phosphorylase
VFMJ11_2165	Transcriptional activator CadC
VFMJ11_2482	Transcriptional regulator, ArsR family
VFMJ11_0898	Uncharacterized protein
VFMJ11_2681	Uncharacterized protein

VFMJ11_2118	Uncharacterized protein
VFMJ11_2480	Uncharacterized protein
VFMJ11_A1010	Uncharacterized protein
VFMJ11_0081	Universal stress protein
VFMJ11_2476	Universal stress protein
VFMJ11_0505	XapX domain, putative

Upregulated genes are highlighted in red, blue instead indicate the downregulated genes

Table 6. List of 26 differently expressed coding sequences found in *V.fischeri* in the presence of artificial functional cells

identifiers	Protein names
VFMJ11_0196	60 kDa chaperonin
VFMJ11_0708	ABC transporter, permease protein
VFMJ11_2390	ATP-dependent protease ATPase subunit HslU
VFMJ11_0818	Copper-transporting P-type ATPase
VFMJ11_0673	Endochitinase
VFMJ11_A0504	Histidine utilization repressor
VFMJ11_A0503	Imidazolonepropionase
VFMJ11_0301	Peptidyl-prolyl cis-trans isomerase
VFMJ11_1809	Recombination protein RecR
VFMJ11_0659	S-(hydroxymethyl)glutathione dehydrogenase
VFMJ11_0663	S-(hydroxymethyl)glutathione dehydrogenase
VFMJ11_A0759	Site-specific recombinase IntIA
VFMJ11_A0805	Type VI secretion system FHA domain protein
VFMJ11_2525	Uncharacterized protein
VFMJ11_2159	AnkB protein
VFMJ11_2134	ATP-dependent NAD kinase
VFMJ11_1225	Carbon starvation protein A
VFMJ11_1948	Lipoprotein VacJ
VFMJ11_0927	Putative transport protein
VFMJ11_0611	TPR-repeat-containing protein
VFMJ11_0189	UDP-D-quinovosamine 4-dehydrogenase
VFMJ11_0693	Urea amidohydrolase subunit gamma
VFMJ11_0694	Urease accessory protein UreD
VFMJ11_0690	Urease accessory protein UreE
VFMJ11_0689	Urease accessory protein UreF
VFMJ11_0688	Urease accessory protein UreG

Upregulated genes are highlighted in red, blue instead indicate the downregulated genes

Artificial cells can sense *Vibrio fischeri* and disrupt *P. aeruginosa* quorum sensing

After showing that artificial cells can be built that can chemically communicate by sensing and synthesizing 3OC6 HSL, we next sought to determine whether such artificial cells could be used for technological purposes. Pathogenic bacteria are known to regulate the expression of their virulent genes through quorum sensing (39). For example, the opportunistic human pathogen *P. aeruginosa* uses N-(3-oxododecanoyl)-L-homoserine lactone, hereafter referred as 3OC12 HSL (Figure 15), to control the initial stages of biofilm formation (40) and the production of virulence factors (39).

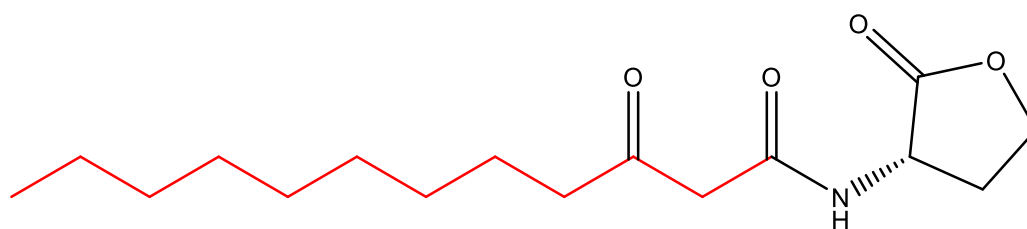


Figure 15. Chemical structure of the *P. aeruginosa* quorum sensing molecule N-(3-oxododecanoyl)-L-homoserine lactone. This amphipathic quorum molecule is composed of a homoserine lactone ring and 12-carbon atoms oxidized acyl chain highlighted in red.

The mechanism of activation of gene expression is similar to that of *V. fischeri*. In the case of *P. aeruginosa*, the activation relies on the transcriptional activator LasR, which upon interaction with 3OC12 HSL binds to a specific DNA binding site termed las box, hereafter referred to as (plas). Reconstituting simplified versions of the quorum sensing mechanism of *P. aeruginosa* was complicated. Several genetic constructs designed and engineered to detect and respond specifically to 3OC12 HSL failed at sensing the molecule in in vitro transcription translation reactions. (Table 7). Only NY008A coding for the *lasR* transcriptional activator under the control of pTet constitutive promoter and GFPmut3b under a LuxR responsive promoter showed a two-fold increase in protein expression in the presence of the quorum molecule (Figure 16). LasR has been shown to also bind the *V. fischeri* LuxR responsive promoter (41).

Plasmid name	Vector	Insert	Function	Ratio RFU (a.u.) end time point
			Sensing	
NY001A	pET21b	<i>lasR</i> -pJ23100-plux-sfGFP	3OC12 HSL	0.71
NY002A	pET21b	<i>lasR</i> -pT7-plux	3OC12 HSL	1.16
NY003A	pET21b	<i>lasR</i> -pJ23100	3OC12 HSL	0.56
NY004A	pET21b	pluxR-sfGFP	3OC12 HSL	
NY005A	pET21b	<i>lasR</i> -pT7-plas-sfGFP	3OC12 HSL	0.91
NY008A	pSB1A3	pTet- <i>lasR</i> -plux-GFPmut3b	3OC12 HSL	2.3

Table 7. Genetic constructs tested for 3OC12 HSL sensing in vitro. TX/TL reactions were assembled with different genetic constructs engineered to sense 3OC12 HSL. Reported are the ratios of the end time point fluorescence values after 6 h from reactions that were supplemented with 10 μ M commercial 3OC12 HSL over the values obtained from reactions that were carried in the absence of quorum molecule. NY002A and NY003A encoding the *lasR* transcriptional activator under the T7 or J23100 constitutive promoters respectively were used in equimolar concentration with NY004A coding for sfGFP reporter under the control of a *pluxR* responsive promoter, in the same reactions. Indicated ratios were obtained from 1 representative experiment. pJ23100 RFU (Relative Fluorescence Unit).

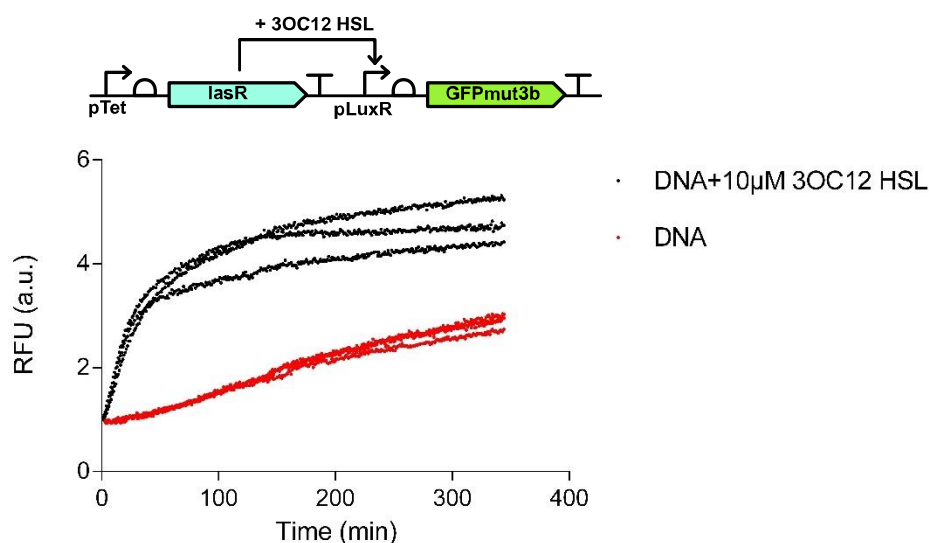


Figure 16. Sensing 3OC12 HSL in vitro. Top: schematic representation of the genetic parts of the quorum sensor DNA (NY008A). Bottom: GFPmut3b expression from *in vitro* transcription-translation reaction in the presence or absence of 10 μ M of commercial 3OC12 HSL was monitored over 6 h by fluorescence spectroscopy. $n=3$ representative experiments.

Artificial cells encapsulating TX/TL machinery and carrying a genetic construct coding for the *lasR* transcriptional activator and firefly luciferase under the control of a LuxR responsive promoter were not responsive to 10 μ M commercial 3OC12 HSL after 4 h of incubation at 37 $^{\circ}$ C (Supplementary Figure 7 and Supplementary Figure 2). Then a

calcein leakage assay showed that the artificial cells were unstable in the presence of *P. aeruginosa* (Figure 17), consistent with previous reports showing that *P. aeruginosa* produce and release phospholipases of various types (42).

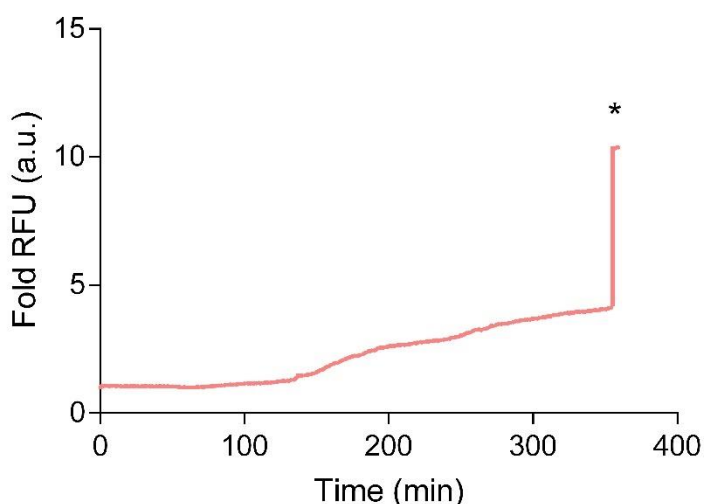


Figure 17. Stability of artificial cells in contact with *P. aeruginosa* determined by a calcein leakage assay. The increase in fluorescence due to calcein release from liposomes, indicated that artificial cells were disrupted in the presence of *P. aeruginosa*. (*) indicates the addition of 0.3% (v/v) Triton X-100. RFU (Relative Fluorescence Units); a.u. (arbitrary units).

Interestingly, acyl-homoserine lactones are degraded by the *Bacillus thuringiensis* enzyme AiiA (43). This suggested that artificial cells capable of sensing homoserine lactones produced by *P. aeruginosa* and in response synthesize and release AiiA could disrupt the QS pathways of pathogenic bacteria. Since 3OC12 HSL sensing did not work inside phospholipid vesicles, (Supplementary Figure 6) a genetic construct was then cloned that encoded *luxR** under a pTet constitutive promoter and *aiiA* under the control of a LuxR responsive promoter (Table 8). DNA was encapsulated together with the cell-free extract inside 1:2 POPC:cholesterol vesicles. Artificial cells were incubated with the supernatant of *V. fischeri* for 4 h at 37 °C to activate the expression of AiiA lactonase. Then a culture of *P. aeruginosa* at $OD_{600\text{ nm}} = 0.3$ was mixed with the suspension of artificial cells and incubated for 2 h at 37 °C. During the incubation time, artificial cells broke and released the AiiA enzyme that degraded the homoserine lactones produced and released by *P. aeruginosa*. Quantification of extracellular 3OC12 HSL was done using an *E. coli* sensor strain transformed with the DNA construct BBa_K575024 which coded for the lasR transcriptional activator (Table 8).

The genetic construct expressing *aiiA* under the control of *LuxR*^{*} allowed the artificial cells to decrease the extracellular 3OC12 HSL by 95% only in the presence of *V. fischeri* (Figure 18). Positive controls were the addition of 100 nM commercial 3OC12 HSL or the supernatant of a culture of *P. aeruginosa* to the *E. coli* reporter strain. Negative controls included the reporter strain without the addition of the quorum molecule or the addition of the supernatant of *V. fischeri* to monitor unspecific interactions.

Plasmid name	Vector	Insert	Function	
			sensing	sending
NY017A	pSB1A3	pTet- <i>luxR</i> [*] - <i>plux</i> - <i>aiiA</i>	C6/C8	<i>AiiA</i>
BBa_K575024	pSB1C3	plas-GFPmut3b-pJ23100- <i>lasR</i>	C12	

Table 8. Genetic constructs used for QS quenching of *P. aeruginosa* experiments. The plasmid BBa_K575024 was extracted from the registry of biological standard parts. C6/C8 (3OC6 HSL and C8 HSL), C12 (3OC12 HSL).

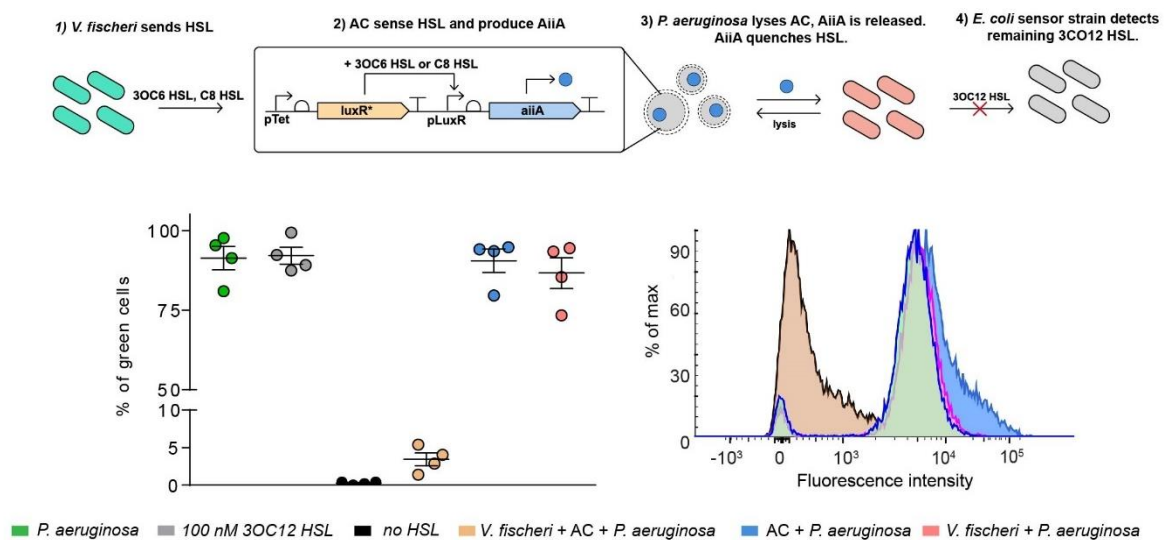


Figure 18. Artificial cells quench *P. aeruginosa* quorum molecules. Top: schematic representation of the experimental setting. Artificial cells (gray, circles) sense homoserine lactones present in the supernatant of a *V. fischeri* culture (teal, oblong) and in response express *aiiA*. Upon incubation with *P. aeruginosa* (pink, oblong), artificial cells break and *AiiA* degrades the 3OC12 HSL released by *P. aeruginosa*. *E. coli* sensor strain (gray, oblong) constitutively expressing *LasR* transcriptional activator detects the remaining 3OC12 HSL by producing GFPmut3b. Bottom: Quantification of extracellular 3OC12 HSL was with an *E. coli* sensor strain by flow cytometry. Bottom left: (% of green cells) indicate the percentage of 3OC12 HSL *E. coli* sensor cells that expressed GFPmut3b in response to the remaining 3OC12 HSL present in the different samples. Bottom right: shown are overlay histograms showing the distribution of the green fluorescence intensity from *E. coli* sensor cells. (% of max) corresponds to the percentage of *E. coli* reporter cells normalized to the total number of counted cells per sample. X-axis is in log scale. *n* = 4 independent experiments; Solid lines represent the means and the error bars correspond to standard error of the mean (SEM). (AC) indicates artificial cells.

Finally, to confirm the use of such technology for therapeutic applications, a preliminary experiment was performed to assess whether artificial cells could be built to disrupt the formation of biofilm from the pathogenic bacteria. A biofilm assay was performed according to O’Toole’s instructions (44). An overnight culture of *P. aeruginosa* grown in LB was diluted, placed in a 96-well plate and incubated for 5 h at 37 °C to allow the formation of the biofilm. The culture was either mixed with artificial cells that constitutively expressed *aiiA* or with artificial cells expressing *aiiA* under the control of a LuxR responsive promoter in response to 3OC6 HSL (Table 9). Negative controls were artificial cells that were not supplemented with DNA or liposomes encapsulating LB. The formation of biofilm was inhibited only in the wells where artificial cells produced AiiA (Figure 19).

Plasmid name	Vector	Insert	Function	
			sensing	sending
NY017A	pSB1A3	pTet- <i>luxR</i> *- <i>plux-aiiA</i>	C6/C8	AiiA
RL089A	pSB1A3	pTet- <i>aiiA</i>		AiiA

Table 9. Genetic constructs used for the biofilm disruption experiment.

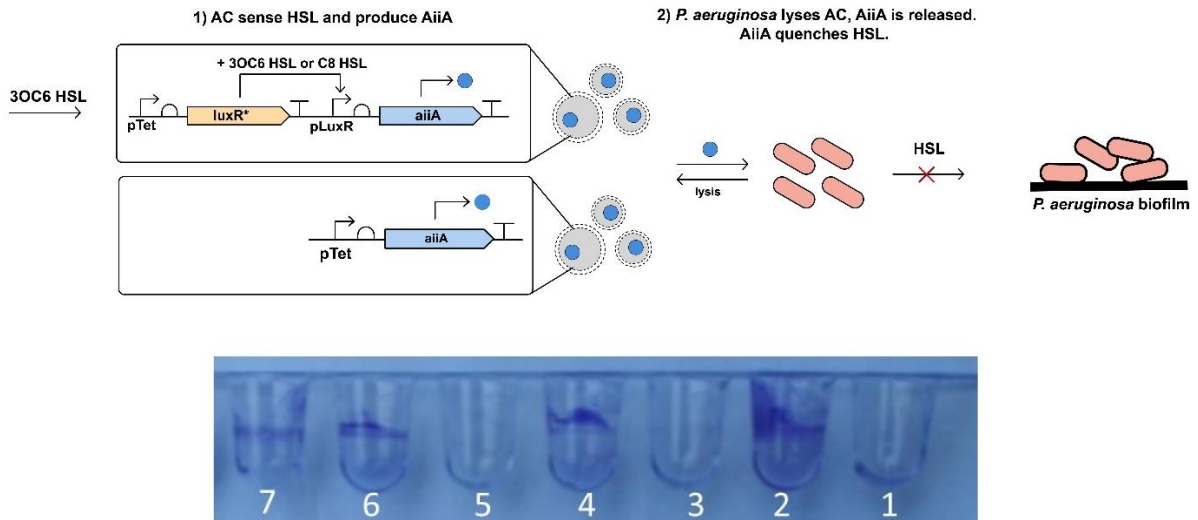
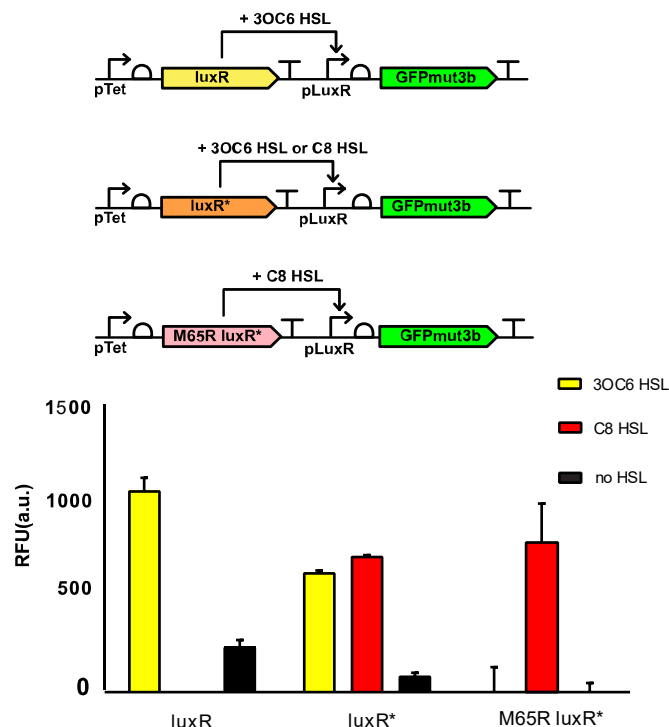


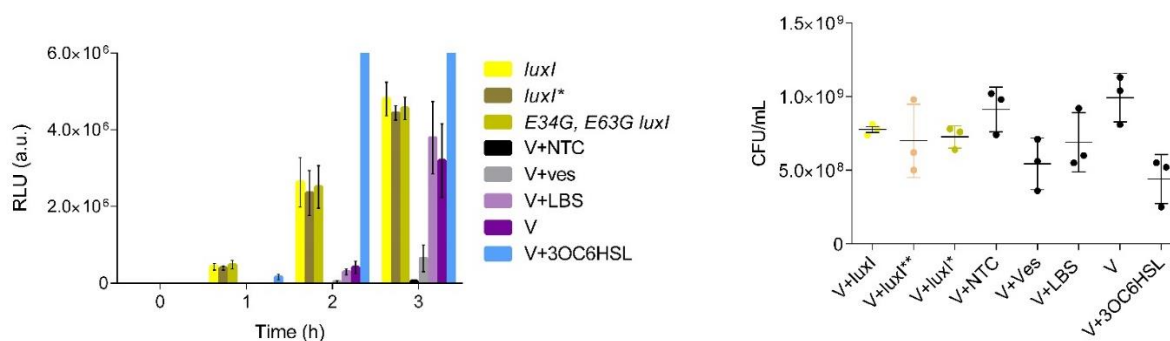
Figure 19. Artificial cells expressing *aiiA* inhibit *P. aeruginosa* biofilm formation. Top: schematic representation of the experimental setup. Artificial cells express AiiA constitutively or in response to commercial 3OC6 HSL. *P. aeruginosa* break artificial cells and AiiA degrades *P. aeruginosa* quorum molecules. The formation of biofilm is assessed by a biofilm assay conducted in a 96-well plate. Bottom: crop image of wells from a 96-well PVC plate after 5 h incubation with *P. aeruginosa* in the presence of either artificial cells constitutively expressing AiiA (well 3), or artificial cells expressing AiiA in response of 10 μ M 3OC6 HSL (well 5). Negative controls were samples with *P. aeruginosa* in the presence of liposomes encapsulating LB (lane 7), artificial cells without DNA (wells 4 and 6). Well 1 was loaded with LB while well 2 contained only *P. aeruginosa*. Biofilm was stained with 0.1% crystal violet aqueous solution.

Although the data need to be reproduced and confirmed and more work is needed to convert such artificial cells into a useful technology, including the development of a membrane that can withstand *P. aeruginosa*, the data suggest that artificial cells could potentially be built to interfere with biofilm formation.

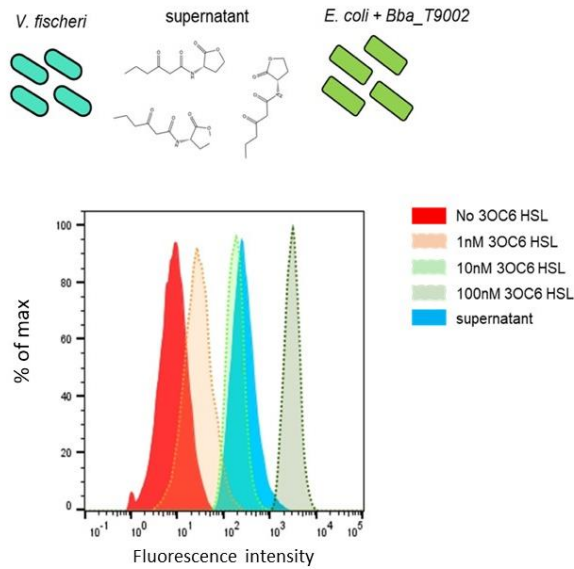
SUPPLEMENTARY FIGURES



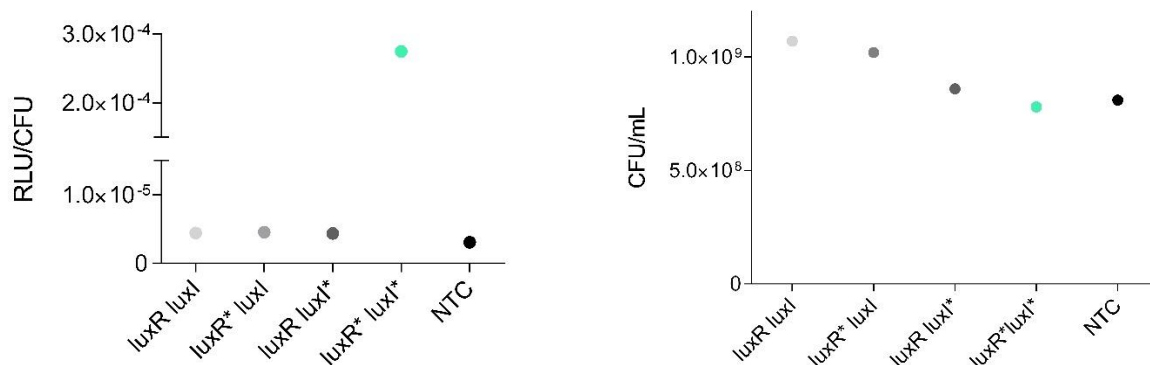
Supplementary Figure 1. Single point mutations are enough to affect the extent of interaction between *luxR* transcriptional activator and *V. fischeri* homoserine lactones and the subsequent activation of gene expression. Top: schematic representation describing the genetic constructs tested for *luxR* activation of gene expression in the presence of commercial 3OC6 HSL and C8 HSL. Bottom: the activity of each genetic construct was assessed by monitoring the *GFPmut3b* fluorescence coming from *in vitro* reactions. Error bars indicate the standard deviation of the mean of $n=3$ independent experiments.



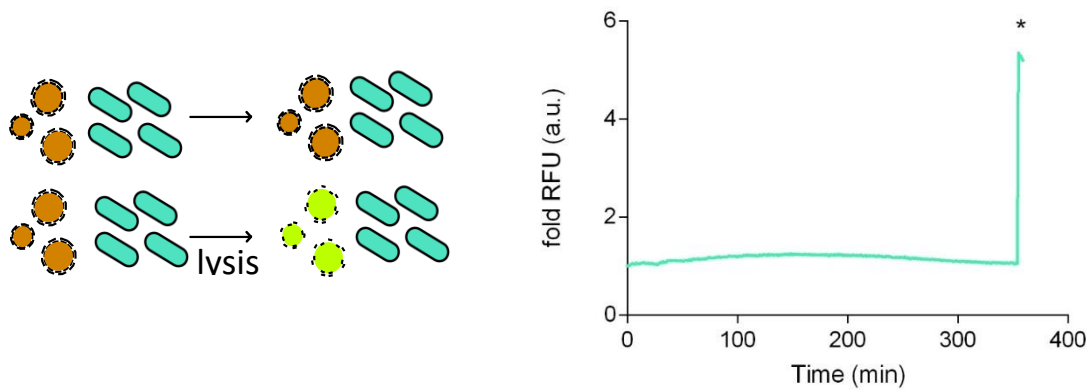
Supplementary Figure 2. Artificial cells expressing different versions of the *LuxI* synthase were inducing similar levels of luminescence to *V. fischeri*. Left: kinetics of *V. fischeri* induced luminescence by artificial sender cells over 3h of co-incubation. Right: colony forming units per mL per sample. Solid lines indicate the mean. Error bars indicates the standard error of the mean of $n=3$ independent experiments.



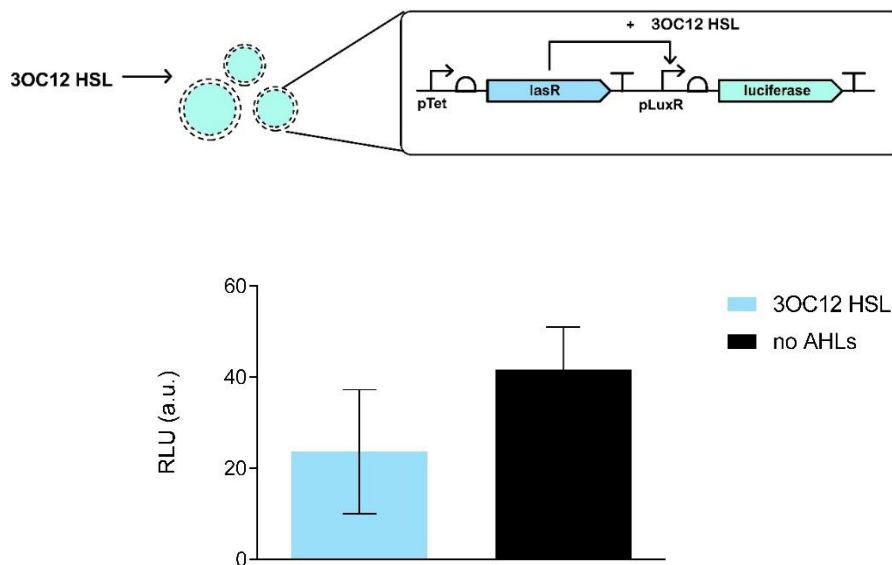
Supplementary Figure 3. 3OC6 HSL detection in *V. fischeri* culture supernatant. Top: schematic representation of the experimental setting. *V. fischeri* produce and release 3OC6 HSL, *E. coli* cells transformed with DNA BBa_T9002 and constitutively expressing LuxR transcriptional activator are incubated with the supernatant of a *V. fischeri* culture at $OD_{600\text{ nm}}=0.25$. 3OC6 HSL diffuses through the *E. coli* sensor strain wall and membranes and activates GFPmut3b expression. The number of fluorescent cells is assessed by flow cytometry. Bottom: overlay histograms showing the distribution of the green fluorescence intensity from *E. coli* sensor cells. (% of max) corresponds to the percentage of *E. coli* reporter cells normalized to the total number of counted cells per sample. X-axis is in log scale. Positive controls were the addition to the sensor strain of 1 nM, 10 nM and 100 nM of commercial 3OC6 HSL.



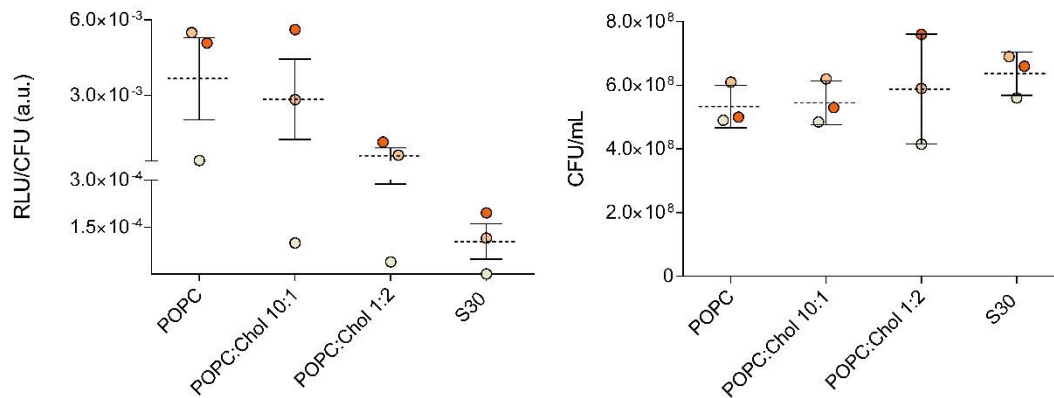
Supplementary Figure 4. Preliminary experiment for two-way chemical communication between artificial and *V. fischeri* cells. Artificial cells expressing LuxR* and LuxI* were the only capable of inducing a detectable luminescence signal per *V. fischeri* colony forming unit (left). Right: Colony forming units per mL (CFU/mL) RLU (Relative Luminescence Unit).



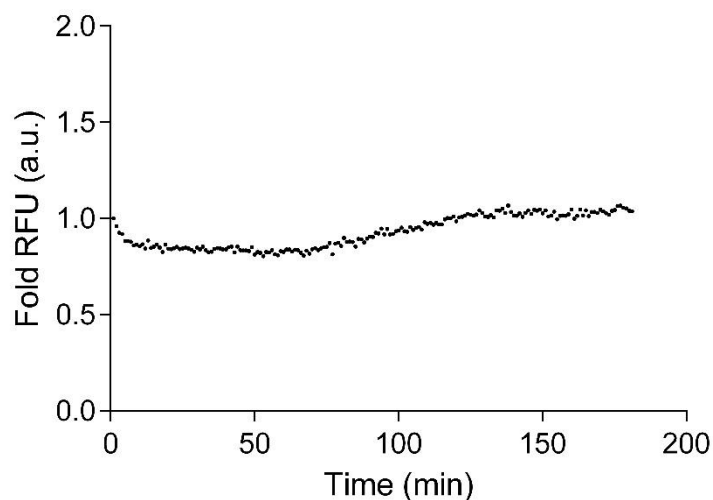
Supplementary Figure 5. Artificial cells stability in the presence of *Vibrio fischeri*. Left: schematic of the calcein leakage experiment. 80mM Calcein, the genetic construct encoding *luxR** and *luxI** mutant and a transcription-translation machinery provided by a commercial *E. coli* extract were encapsulated inside 1:2 POPC:cholesterol liposomes. Artificial cells were incubated with *V. fischeri* for 3h at 30 °C. At this concentration, calcein fluorescence is low due to self-quenching. Upon liposome breakage, calcein is released thus giving rise to increased fluorescence. Right: graph showing the fold increase of calcein fluorescence over time. (*) indicates the addition of 0.3% Triton (v/v) to break the liposomes.



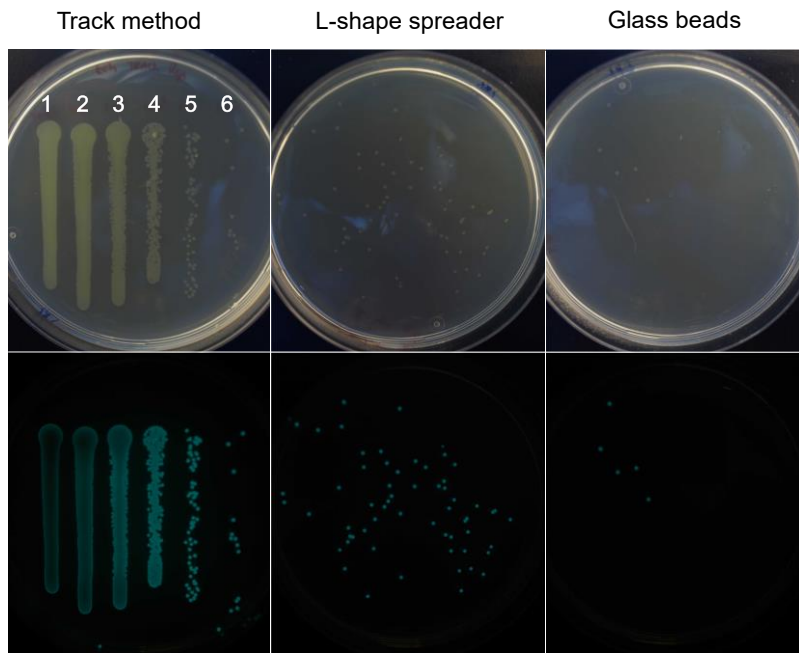
Supplementary Figure 6. Artificial cells failed at sensing 3OC12 HSL. Artificial cells constitutively expressing the transcriptional activator LasR did not activate firefly luciferase expression in response to 10 μ M of commercial 3OC12 HSL after 4 h incubation at 37 °C. Error bars correspond to the standard deviation. $n=3$ independent experiments.



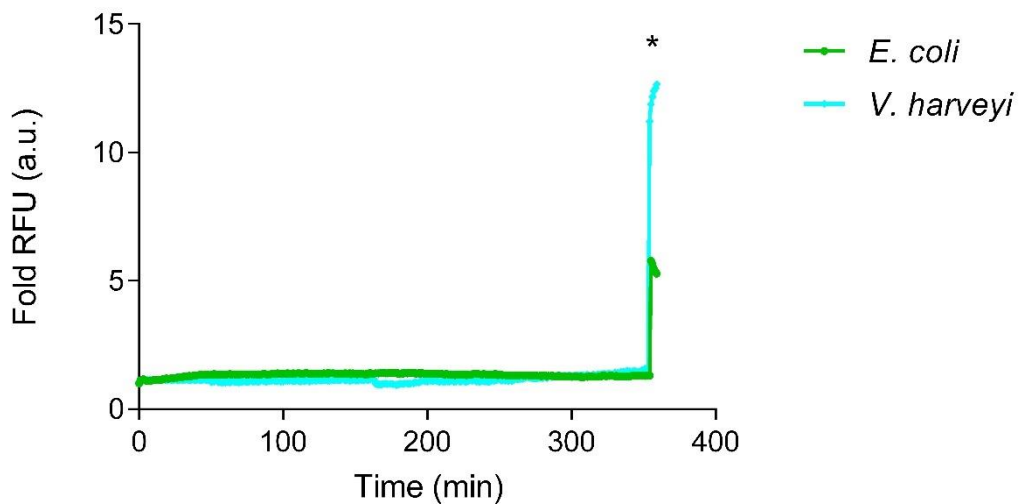
Supplementary Figure 7. Influence of the artificial cell membrane composition on chemical communication with *V. fischeri*. Left: Artificial cells with different membrane composition (POPC only, 10:1 or 1:2 POPC:cholesterol molar ratios) expressing DNA encoding *luxR** and *luxI** were tested for communication with *V. fischeri*. The luminescent response per single cell of *V. fischeri* after 3 h of incubation showed a clear dependence on the concentration of cholesterol. Right: The number of viable *V. fischeri* cells per sample was determined by counting the colony forming units. The negative control was an unencapsulated S30 reaction containing the same DNA and necessary components for transcription-translation. RLU/CFU (Relative Luminescence Units/Colony Forming Units per milliliter), CFU/mL (Colony Forming Units per milliliter). Solid lines indicate the mean. Error bars indicate the standard error of the mean (SEM). $n=3$ independent experiments (data values obtained from each experiment are labelled with a different color).



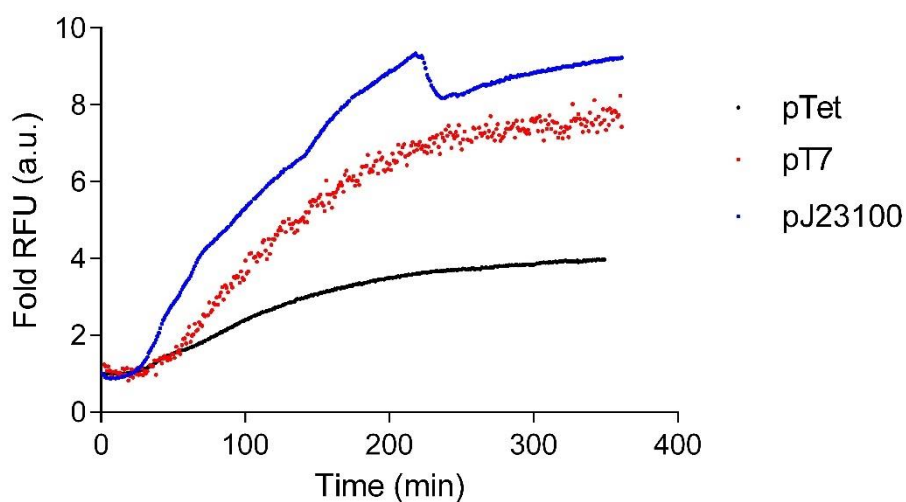
Supplementary Figure 8. Control experiment to assess the activity of non-encapsulated transcription and translation reactions. A TX/ TL reaction was assembled with the 3OC6 HSL sensor construct BBa_T9002. As for encapsulated reactions in artificial cells, proteinase K and RNaseA/T1 were added and the reaction was diluted 1:1 (volume ratio) with a *V. fischeri* culture at $OD_{600\text{ nm}}=0.3$. No GFP expression was detected over 3h of incubation at 30 °C indicating that proteinaseK, RNases and the dilution factor were inhibiting any potential activity of non-encapsulated transcription translation reactions. RFU (Relative Fluorescence Unit), a.u. (arbitrary unit).



Supplementary Figure 9. Comparison of different plating methods for enumerating CFU of *Vibrio fischeri* cells. Bacteria were grown at 30 °C, 145 rpm until $OD_{600\text{ nm}} = 0.3$ in 5mL of LBS starting from a 200 μ L glycerol stock aliquot. Before plating, cells were 10-fold serially diluted and 10 μ L of the non-diluted culture (line 1) or the serial dilutions, 10^{-1} (line 2), 10^{-2} (line 3), 10^{-3} (line 4), 10^{-4} (line 5), 10^{-5} (line 6) were plated in LBS agar plates with the track dilution method (45). 10 μ L of the 10^{-4} dilution were combined with 90 μ L of water and were also plated with an L-shape spreader or with glass beads. Top pictures (day light) bottom pictures (luminescence). The glass bead method was discarded because of the consistent and substantial loss of cells during each spreading. The track method offered instead an easy way to plate and count cell colonies from different samples and different dilutions in the same plate.



Supplementary Figure 10. Stability of artificial cells in contact with *E. coli* sensor strain and *V. harveyi* BB170 determined by a calcein leakage assay. The low and constant values of calcein fluorescence measured over 6h of incubation with bacteria indicated that artificial cells were stable. (*) indicates the addition of 0.3% (v/v) Triton X-100. RFU (Relative Fluorescence Units); a.u. (arbitrary units).



Supplementary Figure 11. Promoter sequences determine different GFPmut3b expression levels. Three genetic constructs coding for *luxR* transcriptional activator under three different promoter sequences were tested for activity in the presence of $10 \mu\text{M}$ of commercial 3OC6 HSL (Supplementary Table 3). Shown is the fluorescence fold increase respect to time 0 min normalized against fluorescence values from the same reactions without quorum molecules. GFPmut3b expression was monitor by fluorescence spectroscopy. DNA coding for pT7 promoter used the *E. coli* T7 high yield commercial cell extract (Promega), while for DNA coding for the *E. coli* endogenous promoters (pTet and pJ23100) used the *E. coli* extract for circular DNA template (Promega.) $n=1$ representative experiment.

SUPPLEMENTARY TABLES

Plasmid name	Vector	Insert	Function
BBa_T9002	pSB1A3	pTet- <i>luxR</i> - plux-GFPmut3b	C6 sensing
RL086A	pSB1A3	pTet-(T33A,S116,M135I) <i>luxR</i> - plux-GFPmut3b	C6/C8 sensing
RL087A	pSB1A3	pTet-(T33A,R65M,S116,M135I) <i>luxR</i> - plux-GFPmut3b	C8 sensing

Supplementary Table 1: list of genetic constructs used for the sensing of *V. fischeri* quorum molecules in *in vitro* transcription-translation reactions. BBa_T9002 was extracted from the registry of biological standard parts.

Plasmid name	Vector	Insert	Function
RL092A	pSB1A3	pTet- <i>lasR</i> -plux-fireflyluciferase	3OC12 HSL sensing

Supplementary table 2. Genetic construct used to check 3OC12 HSL sensing activity inside artificial cells.

Plasmid name	Vector	Insert	Function
BBa_T9002	pSB1A3	pTet- <i>luxR</i> - plux-GFPmut3b	C6 sensing
NY006A	pSB1A3	pT7- <i>luxR</i> - plux-GFPmut3b	C6 sensing
NY007A	pSB1A3	pJ23100- <i>luxR</i> - plux-GFPmut3b	C8 sensing

Supplementary Table 3: list of genetic constructs tested for 3OC6 HSL sensing activity.

MATERIAL AND METHODS

Bacterial strains and media

Allivibrio fischeri MJ11 (46) was grown in LBS (10 g/L tryptone, 5 g/L yeast extract, 20 g/L NaCl, 50mM Tris-HCl, 0.3% glycerol) in absence of antibiotics. *E. coli* NEB express and *Pseudomonas aeruginosa* PT5 PAO1 (47) were grown in LB (10 g/L tryptone, 10 g/L NaCl and 5 g/L yeast extract). Cultures from *E. coli* NEB express cells transformed with plasmids BBa_T9002 or BBa_K575024 were supplemented with either 100 µg/mL ampicillin or 50 µg/mL chloramphenicol respectively. *P. aeruginosa* PT5 PAO1 was grown in absence of antibiotics. *V. harveyi* BB170 was grown in Autoinducer Bioassay (AB) media (17.5 g/L NaCl, 12.3 g/L MgSO₄•7H₂O, 2 g/L casamino acids, 10 mM potassium phosphate pH 7, 1 mM L-arginine, 1% (v/v) glycerol) with 50 µg/mL kanamycin.

Colony forming unit assay

To enumerate viable *V. fischeri*, cells were plated in LBS agar plates (without antibiotics) with the Track dilution method (45). Briefly, 5 µL of each sample containing *V. fischeri* were 100-fold diluted in LBS for two consecutive times. The 10⁻⁴-fold dilutions were diluted 10-fold. 10 µL of the serial dilutions 10⁻⁵ were spotted at the top side of the plates. To distribute cells over the surface of the agar plates, plates were left tilted until the spotted droplet reached the bottom of the plates. After 5 min drying, plates were incubated at 30 °C overnight. Luminescent bacteria colonies were photographed in a dark room with an Olympus OM-D EM5 camera coupled with a M-Zuiko ED 12-50 mm 1:3.5-6.3 EZ objective lens using an exposure of 40 s at F 5 and an ISO of 200. The number of luminescent colonies or colony forming units (CFU) were counted manually from one plating per sample per experiment. To avoid unbiased counting, colonies were counted without previously knowing from which sample they were coming from.

Preparation of liposomes

Starting from 1-Palmitoyl-2-oleoyl-sn-glycero-3-phosphocholine (POPC) and cholesterol stocks solutions dissolved in chloroform to 100 and 40 mg/mL respectively, the required volume from each solution was calculated according to the molar ratio between the two components, then mixed and transferred into a 5mL round flask. The solvent was evaporated for about 30min at room temperature using a rotary evaporator (Buchi). The thin lipid films created at the bottom of the flask were resuspended in distilled water to a final concentration of 24 mM with different POPC and cholesterol molar ratios. The suspended liposomes were homogenized for 1min with T10 basic ULTRA-TURRAX disperser set at power 4. The solution was split into 100 μ L aliquots in 2 mL Eppendorf tubes, flash-frozen in liquid nitrogen and dehydrated overnight at 37 °C with a benchtop vacuum concentrator (Labconco). Aliquots were stored at -20 °C. Thin lipid films were hydrated with in vitro transcription translation reactions containing DNA by vortexing for 30 s. Suspended liposomes solutions were used directly for the experiments without further purification. Note that all experiments involving artificial cells in chapter 1 were performed with 1:2 POPC cholesterol liposomes apart from the experiment in Supplementary Figure 7 where POPC and 10:1 POPC cholesterol liposomes were also used.

In vitro transcription-translation reactions

Genetic constructs designed and cloned to reconstitute *P. aeruginosa* and *V. fischeri* quorum pathways parts used either a cell-free *E. coli* S30 extract for circular DNA (Promega) (20 μ L premix, 15 μ L S30 extract, 5 μ L amino acids mix, 40 U of RNase inhibitor, and 2 μ g of DNA) or *E. coli* S30 T7 High Yield Protein Expression System (Promega) (20 μ L S30 premix, 18 μ L T7 S30 extract, 40 U of RNase inhibitor, and 1 μ g of DNA). 10 μ M of 3OC12 HSL, C8 HSL or 3OC6 HSL (Sigma Aldrich or Cayman Chemical) were used to activate gene expression. In vitro reactions were monitored for 6 h at 37 °C. Reactions that were assembled for sensing 3OC12 HSL with NY008A, were shaken for 50 s (1 mm orbital amplitude) prior to fluorescence acquisition every min) in 384 microwell plates (781076 Greiner Bio One) during incubation in an Infinite

m200 plate reader (Tecan). Fluorescence from in vitro reactions assembled for the sensing of 3OC12 HSL using NY001A, were acquired at the Rotor-gene Q 6plex (Quiagen) with green channel (excitation: 470 ± 10 nm; emission: 510 ± 5 nm). Negative controls were the same reactions in the absence of quorum molecules. Fluorescence from in vitro reactions assembled with genetic constructs coding for *luxR* mutants was measured with a CFX96 Touch Real-Time PCR Detection System (Bio-Rad) with the FAM channel (excitation: 450-490 nm; emission: 510-530 nm). For the rest, fluorescence was measured with a Photon Technology International (PTI) QuantaMaster 40 UV-vis spectrofluorometer, for GFPmut3b (excitation: 501 nm; emission: 511 nm) for sfGFP (excitation: 485nm; emission: 510 nm).

Artificial sensing cells

1:2 POPC: cholesterol thin lipid film aliquots were hydrated with 50 μ L of S30 *E. coli* extract containing 20 μ L S30 premix, 15 μ L S30 extract, 5 μ L amino acids mixture, 40 U of RNase inhibitor, and 4 μ g of DNA RL082A, RL093A or RL094A (Table 1). For sensing of natural quorum molecules, *V. fischeri*, bacteria were grown from 200 μ L glycerol stock aliquot at (30 °C, 145 rpm) in 5 mL of LBS until $OD_{600\text{ nm}} = 1.8$. Bacteria were then harvested, and the supernatant was filtered through a 220 nm pore membrane (Sartorius). 100 μ L of supernatant was mixed with 50 μ L of artificial cells. 0.7 mg/mL proteinase K, 0.07 mg/mL RNase A, and 170 U/mL RNase T1 (Thermo Fisher Scientific) were supplemented to avoid any residual activity outside the liposomes. As a negative control LBS was used in place of the *V. fischeri* supernatant. Instead, for sensing commercial quorum molecules, 10 μ M of 3OC12 HSL (Sigma Aldrich) was added to the suspension of artificial cells carrying DNA RL092A. Samples were incubated at 30 °C with the supernatant of *V. fischeri* or at 37 °C with commercial 3OC12 HSL for 4 h, then artificial cells were collected and loaded into 96 well plates (Thermo Fischer Scientific, 216305). 0.3% (v/v) Triton X-100 was added to disrupt the artificial cells, and 150 μ L of the luciferase assay reagent (Promega) containing luciferin was added to the samples. Luminescence was recorded immediately with a plate reader (Tecan). Firefly luciferase catalyzes the oxidation of luciferin using $ATP \bullet Mg^{2+}$ as co-substrate and forming oxyluciferin as product. In the process light is emitted.

Artificial sender cells

1:2 POPC:cholesterol thin lipid films were hydrated with 50 μ L of S30 T7 High-Yield Protein Expression System supplemented with 2 μ g of DNA encoding the corresponding synthase behind a T7 promoter (constructs MC002A, NY018A, NY019A Table 2). 1 mM S-adenosyl-L-methionine and 700 μ M acetyl coenzyme A were added for the synthesis of acyl homoserine lactones. Artificial sender cells were diluted 1:1 (v/v) with *V. fischeri* MJ11 at OD_{600 nm} = 0.2-0.3 and 0.7 mg/mL Proteinase K, 0.07 mg/mL RNase A, and 170 U/mL RNase T1 (Thermo Fisher Scientific) were also added to avoid any residual activity of the S30 reactions outside the artificial cells. Samples were incubated at 30 °C in 96-well plates (Thermo Fischer Scientific, 216305) without shaking. Every hour luminescence was measured with an Infinite M200 plate reader (Tecan). After 3 h of incubation, 5 μ L of each sample were serially diluted and 10 μ L of the 10⁻⁵-fold dilution were plated on LBS agar following the “track dilution” method to enumerate the colony forming units (CFU) with one plating per sample per experiment. Pictures from luminescent bacteria colonies were captured in a dark room with an Olympus OM-D EM5 camera and a M-Zuiko ED 7 12-50 mm 1:3.5-6.3 EZ lens using an exposure of 40 s at F 5 and an ISO of 200. Negative controls were liposomes encapsulating the S30 extract without DNA or liposomes encapsulating only LBS. Positive control was the addition of 100 nM 3OC6 HSL. *V. fischeri* non-diluted and 1:1 (v/v) diluted cultures were also tested.

Cellular Imitation game

1:2 POPC:cholesterol thin lipid films were hydrated with 50 μ L S30 *E. coli* extract for circular DNA template (Promega) supplemented with 4 μ g of DNA, 700 μ M acetyl coenzyme A and 1 mM S-adenosyl-L-methionine. 200 μ L of a 20% glycerol stock of *V. fischeri* MJ11 were grown in 5 mL of LBS (30 °C, 145 rpm) until OD_{600 nm} = 0.2-0.3. Cells were undiluted (*Vibrio fischeri*-*Vibrio fischeri* sample) or mixed in a 1:1 volume ratio with either functional artificial cells encapsulating DNA plasmids RL078A, NY009A, NY013A, or NY014A (Table 3) coding for the multiple versions of *luxI* and *luxR* or nonfunctional artificial cells containing RL081A (Table 3) coding for *luxR* and T7 RNA polymerase. 0.7 mg/mL Proteinase K, 0.07 mg/mL RNase A, and 170 U/mL

RNase T1 (Thermo Fisher Scientific) were added to the extravesicular solution to avoid any unwanted activity of the S30 *E. coli* extract outside of the artificial cells. Samples were placed in 96-well plates (Thermo Fischer Scientific, 216305) with at least 2 wells of interspace separation between each sample. Plates were incubated at 30 °C without shaking. Luminescence was acquired with an Infinite M200 plate reader (Tecan) every hour with the following settings (prior each luminescence acquisition, the plates were shaken for 5 s with 3 mm orbital shaking, attenuation= OD1; integration time= 500 ms). At 3 h of incubation, 5 µL of each sample were serially diluted and 10 µL of the 10⁻⁵-fold dilution were plated on LBS agar plates without antibiotics with the “track dilution” method (45). The rest of the samples were collected for RNA extraction. Plates were incubated overnight at 30 °C. Total RNA isolation was performed with the GeneJET RNA Purification Kit (Thermo Fischer Scientific), and 500 ng of RNA was retro transcribed with the RevertAid Reverse Transcriptase kit (Thermo Fischer Scientific). 5 ng of cDNA was mixed with the iQ SYBR Green supermix (Bio-Rad) and supplemented with the appropriate primers. 10 µL reactions were loaded in 96-well plates (HSP9655 Bio-Rad), and the cDNA was quantified with a CFX96 Touch real-time PCR (Bio-Rad) with SYBR green detection. The real-time PCR run protocol was one initial cycle of denaturation at 95 °C for 3 min followed by 40 cycles of denaturation (95 °C, 10 s) and annealing + extension (60 °C, 30 s) followed by one melt curve cycle (55-95 °C with 0.5 °C, 40 s). Primers used to quantify the cDNA of luxA and luxB were luxA FW: 5'-cagagtttggtcttacgggaaat-3', luxA REV: 5'- ggggtgtgctgtcggaataac-3', luxB FW: 5'-attaccacccatcacctgt-3', luxB REV: 5'- gtcactaaaaccaagaatgaagcg-3'. The concentration of luxA primer was 150 nM and for luxB primers was 250 nM. Gene expression of both genes was normalized to the expression of the malate dehydrogenase (mdh) housekeeping gene that was amplified with the following primers mdh FW: 5'-cactctggtgttactatcttacctct-3' and mdh REV: 5'-actctgttcccgcattttg-3' at 300 nM. Primers were designed with Primer3 software.

RNAseq analysis

Total RNA was treated with DNase (RapidOut DNA Removal kit, ThermoFisher) prior to RNA quantification with a spectrofluorometric detection method using the Quant-iT™ RiboGreen™ RNA assay kit (Life-Technologies). Library preparation and sequencing were performed at Edinburgh Genomics (Ashworth laboratories,

University of Edinburgh). Briefly, libraries were prepared using the TruSeq stranded total RNA-seq kit (Illumina) and the depletion of ribosomal RNAs was accomplished with the RiboZero rRNA removal kit for Gram negative bacteria (Illumina). Libraries were then sequenced on one lane of an Illumina HiSeq2500 in high output mode with v4 chemistry to a length of 125 base paired end. The quality of the raw sequence data was assessed with FastQC (48). The average number of reads were 10,397,486, 11,006,173, and 11,077,471 for samples containing functional artificial cells, nonfunctional artificial cells, and no artificial cells, respectively. Reads in FASTQ format were mapped to the *V. fischeri* MJ11 genome reference sequence using bowtie (49). Transcripts were assembled with cufflink and cuffmerge and the quantification of isoforms was with cuffdiff (50–52). The sample size for the RNA-seq experiments was chosen based on the average number of reads per sample (10M), read length (200 bp), preliminary results, and prior reports (53) showing an effect size of at least two for lux operon gene expression from activation by quorum sensing. Therefore, to ensure a statistical power of at least 0.8 at a significance level of 0.05 for a standard two-tailed t-test, the sample size was set to six. Differences in the mean between groups were assessed using an unpaired two-tailed standard t-test. Standard errors of the mean are shown in the bar plots as a measure of variability. RNA-seq differentially expressed genes were determined by cufflinks/cuffdiff after p value adjustment for multiple comparisons using FDR (False Discovery Rate).

Quenching *P. aeruginosa*

Dehydrated aliquots of 1:2 POPC:cholesterol vesicles were hydrated with 50 μ L of S30 *E. coli* extract supplemented with 4 μ g of DNA NY017A (Table 8). An aliquot of a *V. fischeri* culture at $OD_{600\text{ nm}} = 0.2-0.3$ was added to the suspension of artificial cells. An aliquot of LB was added instead to another batch of artificial cells as negative control for the production of AiiA. Samples were incubated at 37 °C for 4 h. *P. aeruginosa* was grown from 200 μ L of a glycerol stock in LB until $OD_{600\text{ nm}} = 0.3$ and added to artificial cells in a 1:1 (v/v) ratio. After 2 h of incubation (37 °C 220 rpm) cells were harvested and the supernatants mixed 1:20 with the 3OC12 HSL *E. coli* sensor strain carrying the BBa_K575024 plasmid. Samples were incubated at 37 °C for 2h. 2 μ L were then collected from each sample, 10⁻²-fold diluted in PBS, and monitored by flow cytometry with a FACSCanto A (BD Biosciences) samples were analyzed with BD

FACSDiva software. Parameters used were: Forward Scatter (FSC) signal (excitation: 488 nm, Type: Area, Voltage: 525); Side Scatter (SSC) signal (excitation: 488 nm, emission: 488 +/- 10 nm, Type: Area, Width, Voltage: 403); Green channel (FITC) signal (excitation: 488 nm, emission: 530 +/- 30 nm, Type: Area, Voltage: 600); Threshold parameters (FCS: 200, SSC: 200, threshold operator: And). 10000 events were acquired per sample. The population distribution was analyzed and plotted with FlowJo software. Positive controls were the addition of 100 nM commercial 3OC12 HSL or the supernatant of a culture of *P. aeruginosa* at OD_{600 nm} = 0.3 to the *E. coli* reporter strain. Negative controls included the reporter strain without the addition of quorum molecule or with the addition of the supernatant of a *V. fischeri* culture at OD_{600 nm} = 0.2-0.3.

Biofilm disruption

Dehydrated aliquots of 1:2 POPC:cholesterol vesicles were hydrated with 50 µL of S30 *E. coli* extract for circular DNA template (Promega) supplemented with 2 µg of DNA NY017A or RL089C (Table 9). 10 µM commercial 3OC6 HSL was added to the suspension of artificial cells carrying NY017A. Artificial cells were incubated for 6 h at 37 °C to allow the production of AiiA. To assess whether artificial cells could disrupt or inhibit the biofilm formation of *P. aeruginosa* a biofilm assay was conducted following O'Toole 's indications (44). *P. aeruginosa* were grown from a 200 µL glycerol aliquot stock in 10 mL of LB at 37 °C, 220 rpm overnight. Cells were diluted 1:100 and 50 µL were loaded in 96-well "U" shape flexible plates (Thermo). Bacteria were mixed in a 1:1 volume ratio with artificial cells expressing aiiA constitutively or in response to 3OC6 HSL. Negative controls were bacteria incubated with liposomes encapsulating LB, or artificial cell containing the cell extract without DNA. As control for biofilm formation one sample consisted of *P. aeruginosa* diluted with LB. Samples were incubated for 5 h at 37 °C without shaking. After the incubation, non-adherent cells were removed by turning upside down the plate. Adherent cells were carefully washed three times by submerging the plate in a water container. Finally, the adherent cells forming the biofilm in the surface of the wells were stained with 0.1% crystal violet aqueous solution.

Vesicle stability

To test whether bacteria could break phospholipid vesicles, a dye leakage assay (54) was performed. Dehydrated aliquots of 1:2 POPC:cholesterol vesicles were hydrated with 60 μ L S30 *E. coli* extract for circular DNA template (Promega) supplemented with 4 μ g of DNA RL081A (Table 3), 1 mM S-adenosyl methionine, 700 μ M acetyl coenzyme A, and 80 mM calcein (Sigma). Liposomes were then extruded 11 times through a 19 mm polycarbonate membrane with 1 μ m pores (Whatman) with an Avanti mini-extruder and purified by gel filtration with a sepharose 4B (Sigma-Aldrich) column. Eluent fractions were collected with a FC 203B fraction collector (Gilson) into flat bottom transparent 96-well plates (Eppendorf). Fractions with suspended liposomes were mixed in a 1:1 (v/v) ratio with a culture of *V. fischeri* grown in LBS at $OD_{600\text{ nm}} = 0.25$ or a culture of *P. aeruginosa* grown in LB at $OD_{600\text{ nm}} = 0.3$. Fluorescence was acquired every minute for 3 h and monitored with a Photon Technology International (PTI) QuantaMaster 40 UV-vis spectrofluorometer with excitation and emission at 495 nm and 515 nm, respectively. Subsequently, 0.3% (v/v) Triton X-100 was added as a control to break the vesicles. The same assay was also performed to test the stability of artificial cells in presence of *E. coli* NEB express sensor strain and *V. harveyi* BB170 (Supplementary Figure 10) that were used in Figure 2C and Figure 3A of the article entitled “Two-way chemical communication between artificial and natural cells”.

The effect of cholesterol on chemical communication

Thin lipid films of POPC containing either 0 mol%, 10 mol%, or 66 mol% cholesterol were hydrated with 50 μ L S30 *E. coli* extract for circular DNA template (Promega) supplemented with 4 μ g of DNA NY013A (Table 3), 700 μ M acetyl coenzyme A and 1 mM S-adenosyl-L-methionine. The experiments were conducted as described in the cellular imitation game section. This test was performed to check the permeability of 3-oxo-hexanoyl homoserine lactone through the membranes of artificial cells.

SUMMARY

Artificial cells expressing wild type or mutant versions of the *luxR* transcriptional activator were shown to sense the quorum sensing molecules produced by *Vibrio fischeri*. Subsequently, artificial cells expressing different versions of *luxI* synthase were also able to produce 3OC6 HSL and induced the expression of the lux genes of the same bacterial cells. Activity was assessed by fluorescence, luminescence and RT-qPCR. Then, artificial cells capable of two-way chemical communication with *Vibrio fischeri* were constructed and tested by a type of cellular imitation test. The extent to which artificial cells could communicate with natural cells, in other words the extent of mimicry, was initially determined by luminescence and RT-qPCR and subsequently evaluated and quantified by RNA-seq analysis. The transcriptome analysis of *V. fischeri* in the presence of functional artificial cells capable of sensing and in response synthesizing and releasing 3OC6 HSL revealed a higher degree of likeness to natural *V. fischeri* than the nonfunctional artificial cells that could only sense 3OC6 HSL. The degree of likeness was quantified according to the difference in the number of differently expressed genes induced by functional and nonfunctional artificial cells with respect to *Vibrio fischeri*. Artificial cells were also constructed that could sense 3OC6 HSL and in response produce a lactonase that disrupted the homoserine lactone QS pathways of *P. aeruginosa*. Finally, preliminary results indicate that artificial cells could be built to disrupt the biofilm formation of pathogenic bacteria.

DISCUSSION AND FUTURE PERSPECTIVES

Considerations on the artificial lipid membrane composition

The lipid composition used for the experiments described above were for historical reasons, i.e. the lipid composition was the best for the activity of artificial cells that depended upon the function of α -hemolysin (29). However, this lipid composition was likely not optimal for quorum signaling with *V. fischeri*. Artificial cells with different membrane compositions (POPC only, 10:1 or 1:2 POPC: cholesterol molar ratios) containing DNA encoding *luxR** and *luxI** and the transcription and translation machinery from a commercial *E. coli* extract were incubated and tested for activity with *V. fischeri* for 3 h at 30 °C. The maximum luminescence response per cell was observed for samples containing liposomes composed of POPC, while bacteria in the presence of liposomes with high cholesterol content showed considerably lower luminescence (Supplementary Figure 15). This effect is consistent with the fact that cholesterol molecules are known to decrease the permeability of phospholipid membranes by increasing the rigidity and the order of the membrane. The rigidity is achieved through hydrophobic interactions between the steroid ring of cholesterol and the fatty acyl chain of the phospholipids. This effect might also explain why *V. fischeri* cells in contact with liposomes encapsulating LBS or the non-template DNA were consistently less luminescent. However, in our case functional artificial cells with 1:2 POPC:cholesterol counteracted the permeability effect by synthesizing 3OC6 HSL. The negative control for this experiment was an unencapsulated S30 reaction containing the same DNA and necessary components for transcription-translation. Such a negative control was chosen to demonstrate that the unencapsulated in vitro reactions that were not discarded neither by dialysis nor gel-filtration after liposome preparation were not capable of engaging in chemical communication with *V. fischeri*.

Considerations on the RNA-seq data interpretation

To avoid confusion or misinterpretation, it should be first emphasized that the functional artificial cells presented in this work are not alive. The cellular version of the imitation game implemented here did not intend to give a definition of life but instead demonstrated an objective way to quantify cellular mimics. It should be clarified in this regard, that the 39% value was calculated with respect to nonfunctional artificial cells that was assumed to be 0% *V.fischeri*-like. In our case, the nonfunctional artificial cells were carrying DNA encoding *luxR** and T7 polymerase but another negative control sample could have been chosen. For instance, liposomes encapsulating LBS only, or artificial cells carrying the same genetic construct as functional artificial cells but lacking an essential component of the transcription or translation machinery. In any of those cases, each comparison with respect to our functional artificial cells would have likely given a different number of genes that were differently expressed and therefore would have given another value for the estimation for *V. fischeri* likeness. Therefore, it is important to interpret the data in the context of the specific controls used in the experiment. 39% did not indicate that functional artificial cells were 39% identical to *V. fischeri*, but instead indicated in a relative way that functional AC were more *V. fischeri* like than the nonfunctional artificial cells. Moreover, if another arbitrary system would have randomly induced the same number of differently expressed genes as the functional artificial cells, the arbitrary system would have been considered as *V. fischeri*-like as functional artificial cells. This might be considered as subjective evaluation of likeness. However, we have to contextualize the data in the frame of an imitation game where functional artificial cells are intended to mimic *V. fischeri* while nonfunctional artificial cells are not and where *V. fischeri* is conceptually interrogating itself, functional artificial cells and nonfunctional artificial cells. In our method, the self-comparison sample (*V. fischeri* interrogating itself) is the key and a more objective reference to compare with. The importance of this work lies in the fact that the natural cell is directly evaluating the performance of both artificial systems with respect to itself by differently expressing different number of genes. The number of differently expressed genes induced by functional or nonfunctional artificial cells were 107 and 175 respectively. This data indicated that functional artificial cells that were specifically intended to mimic quorum sensing communication were considered more similar to

bacteria because the induced number of differently expressed genes was lower. This method is then a more direct and objective way of assessing cell-likeness because these numbers resulted from the direct comparison respect to the target natural cell to be mimicked.

Consideration on the cellular imitation game

In the original imitation game or Turing test, one human is intended to interrogate one computer and both human and computer are supposed to be physically separated to avoid any direct recognition. In the type of cellular imitation game that we have implemented, a culture of *V. fischeri* was in direct contact with many artificial cells. In the latter case, the observed effect was the result of the average chemical communication that took place in each sample. To test the individual activity of artificial cells, artificial cells made by hydrodynamic flow focusing (55) could be mixed with natural cells within a microfluidic device. With the current technology it is possible to build microfluidic chips with the design and geometry of interest. Two parallel arrays of micro-chambers connected by a semipermeable membrane would be ideal for chemical communication. With hydrodynamic cell isolation array techniques (56), it would also be possible to trap in each micro-chamber, either one artificial or one natural cell. Before natural cells start dividing, cells should be collected, their RNA extracted and subjected for analysis to bacterial single cell RNA-seq (57). Using these technologies, it would be also possible to assess the variability in response among natural cells since it is well known that bacteria are rarely 100 % identical. Improved versions of functional cells with a compartment that better mimics the compartment of natural cells could help in gaining a better understanding of other types of communications since communication might not only involve the sensing and release of chemical signaling molecules. Physical recognition by direct contact might also play a role in the way natural cells communicate. In the future other potential imitation games could be implemented. For example, artificial cells that mimic the light organ environment of the squid or the fish with which *V. fischeri* are typically found in symbiosis. Or conversely, artificial cells capable of colonizing. A similar method as proposed in this chapter to measure progress can be used for those case since transcriptome analysis of *V. fischeri* over the different stages of the colonization of the light organ have been conducted and reported in literature (58). Other types of

imitation games that test for other properties of living cells will only be possible to implement in the future if we will find the way to observe and quantify the natural cell assessment of the artificial system.

Improving artificial cells for chemical communication with *V. fischeri*

Several aspects can be taken into consideration to improve artificial cells capable of chemically communicating with *V. fischeri*. If liposomes can be made that better mimic the *V. fischeri* cell wall and membrane composition, first, the robustness and stability of the artificial cells would improve, second, the diffusion of homoserine lactones across the artificial cell membranes would take place in a more similar and reliable way and third, other types of communication relying on physical interactions could take place. To better mimic the production levels of homoserine lactones in the presence of bacteria, genetic constructs can be fine-tuned to produce similar levels. In this regard, simply by changing the promoter sequence of the genetic construct responsive to 3OC6 HSL was enough to activate the expression of the fluorescent reporter gene at different levels. (Supplementary Figure 11 and Supplementary Table 3). Artificial cells carrying more complex genetic circuits including for example the whole *lux* operon or even the complete quorum sensing pathway would allow for a more complete and natural response in the presence of homoserine lactones. Moreover, artificial cells with the ability to replicate their genetic content and divide would be able to engage in chemical communication for longer periods of time but the risk exists that such artificial cells could evolve and lose their functionality.

Here we have proposed an objective method to quantify the life-likeness of artificial cells respect to a target natural cell by analyzing the response of the natural cell in the presence of the artificial cell. The artificial cells presented in this chapter were not perfect and leave much room for improvement but we hope to have built the foundations that will pave the way to guide the construction of artificial cells that will better display the features and properties of living cells.

Chapter 2: Cellular mimics inside non-equilibrium, open thermophoretic chambers.

INTRODUCTION

Cell membranes

Extant living cells, from a simplistic point of view, can be described as compartments containing a crowded mixture of DNA, RNA and protein. DNA contains the genetic information that codes for proteins through the intermediary messenger RNA. Proteins, in turn, catalyze cellular metabolic reactions, including the synthesis of RNA and proteins, that allows the cell to adapt to the environment, persist over time, and grow and divide. Importantly, the content of the cell is separated from the environment and is confined to a defined space by a lipid membrane. Compartmentalization allows, for example, for cellular evolution to take place by maintaining a link between the genotype (DNA) and the phenotype (the activity of the cell mediated by encoded proteins and RNAs). Confinement within compartments also facilitates interactions among the components of the cell and provides a spatial organization that favors flux down specific pathways. Moreover, cell membranes contain a large percentage of proteins that are responsible, in part, for converting metabolic activity into concentration gradients that are then used to fuel the cell. For example, the lipid compartment controls the passive and active transport of ions and molecular feedstocks leading to the generation of electrochemical gradients that can be used to drive the synthesis of ATP. In other words, lipid membranes are essential to keeping cells alive, i.e. in a state of thermodynamic disequilibrium. Although concentration gradients across lipid membranes is how life as we know it operates, in theory, it should be possible to generate similar disequilibrium states in the absence of a physical membrane.

Thermophoresis

Thermophoresis, sometimes referred to as thermal diffusion or the Soret effect, is a physical phenomenon that can be described as the directed movement of particles induced by a temperature gradient. The thermophoretic velocity “ v ” of particles in a fluid, $v = -S_T D \nabla T$, is directly proportional to the thermal gradient “ ∇T ,” the diffusion coefficient “ D ” and the Soret coefficient “ S_T ” (59). The Soret coefficient, in turns,

depends on the surface charge, the hydration shell, and the size of the molecule (60, 61). Molecules with a positive Soret coefficient that are dissolved in aqueous solution and are located within a chamber are driven by thermophoresis from the hot to the cold region of a thermal gradient. Additionally, temperature differences generate thermal convective flows resulting from density changes. Within the hot region, the liquid expands and moves upwards while in the cold region the liquid contracts and moves downwards. Combined, both phenomena result in an accumulation of molecules at the bottom, colder side of the chamber until a steady state of thermodiffusion and counteracting Brownian diffusion is reached (Figure 1). This accumulation of molecules is also known as thermal trapping. In the past decade, thermophoresis coupled with convective fluid flow was used to amplify DNA by PCR and to selectively accumulate oligonucleotides (62). Similarly, molecules of fatty acids were accumulated and self-assembled into vesicles within a chamber with an applied thermal gradient (63), and the partitioning of charged molecules was shown to generate a pH gradient (64). Thermophoresis alone has even been developed as a commercial technology to measure binding affinities between biomolecules (65). However, all of these examples exploited relatively simple mixtures of molecules. What is unclear is whether vastly different molecules can be accumulated together into a functioning system.

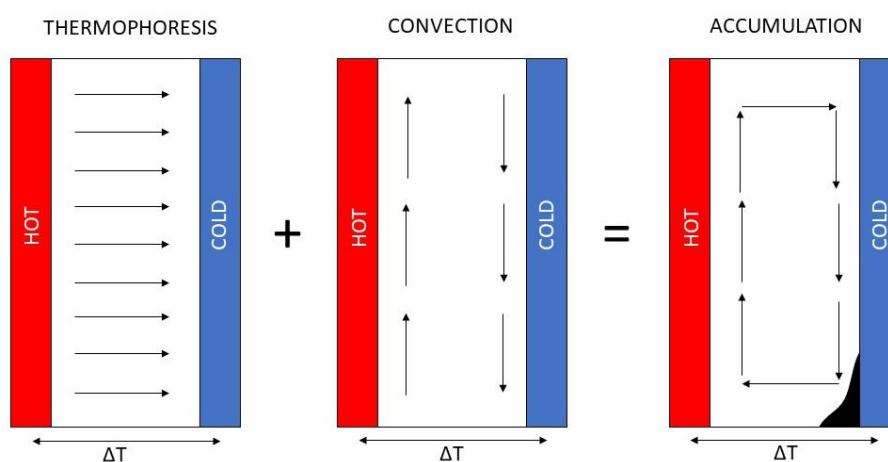


Figure 1. Thermophoresis and convection drive the accumulation of molecules. In the presence of a thermal gradient (∇T) across a chamber, thermophoresis transports molecules with a positive Soret coefficient from the hot to the cold side, while convective flows move molecules vertically. The combination of both effects results in the accumulation of molecules in the corner of the cold side of the chamber. Arrows indicate the direction of the movement of the molecules inside the chamber.

Cellular mimics in out-of-equilibrium conditions

The construction of cellular mimics is intended to provide a deeper understanding of how living cells work by reconstituting the cellular functions and properties from their component parts. As presented in the first chapter, this approach has typically relied upon vesicles composed of natural lipids or synthetic amphiphiles that form structures similar to biological membranes encapsulating the biological components needed to confer upon the artificial cells the ability to mimic specific cellular functions. Here, we chose to begin building a cellular mimic that possesses some of the functionalities of a lipid membrane without containing a physical barrier at all. Instead, convection and thermophoresis are used to compile the cellular components in the absence of lipids and to generate a disequilibrium state reminiscent of natural living cells. To build such an artificial system, a microfluidic chamber was designed, built, and subjected to a thermal gradient in order to accumulate the hundreds of components needed to reconstitute transcription and translation from a diluted extract of *E. coli*. In this chapter, preliminary experiments are shown that suggest that in the presence of a thermal gradient the components of an *E. coli* extract accumulate in confined and defined spaces at the air-water interphase where transcription and translation were shown to likely work. The feasibility of reconstituting complex cellular mimics under out-of-equilibrium conditions driven by thermal gradients is explored and discussed.

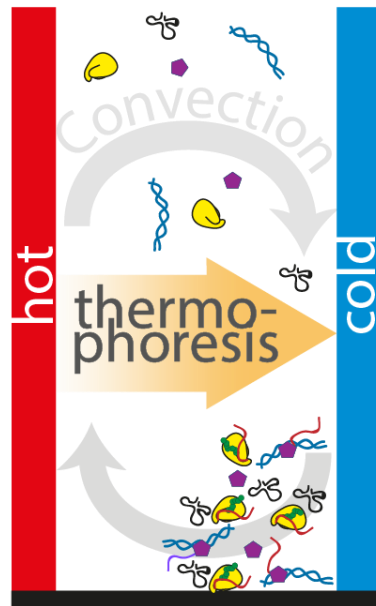


Figure 1. Schematic representation of the accumulation of the components of a cell-free extract by thermophoresis and convection. Upon accumulation of DNA and the transcription and translation machinery, RNA and protein synthesis are localized to a confined and defined space without the need of a membrane compartment. The disequilibrium state is generated by a thermal gradient applied across the chamber. Blue double helix structures represent DNA, the purple hexagons represent RNA polymerase, the black clover-like structures represent tRNA, red filaments represent mRNA transcripts, chains of green circles represent nascent protein, and ribosomes are represented in yellow.

RESULTS

To assess whether complex reactions, such those mediated by transcription and translation, could be reconstituted in a manner dependent upon convection and thermophoresis, a crude cell extract providing the transcription and translation machinery of *E. coli* supplemented with DNA coding for a fluorescent protein were loaded inside of a microfluidic container referred to as thermophoretic chamber. In other words, the goal was to have a solution that was too dilute to support transcription-translation in the absence of a thermal gradient. Then, due to convection and thermophoresis, the molecular components needed to support transcription and translation would accumulate within the same region of the thermophoretic chamber when the thermal gradient was established, thus leading to the onset of activity. The assessment of the activity of the system was by fluorescence, as both the synthesized RNA and protein led to fluorescence in the described system.

Cell-free extract

To mimic the internal content of the cell we decided to use a crude cell extract from *E. coli*. The preparation of the cell extract included the following steps. First, *E. coli* cells were cultured under aerobic conditions to mid-exponential phase. Then the cells were harvested and lysed, membranes and debris were removed by centrifugation and the endogenous nucleic acids were digested by the endonucleases present in the lysate. The lysate, composed mainly of ribosomes and proteins, was subsequently dialyzed to remove metabolic waste products. After dialysis, the cell-extract was ready to use or to be stored at -80 °C by the flash freezing of aliquots (Figure 1). The cell extract provided the endogenous transcription and translation machinery of *E. coli*. However, to function in vitro the extract needed to be supplemented with tRNAs, the 20 canonical amino acids and the ribonucleotide triphosphates required for the synthesis of RNA and protein, which were lost during dialysis. The cell extract was typically also supplemented with other additives that helped the efficiency of in vitro transcription and translation, such as salts, crowding agents and components needed to regenerate ATP (Figure 2 and material and methods). To assess the activity of the cell-free extract, a genetic construct was built that coded for a monomeric A206K Ypet fluorescent

protein under the control of a constitutive promoter (Tac). We chose Ypet because of the high brightness and photostability of the protein (66, 67). To monitor transcription, three malachite green aptamers were cloned inside of a pRNA-3WJ motif (68) at the 3' UTR of the coding sequence of Ypet. The pRNA-3WJ is an RNA motif composed of three interspaced interacting 18 nt fragments that fold in a three-way junction ultra-structure and that can accommodate the insertion and proper folding of other RNA sequences of interest. One malachite green aptamer was cloned per junction. The detection of the RNA transcripts occurred upon the binding of malachite green to the malachite green aptamers.

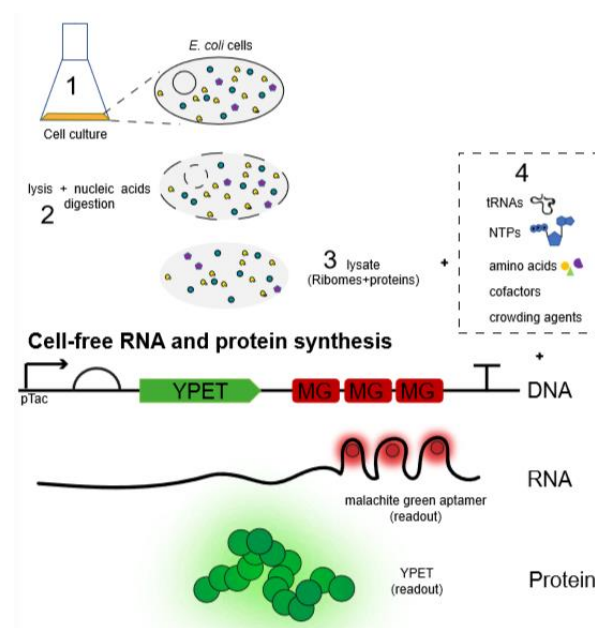


Figure 2. Homemade cell-free extract and in vitro transcription translation reactions. Top: Schematic representation of the main steps for the preparation of an *E. coli* cell-free extract. Bottom: Schematic diagram showing the genetic construct used for the experiments of this chapter. The DNA codes for A206K Ypet, a monomeric version of the Ypet fluorescent protein. Three malachite green aptamers were cloned downstream of the Ypet coding sequence to allow for the monitoring of RNA synthesis upon the addition of malachite green.

Thermophoretic chamber

The thermophoretic chamber was composed of various material parts (Figure 3). The shape and thickness of the chamber were determined by the thickness and the geometry of the Teflon, fluorinated ethylene propylene (FEP) foil 6), which was cut with a 2D plotting cutter (material and methods). The chamber was placed between two heat-conductive materials, that is, a silicon wafer 5) on one side and a sapphire block

(14 x 30 mm) 7) on the other side. Both materials contained flat surfaces that provide a homogenous distribution of heat over the entire surface. Moreover, the sapphire block was transparent, which allowed for the monitoring of fluorescence. To complete the assembly of the thermophoretic chamber (Figure 3), the silicon wafer was placed and glued with thermal paste on top of a copper block 8). Copper is known for its high heat capacity so that the chamber could be kept on ice or at 4 °C to avoid any potential activity of the cell-free extract prior to starting the experiment. A copper holder for the heat resistors 3) was placed and glued on top of the sapphire block with thermal paste. A steel mounting support 4) held the whole structure of the chamber together with plastic screws. PTFE poly(tetrafluoroethylene) Teflon tubing 2) was used to load the cell-free reaction inside the thermophoretic chamber. Teflon was chosen since this material is inert and thus minimizes possible unwanted interactions between the components of the cell extract and the tubing. The inner diameter of the tubing was 0.18 mm, which minimized the dead volume.

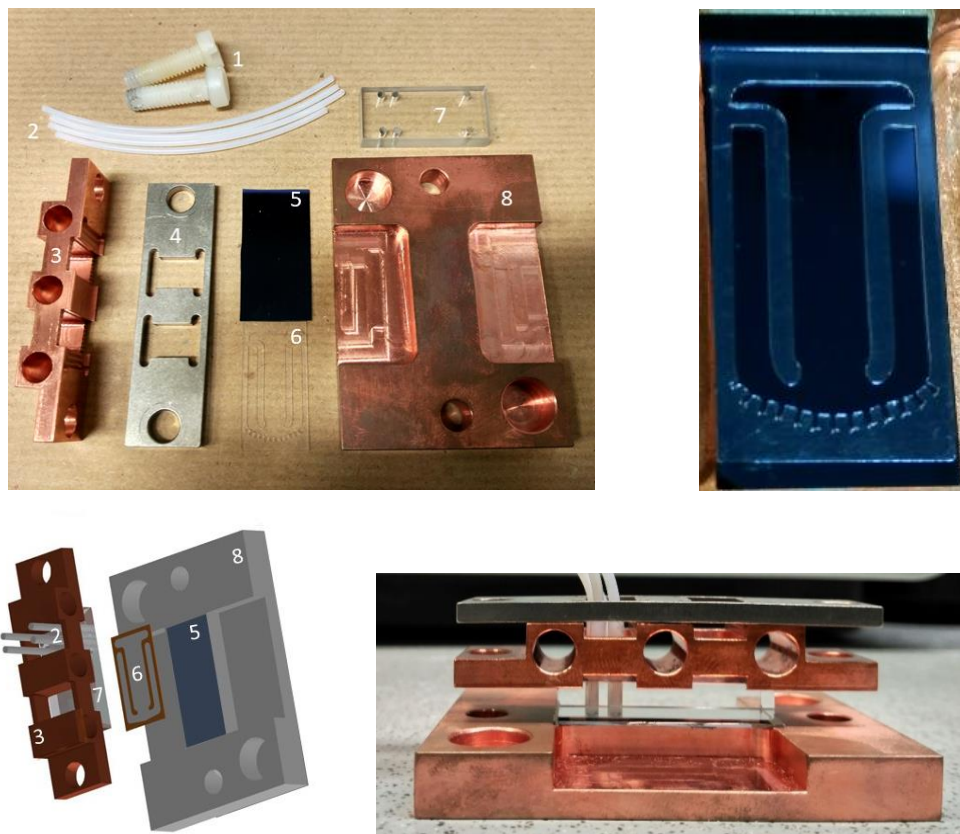


Figure 3. Thermophoretic chamber. Top left, Parts of a thermophoretic chamber. 1. plastic screws, 2. Teflon PTFE (Polytetrafluoroethylene) tubing, 3. Copper holder for heater resistors, 4. Steel mounting support, 5. Silicon wafer, 6. Teflon FEP (fluorinated ethylene propylene) with the trap geometry of interest, 7. Sapphire and 8. Copper block. Top right: Teflon geometry on top of a silicon wafer. Bottom left: schematic representation of the assembly of the different parts of a thermophoretic chamber.

Bottom right: profile view of an assembled thermophoretic chamber.

The dimensions of the trap were (11.2 x 21.2 mm) (Figure 4). The reasoning behind the trap geometry was to optimize the loading process by avoiding the formation of bubbles that could eventually alter the continuity of the thermal gradient and thus alter the accumulation of the transcription-translation machinery. Another trap geometry was also designed to maximize the amount of oxygen available for the maturation of the chromophore of the fluorescent protein. The posttranslational formation of the chromophore of GFP and GFP related fluorescent proteins, as in the case of A206K Ypet, requires molecular oxygen. More specifically, the polypeptide backbone of the protein has to undergo folding, the cyclization of side-chains, oxidation and dehydration. Without the oxidation and dehydration steps, the conjugate double bonds of the chromophore cannot be formed (69). Several notches (indentations) were included to create small oxygen reservoirs at the bottom of the chamber (Figure 4). Upon loading, water could not go inside the notches because of the surface tension at the interphase with the air.

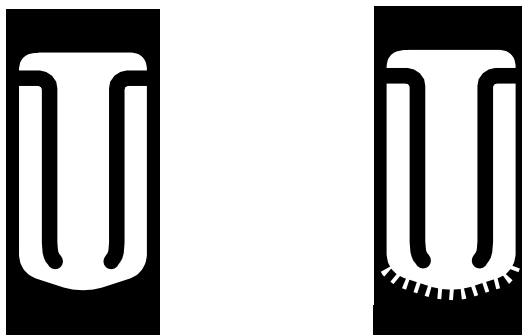


Figure 4. Thermophoretic chamber geometries. Left, regular geometry. Right, geometry containing small indentations at the bottom to create oxygen reservoirs. White area corresponds to the geometry of the thermophoretic chamber while the black area indicates Teflon.

Setup

The custom-built setup (Figure 5) was composed of a metallic multi-support for the thermophoretic chambers, a microscope and software. The microscope was equipped with a 4x objective, a CCD camera and two light emitting diodes (470/625 nm) that allowed for the monitoring of the fluorescence of Ypet and malachite green. The microscope was mounted on top of a motorized stage (attached to the multi-support) and controlled by three-step motors that could be moved in three dimensions. This setup allowed for the acquisition of fluorescence at multiple positions of the thermophoretic chamber. The metallic multi-support could hold up to 10 trap chambers. Each chamber support was composed of a metallic magnet that held the chamber in a fixed position, and the chamber was directly connected to a thermal bath with water filled tubes.

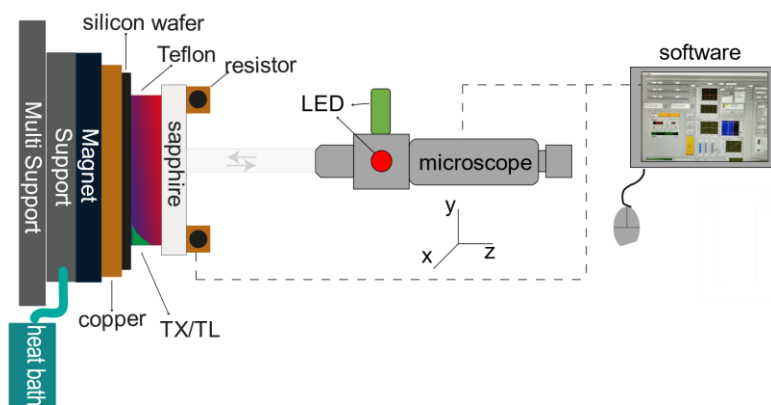


Figure 5. schematic representation of the custom-built set up to monitor de fluorescence coming from the thermophoretic chamber. The set up includes a microscope and a multi-support for the thermophoretic chambers and a computer that controls the data acquisition.

The LabVIEW-based software allowed for the sequential read-out of fluorescence at specific selected positions of multiple thermophoretic chambers (Figure 6). To create a thermal gradient inside the chamber, the cold temperature was set manually with a heat bath, while the hot temperature was set via the software that controlled the resistor's temperature.

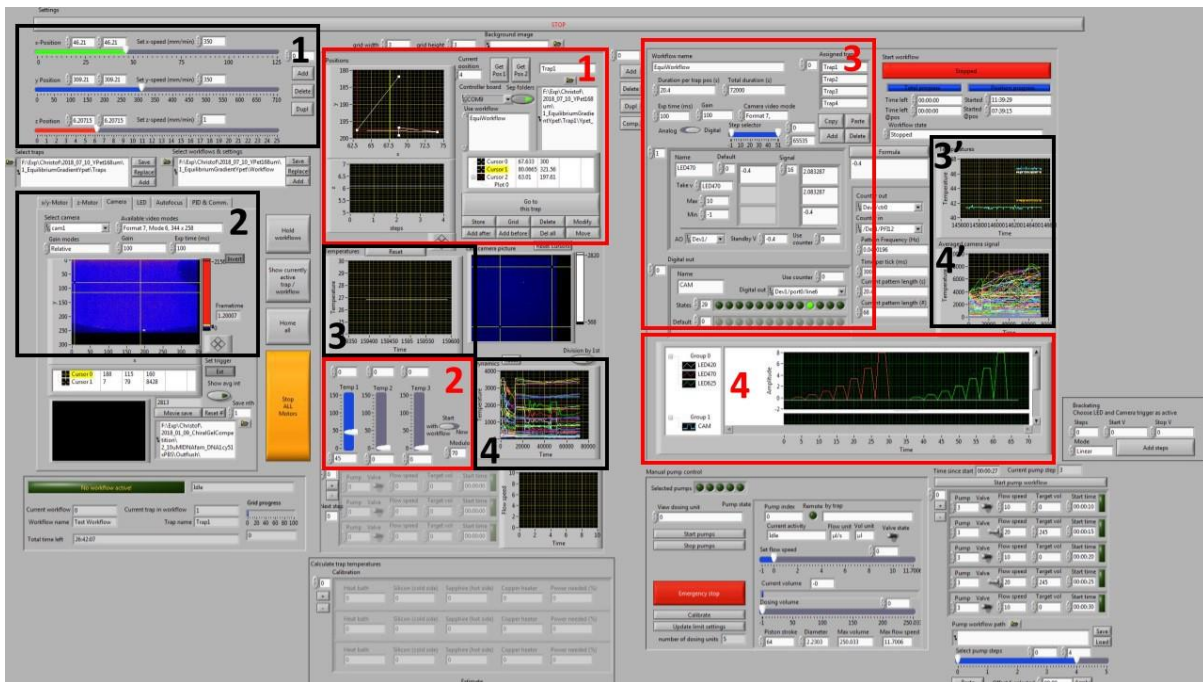


Figure 6. User interface of the LabVIEW software. The software allows for data acquisition and contains the following implementations: 1- Real time control (black rectangles). Allows the visualization in real time of the position of the microscope (1), the temperature of the heat resistors for the current trap (3) or for all the traps belonging to the same workflow (3'), the camera image (2) and the acquired fluorescence signal from the current trap (4) or all the traps belonging to the same workflow (4'). 2- Workflow settings (red rectangles). Allows the setting of the workflow parameters. Selection of the positions inside the chamber to be acquired (1), temperature at the resistors (2), which exposition time and LED to use (3), how many acquisitions per chamber (4), camera trigger, overall time course (duration) of the experiment (3).

Thermal accumulation experiments

Before starting the accumulation experiments, transcription and translation reactions, hereafter referred to as (TX/TL), were assembled and supplemented with DNA coding for Ypet and malachite green aptamers. TX/TL reactions were run in test tubes at different temperatures ranging from 20 to 45 °C. According to the fluorescence arising from the reactions over 8 h, the working temperature range was from 25-40 °C with a maximum of protein and RNA production observed in the range of 28-31 °C (Figure 7). This data indicated the maximal temperature gradient that could be applied to the thermophoretic chamber that did not impair substantially the efficiency of the TX/TL reactions.

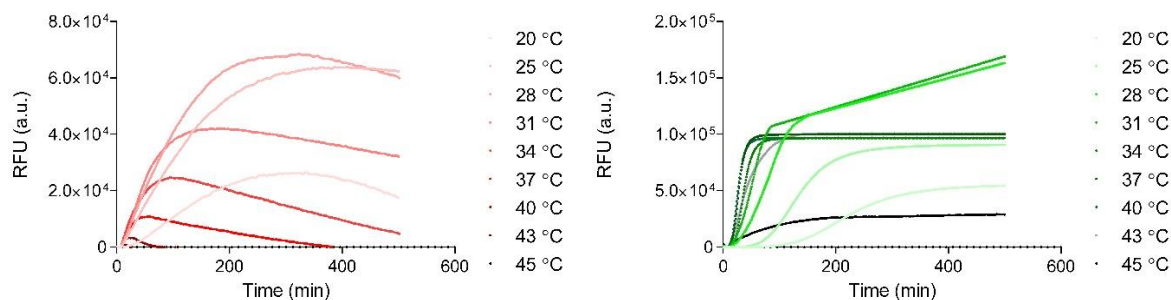


Figure 7. Working temperature range of *in vitro* TX/TL reactions. The activity of TX/TL reactions from an *E. coli* homemade extract supplemented with malachite green and a genetic construct coding for Ypet and three malachite green aptamers was checked at different temperatures. Fluorescence was monitored with the appropriate channels using a qTower³ thermal cycler. Protein production is shown in green and the levels of mRNA are shown in red.

To assess whether the components of the cell-free extract and the DNA could accumulate and still function to produce RNA and protein inside the thermophoretic chamber, a cell-free TX/TL reaction was assembled containing the genetic construct encoding Ypet followed by three malachite green aptamers. The solution was loaded inside a 250 μm chamber and a temperature gradient of ~ 10 °C (28 °C cold side/ 38 °C hot side) was applied. RNA and protein expression were monitored over 2.5 h at 5 different positions of the chamber (Figure 8).

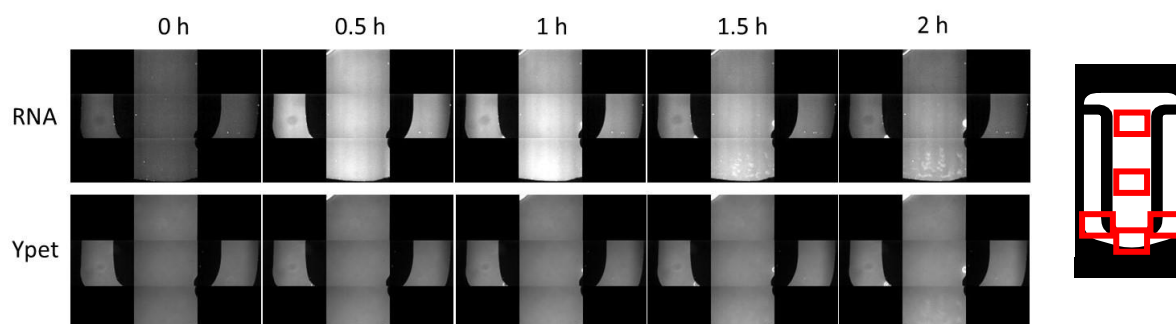


Figure 8. RNA and protein expression inside a thermophoretic chamber subjected to a temperature gradient. Shown are frames selected at the indicated time points over the experiment. Each frame is composed of 5 different subframes that correspond to 5 different positions of the thermophoretic chamber (highlighted in red). The temperature gradient was ~ 10 °C.

Fluorescence arising from the malachite green aptamers within the mRNA was rapidly detected all over the chamber (Supplementary movie 1 and 2). The intensity of the signal began to decrease at the top of the chamber after 1 h and after 1.5 h aggregate-like structures were observed at the bottom of the chamber, potentially indicating a slight accumulation of synthesized RNA. Conversely, the fluorescence signal of Ypet

only slightly increased over time. A lack of fluorescence in this case did not necessarily indicate a lack of protein expression. As explained above, molecular oxygen was required for the maturation of Ypet. Therefore, the concentration of oxygen present in the cell-free reaction solution might not have been enough to support the formation of the chromophore. Similarly, previous reports have observed that protein synthesis correlated with oxygen availability in TX/TL reactions (70, 71). To confirm that protein expression could take place inside the thermophoretic chamber, the experiment was repeated with the same batch of cell-free extract and genetic construct. However, for this test a thermophoretic chamber of the same thickness, i.e. 250 μm , was built that contained a slightly modified geometry that included several notches to facilitate the formation of small air/oxygen reservoirs at the bottom of the chamber. In this way, if Ypet was produced and was properly folded, then the chromophore would form due to the presence of oxygen. The thermophoretic chamber was subjected to a temperature gradient of ~ 10 $^{\circ}\text{C}$ (28 $^{\circ}\text{C}$ cold site/ 38 $^{\circ}\text{C}$ hot site). Fluorescence was monitored for 20 h (Figure 9) at the same positions described above. The data revealed fluorescence arising from both Ypet and RNA but only at the air-water interphase at the rim of the notches (Figure 9 and supplementary movie 3 and 4).

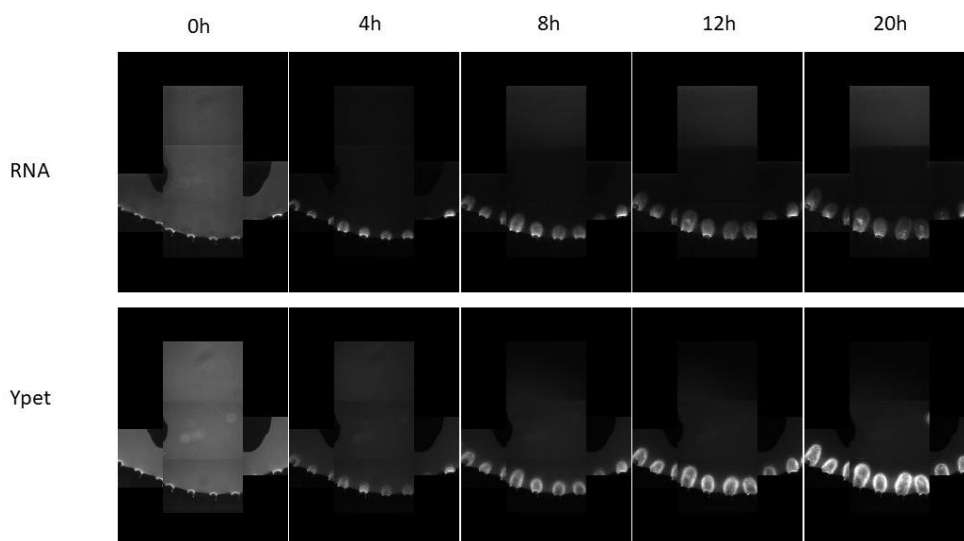


Figure 9. Accumulation kinetics of RNA and protein inside a thermophoretic chamber containing multiple air-water interphases. Selected acquired frames at the indicated time points showed the accumulation of RNA and protein at the air-water interphase. The temperature gradient was ~ 10 $^{\circ}\text{C}$.

Interestingly, over time at the air-water interphase bubble like structures were growing inwards. The fluorescence signals from both RNA and protein were co-localized within the “growing” bubbles. The same effect was observed when the experiment was repeated under the same conditions with a temperature gradient of ~ 5 °C (28 °C cold side/ 33 °C hot side) (Figure 10).

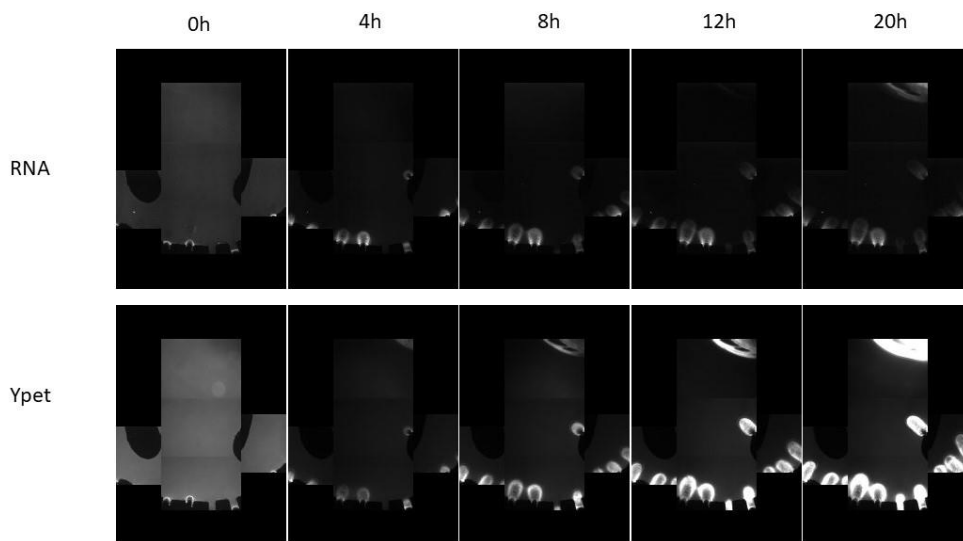


Figure 10. Accumulation kinetics of RNA and protein inside a chamber containing multiple air-water interphases. Selected acquired frames at the indicated time points show the accumulation of RNA and protein at the air-water interphase. The temperature gradient was ~ 5 °C.

After the experiment concluded, the chamber containing the air bubbles was photographed. A remarkable white precipitate could be observed at the air-water interphase, likely indicating a strong accumulation of protein, RNA and the components of the cell extract (Figure 11).



Figure 11: left, photograph of a thermophoretic chamber containing a cell-free TX/TL solution and DNA after being subjected to temperature gradient of 10 °C for 20 h. Right, magnification of the bottom of the chamber at the air-cell-free extract interphase.

The observed accumulation of RNA and protein at the air-water interphase did not seem to depend on thermophoresis. The Braun group has also observed a strong accumulation of DNA at air-water interphases inside similar thermophoretic chambers (manuscript in preparation by Morash et al.). Simulations have been conducted that indicated that the thermal gradient applied to the thermophoretic chamber generates a convective flow that transports molecules to the air-water interphase. The temperature gradient also induced a surface tension gradient along the air-water interphase generating a fluid motion from low surface tension (hot side) to high surface tension (cold side) regions. This phenomenon is known as thermo-capillary convection or the Marangoni effect. However, a key point is that water evaporates at the hot side of the chamber and condenses at the cold side. This creates strong local flows that overcome Marangoni and convection flows at the meniscus, allowing the concentration of molecules at the air-water interphase at the hot side of the chamber (Figure 12).

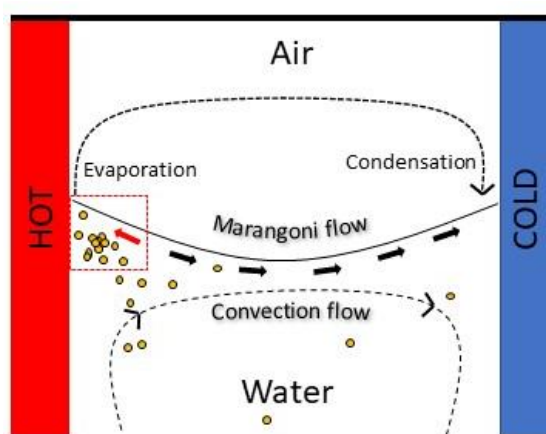


Figure 12: Schematic explanatory diagram of the accumulation inside the thermophoretic chamber. Yellow circles represent the accumulated molecule. Red arrow indicates the direction of accumulation of molecules induced by a strong flow that opposes Marangoni and convection effects.

The inefficient accumulation of the components of the *E. coli* cell extract observed with the thermophoretic chambers without notches were also confirmed by COMSOL simulations. The simulations screened the accumulation of DNA oligonucleotides of different lengths (1, 50, 100, 150, 200 bp) in chambers with different thicknesses in the range of 50-500 μm with the same volume and geometry as the chambers used for the experiments shown earlier and subjected to a temperature gradient of $\sim 10^\circ\text{C}$. The COMSOL simulations indicated that 100 μm was the optimal thickness for favoring the highest accumulation after either 2 h or after reaching steady state (Figure 13). For a 250 μm chamber instead, the accumulation was one or several orders of magnitude lower at 2 h or at steady state, respectively. These data suggest that thermophoresis and convection for chambers thicker than 100 μm cannot enrich more than 10-fold. This is in agreement with the fact that the thicker the chamber, assuming the same temperature difference at both ends, the less steep the thermal gradient is, which leads to lower thermophoretic mobility.

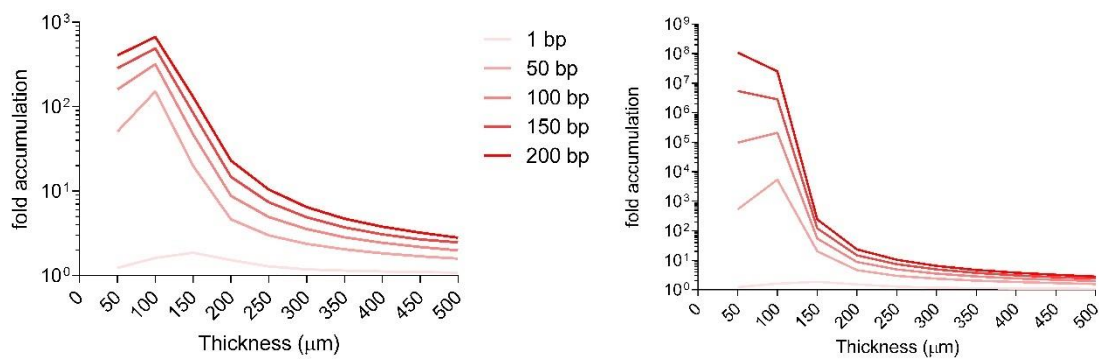
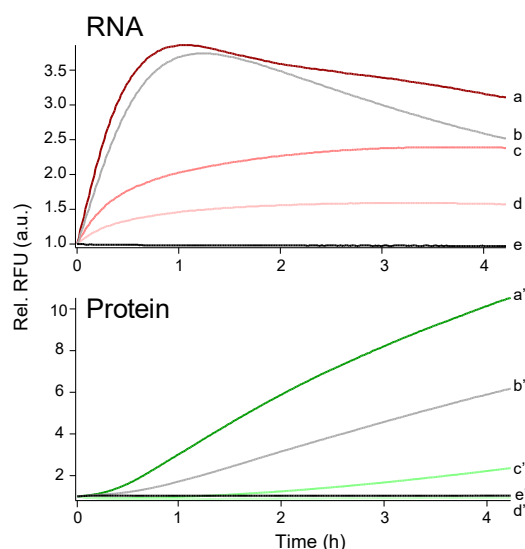
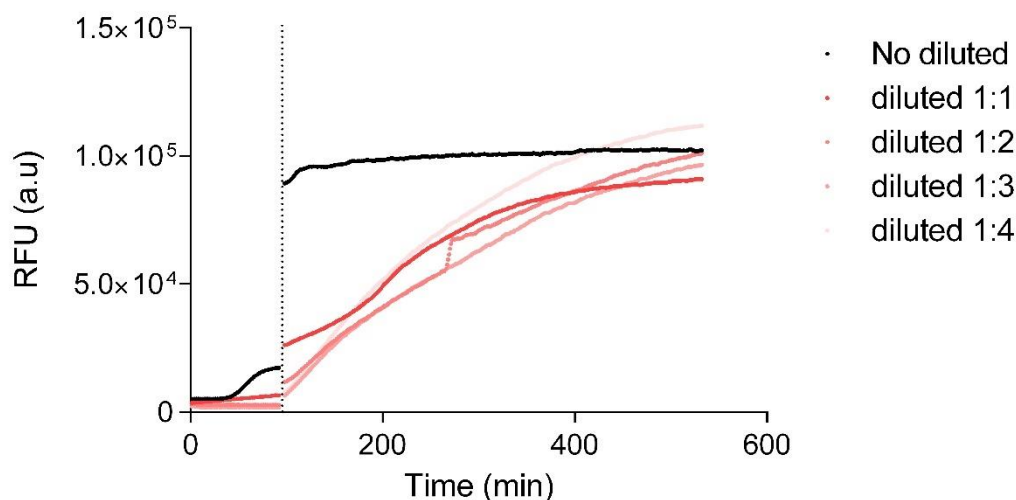


Figure 13. Simulations of the accumulation of different DNA oligonucleotide lengths in chambers of different thicknesses. Accumulation shown after 2 h (left) or after reaching steady state (right) within a thermal gradient of 10 °C.

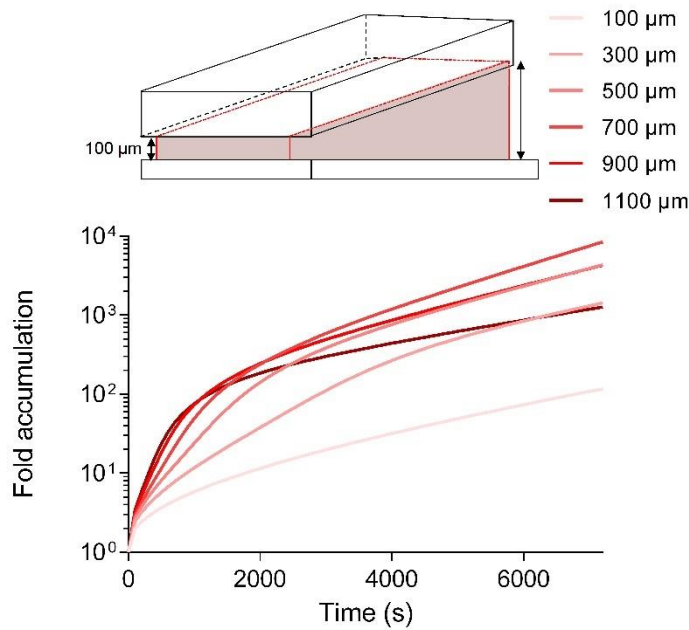
SUPPLEMENTARY FIGURES



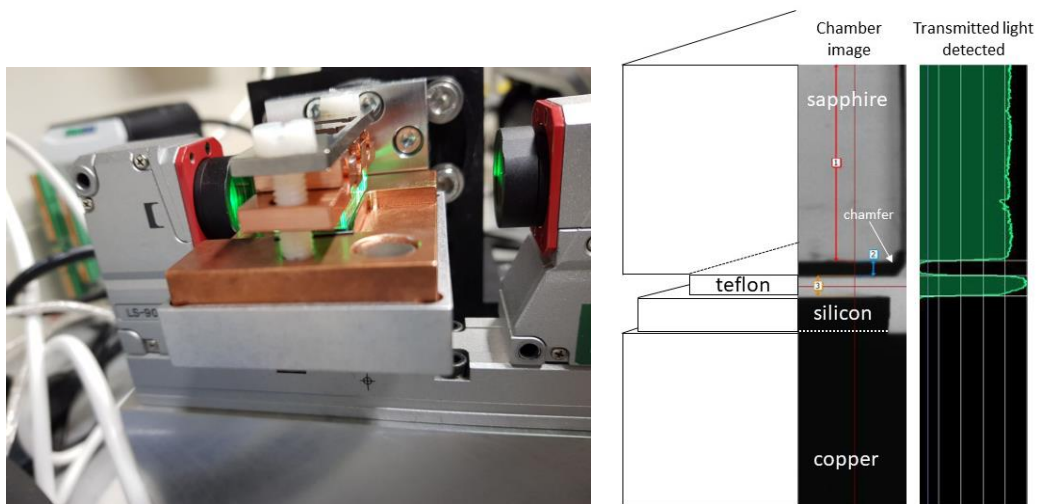
Supplementary Figure 2. The effect of dilution and crowding agents on RNA and protein synthesis in cell-free TX/TL reactions in batch mode. DNA encoding Ypet and three malachite green aptamers allows for the monitoring of the production of Ypet fluorescent protein and RNA upon addition of malachite green. Cell-free reactions were conducted at 33 °C in batch mode. Non-diluted samples (a,a') or samples either diluted 1:1 (volume ratio) (c,c') or 1:2 (volume ratio)(d,d') with water. Samples (b,b') did not contain PEG-8000, while samples (e,e') were the non-DNA template controls.



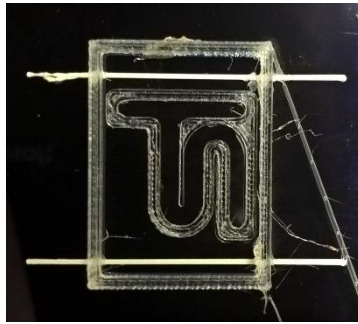
Supplementary Figure 3. Recovery of activity of an *E. coli* cell extract after lyophilization and rehydration. To show, as a proof of concept, that a diluted nonfunctional extract can be made active again upon concentration, TX/TL reactions were assembled and supplemented with DNA coding for A206K Ypet under a constitutive T7 transcriptional promoter. The reaction was either non-diluted or diluted in a 1:1, 1:2, 1:3, 1:4 volume ratios with water. Fluorescence arising from the reactions was acquired for 1.5 h. Then samples were flash-frozen and lyophilized with a Genevac evaporator EZ-2elite set for aqueous solvents until complete dryness. The sample pellets were rehydrated with water up to the initial volume before dilution to give a 1x concentration and fluorescence was acquired again with the appropriate channels using a qTower³ thermal cycle



Supplementary Figure 4. COMSOL simulations showing the accumulation of a 100 bp DNA oligonucleotide inside of a thermophoretic chamber with homogenous 100 μM thickness or inside of differently tilted thermophoretic chambers (100-300, 100-500, 100-700, 100-900 and 100-1100 μM). DNA is shown to accumulate 1000-fold more in a tilted chamber with a gradient of thickness. The temperature gradient was set to 10 °C.



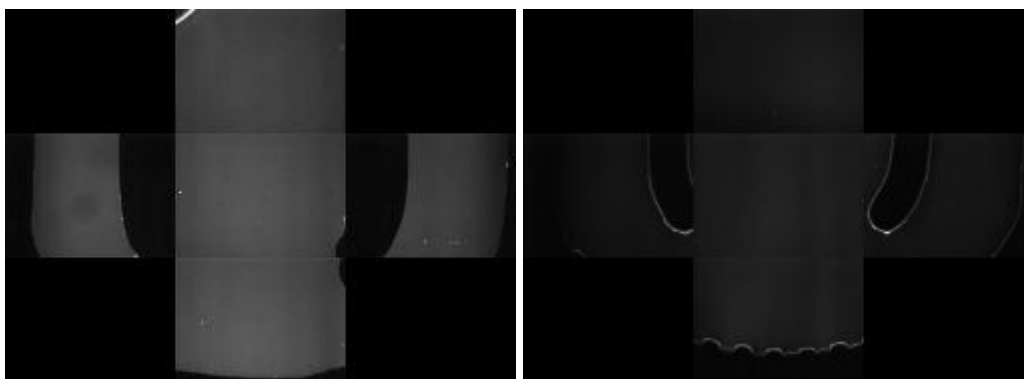
Supplementary Figure 5. High precision optical micrometer used to measure the thickness of the thermophoretic chambers. Left: The chamber is placed on top of a stage between an LED and a CMOS sensor. The stage can be manually controlled in the x and z- axis to position the chamber in the appropriate position to allow for thickness measuring. Transmitted green light passing through the chamber is detected by a sensor. Right: the device is connected to a computer that displays the chamber image. The sensor detects the position of the edges between light and dark edges and calculate the distances.



Supplementary Figure 6. Example of 3D printed thermophoretic chamber. PLA was used to print the geometry of the chamber on top of a silicon wafer while two parallel lignine spacers were printed next to determine the thickness of the chamber.



Supplementary Figure 7. Descriptive pictures for the printing of a resin-based thermophoretic chamber. Left: example of a 2D geometry mask design printed in a transparent foil. Middle: shown is the homemade 64 LED array printing device. Right: resin geometry printed directly on top of a silicon wafer.



Supplementary Figure 8. Left: RNA fluorescence signal distributes homogenously inside a Teflon-based thermophoretic chamber. Right: RNA fluorescence signal inside a resin-based thermophoretic chamber was detected at the border and in contact with the resin surface.

SUPPLEMENTARY TABLES

Chamber version	Printing device	Thickness	Material	Main advantages	Main Disadvantages
1.0	3D printer	Lignine spacer	PLA and PC	biocompatible	leakage
2.0	LED array	Steel spacer	Flexible resin	Fast building	Extract interaction
3.0	No	Teflon foil	Teflon FEP	Chemically inert	No tilting trap

Supplementary Table 1. Thermophoretic chamber versions built with different methods for the accumulation experiments.

MATERIAL AND METHODS

***E. coli* homemade cell extract**

E. coli Rosetta 2(DE3), provided by Prof. Friedrich C. Simmel, was grown from a 10% glycerol stock in 2xYTP media supplemented with 40 mM K₂HPO₄, 22 mM KH₂PO₄, and 34 µg/mL of chloramphenicol for 15 h at 37 °C, 220 rpm. The culture was diluted to OD_{600 nm} = 0.01, and isopropyl-β-D-1-thiogalactopyranoside (IPTG) was added to a final concentration of 0.1 mM to induce the expression of the T7 RNA polymerase. In this way, the cell extract could also be used with T7 transcriptional promoter containing plasmids. The culture was then incubated for 3.5 h at 37 °C, 220 rpm. Flask volume to the cell culture volume was always kept at a ratio 5:1. Cells were harvested at 6,000 xg for 10 min at 4 °C. Starting from the bacterial pellet, the S30 extract was prepared following Noireaux's protocol (72) with some exceptions. For simplicity, only the main steps are described. The cell pellet was washed twice in S30 A buffer (14 mM Mg-glutamate, 60 mM K-glutamate, 50 mM Tris, 2 mM DTT buffered with glacial acetic acid to pH 7.7). Bacterial cells were lysed with ~ 0.1 mm Ø glass beads using the Fastprep-24 homogenizer (MP) in place of the Mini-Beadbeater-1 (BioSpec) in two rounds of 1 min at 6.5 m/s with an interval of 5 min incubation on ice. To discard lipid membranes and cellular debris, the cell extract was centrifuged at 12000 xg for 10 min at 4 °C. Remaining nucleic acids in the cell extract were digested by endogenous nucleases for 80 min at 37 °C 220rpm. Then the cell extract was dialyzed at 4 °C for 3 h against 180 volumes of S30 B buffer (14 mM Mg-glutamate, 60 mM K-glutamate, 1 mM DTT buffered to pH 8.2 with 2M Tris). For the dialysis step, SnakeSkin™ Dialysis Tubing (Thermo Fisher Scientific) was used in place of Slide-A-Lyzer dialysis cassettes. The S30 Crude Extract final solution was aliquoted, flash-frozen and stored at -80 °C as 3x concentrated stock. The S30 energy solution was prepared as 14x concentrated stock and contained: HEPES pH 8 700 mM, ATP 21 mM, GTP 21 mM, CTP 12.6 mM, UTP 12.6 mM, tRNA 2.8 mg/mL, CoA 3.64 mM, NAD 4.62 mM, cAMP 10.5 mM, folinic acid 0.95 mM, spermidine 14 mM and 3-PGA 420 mM. The amino acid solution contained the 20 canonical amino acids at equimolar concentration, was adjusted to pH 7.86 with glacial acetic acid and was prepared according to Noireaux's indications (73). The S30 in vitro transcription translation reaction used for the

experiments contained: 1x S30 Crude Extract, 1.5 mM of each amino acid, 1x energy solution, 12 mM maltose, 7.5 mM Mg-glutamate, 2% (w/v) polyethylene glycol (PEG) 8000, 50 μ M Malachite green and 10 nM plasmid DNA template. The working concentrations of maltose, Mg-glutamate and Malachite green were calibrated. Maltose was used to prolong the functionality of the TX/TL reactions for longer periods of time since it allows the inorganic phosphate recycling and ATP regeneration (71). Mg glutamate is essential for TX/TL functionality, Mg^{2+} ions participate in transcription elongation (74), translation initiation (75) and maintain the structure of the ribosomes (76). If Mg glutamate was not added, no RNA or protein synthesis was observed.

Uninterrupted bacterial cell growth was of fundamental importance for achieving a good working extract. Initially, Noireaux's protocol was strictly followed (72). The bacterial growth consisted in an initial overnight incubation at 37 °C of *E. coli* Rosetta2(DE3) streaked on 2xYTP agar plates, one colony was then inoculated in 4 mL of 2xYTP and incubated for 8 h (37 °C 220 rpm), an aliquot was diluted 50x in 50 mL 2xYTP and incubated for 8 h (37 °C, 220 rpm), subsequently an aliquot was diluted 100x into 660mL of 2xYTP and incubated for 3-3.5 h at 37 °C, 220 rpm). Many trials following that protocol failed to provide a good working extract because bacterial growth was interrupted several times to monitor OD_{600} . Interruption of cell growth increased the doubling time. Therefore, cells were never collected at doubling times \leq 30 min or corresponding to exponential phase. Different conditions to try to improve the performance of the extract were tried, including growing cells in 2xYTP supplemented with 2.5% maltose, collecting cells at different time point during the growth curves and preparing the cell extract without the dialysis step. None of the trials gave extract that worked as well as from the procedure described above.

Cutting the geometry of the thermophoretic chamber

The geometry of interest was cut directly on the Teflon foil with the Graphtec ce6000-40 computer-controlled 2D cutting plotter. The software recognizes the geometry and the cutter cuts it precisely along the path. The thickness of the thermophoretic chamber was determined by the thickness of the Teflon foil.

Thickness measurement of the thermophoretic chamber

After the complete assembly of the thermophoretic chambers, the thicknesses of the chambers were measured with a LS-9501P Keyence device. It is a high-precision optical micrometer equipped with a complementary metal oxide semiconductor (CMOS) sensor and a high-intensity green LED. The thermophoretic chamber is placed in between the sensor and the LED on top of a stage. The green light is emitted as a uniform collimated beam that goes through the chamber and the CMOS sensor detects the position of the edge between light and dark edges of the transmitted light and calculates measured values (Supplementary Figure 5). The measurement accuracy is of $\pm 0.5\mu\text{m}$.

Temperature measurement inside the thermophoretic chamber

Despite the good heat conductivity properties of the materials used to assemble the thermophoretic chamber, heat is not transferred completely from one material to another. Consequently, if two different temperatures are applied at both ends of the thermophoretic chamber (cooper parts), the temperature at the silicon and at the sapphire will not be the same because the temperature gradient will distribute over the different materials composing the chamber. To estimate the temperature inside the thermophoretic chamber, the fluorescent dye 2',7'-Bis-(2-carboxyethyl)-5(6)-carboxyfluorescein (BCECF) in combination with Tris buffer were used. Tris is known to have temperature dependent pK_a values, when the temperature varies the pK_a value of Tris changes and modifies the pH of the solution accordingly. BCECF in turn, is a pH sensitive ratiometric dye. A calibration curve was obtained by plotting and fitting the BCECF ratio (420/470 nm) data values obtained for different temperatures. First, different temperatures were set manually in the thermal bath, the temperature was then measured with a thermistor directly on the surface of the silicon wafer to have a more precise correlation between BCECF fluorescent signal and temperature. This method was also used to assess the average temperature inside the thermophoretic chamber when a thermal gradient was applied by comparing the expected values of BCECF from the cold and hot set temperatures and calculating the offset (difference) with the real values obtained.

Labview software for data acquisition analysis

A labview software was programmed to analyze and plot the fluorescent data acquired by the setup. The software allows the visualization of the acquired frames and computes the average pixel intensity of a selected region of interest (ROI). To show the fold intensity over time, the average pixel intensity of each selected ROI is divided by the average pixel intensity of the same ROI of the first acquired frame. To subtract background noise of the thermophoretic chamber or the background noise of the CCD camera, normalization against a water filled chamber or with LED switched off can be also performed. The software allows for the analysis and plotting of multiple ROI per thermophoretic chamber positions and will be used for future experiments.

Finite element simulations

Simulations were performed with COMSOL, a discrete solver that was used to simulate the movement and the accumulation of DNA oligonucleotides of different lengths over time with a given series of parameters that included the thickness and geometry of the chamber, the temperature gradient and the Soret coefficient. For the simulation, the software first divides the total volume of the chamber into a 3D mesh of arbitrary small volumes. Then, for each volume COSMOL solves and finds the numerical solutions of Navier Stokes diffusion and thermophoresis equations that explains the movement of the particle within each volume. The simulations presented in the chapter show the accumulation of DNA oligonucleotides of different lengths in chambers of different thicknesses subjected to different temperature gradients. Included are also simulations inside titled thermophoretic chambers.

Previous thermophoretic chambers

A considerable amount of time was spent to optimize the thermophoretic chamber. We started building chambers by 3D printing the geometry on top of silicon wafers with biocompatible thermoplastics, such as polylactic acid (PLA) or polycarbonate (PC), using a Ultimaker² 3D printer. The thickness of the chamber was determined by two parallel lignine filaments that served as thickness spacers that were printed on the

sides of the chamber structure (Supplementary Figure 6). The disadvantages of this method were that the complete assembly of the chamber on average took around 90-120 min, the top layer of the lignine spacers was not completely straight and from time to time there were irregularities in the surface causing leakage problems since the thermophoretic chambers could not be completely tightened (Supplementary Table 1). The next method we tried consisted of a black and white 2D geometry design that was printed on transparent foil that served as a printing mask. The printing device was a homemade 64 blue LED array with a microcontroller that controlled the exposure time of light. Two steel spacers of the selected thicknesses and a blue light photoactivatable resin (Photocentric 3D day light flexible resin) were added on top of the printing mask. Then a piece of silicon wafer was added on top. Upon irradiation with 475 nm light the resin was cured only in the transparent areas of the mask remaining attached to the silicon (Supplementary Figure 7). The thermophoretic chamber was then assembled as described in the main text. This method provided a faster assembly procedure. A thermophoretic chamber could be built in less than 30 min. However, a similar problem of leakage was encountered and furthermore, we have observed that RNA from TX/TL reactions interacted with the resin. While it was not the case for the Teflon-based thermophoretic chambers since Teflon is chemically inert (Supplementary Figure 8 and Supplementary Table 1).

SUMMARY

The construction of cellular mimics has relied thus far on the compartmentalization of biological components in defined, self-assembled structures typically made of natural lipids or synthetic amphiphiles. Examples of alternative membrane-free cellular mimics have also been reported that exploited coacervation (77), aqueous two-phase systems (ATPS) (78) or microfluidic devices (79). These three systems have been shown to support cell-free transcription and translation reactions. However, in the aforementioned cases, the cellular mimics were typically confined within regions physically demarcated in some way. For example, confinement was to the aggregates that formed the coacervate droplets, the phase separated polymers, water-in-oil emulsion droplets or a microfluidic chip, respectively. Here instead, we have begun to build cellular mimics through thermophoretic/convection-mediated confinement in an open microchamber.

Our cellular mimics rely on transcription and translation machinery from an *E. coli* homemade cell extract supplemented with DNA coding for the fluorescent protein A206K Ypet and for RNA aptamers that could also be monitored by fluorescence. To mimic some of the functionalities provided by cellular compartmentalization (i.e. spatial localization and concentration) in the absence of a membrane defined compartment, the cell extract was loaded inside of 250 μm Teflon-based microchambers that were subjected to mild temperature gradients (~ 10 $^{\circ}\text{C}$). Thermal gradients, in this case, provided the disequilibrium conditions required to accumulate and concentrate the numerous components of the cell-extract by thermophoretic and convective flows. Preliminary results indicated that the RNA fluorescence signal was slightly more localized at the bottom of the chamber with respect to the top of the chamber, indicating an inefficient accumulation of the cell-extract components after 2 h incubation within the thermal gradient. Instead, the signal corresponding to A206K Ypet was poorly detected. The inefficient accumulation of RNA was confirmed by finite element simulations conducted under similar conditions as the wet lab experiments. The simulations indicated that 100 μm was the optimal thickness for accumulation of components by thermal trapping. When the same experiment was repeated inside of the same microchambers that also incorporated notches at the bottom to provide small

air reservoirs, a strong signal for both RNA and protein was only detected at the rim of the air-water interphase, likely indicating an efficient accumulation of RNA, matured protein and the components of the cell extract. The data likely reflect phenomena not dependent on thermophoresis but rather on the strong flows near the air-water interphase originating at the hotter regions of the chamber due to the evaporation of water.

DISCUSSION AND PERSPECTIVES

The goal of this project is to build cellular mimics that possess the functionality of cell membranes without actually possessing a physical barrier or compartment, i.e. without possessing a cell membrane. The presented preliminary data suggest that a thermal gradient might be sufficient to accumulate and concentrate the components of a cell extract in defined and localized regions in a way that can still interact and function in the absence of encapsulation. The next step is to reconstitute the activity of transcription and translation from a diluted and thus non-functional cell extract. RNA and protein synthesis from diluted TX/TL reactions in test tubes are considerably impaired (Supplementary Figure 1), but the activity can be recovered upon concentrating the TX/TL solutions (Supplementary Figure 2). *E. coli* transcription and translation machinery can also function outside of artificial compartments and can be used, for example, to characterize and test new genetic circuits. The main difference between an in vitro transcription and translation reaction that is unencapsulated in a test tube and the same reaction that is thermally trapped inside a microchamber is that in the latter case, the accumulated components are continuously kept under disequilibrium. However, unencapsulated reactions require the continuous addition of consumable components to allow for continuous gene expression. Thermal trapping may provide a continuous accumulation of large components, such as proteins, RNA and other factors, while small molecules and building blocks such as amino acids, tRNA, nucleotides triphosphate are moderately accumulated or metabolic waste products can leave the trap by diffusion. We would like to build such a system that can be maintained in an out-of-equilibrium state as in the case of living cells. The accumulation of diluted biomolecules is also of interest from an origin of life perspective where the “concentration problem” is one of the problems scientists in the

field are facing. Reconstituting primitive cell-like systems with diluted prebiotically plausible molecules may provide a deeper knowledge on the series of transitions that took place from non-living matter to living cells.

From a technical point of view, we are still in the process of improving the thermophoretic chambers used for the accumulation experiments. We plan to substitute the silicon wafer with a thin layer of Teflon foil. In this way, the chamber would be completely delimited by chemically inert material avoiding potential interactions with the cell extract and DNA. When we were conducting the first accumulation experiments, we did not have Teflon foils thinner than 250 μm . The strong accumulation of the components of the *E. coli* cell extract at the air-water interphase is an interesting phenomenon that can be used to accumulate different DNA constructs coding for different functionalities. With sufficient time, bubble-like structures will fuse and emerging new activities could be reconstituted through the cooperation of individually concentrated components (genetic circuits, for example, could be implemented in this way). However, we will also try to accumulate the components of the cell extract by thermophoresis and convection. We will build, with the same geometry, thermophoretic chambers of 100 μm to maximize accumulation, as the simulations indicated. To avoid accumulation at the air-water interphase, we will use a genetic construct coding for a fluorescent protein based on the flavin-binding LOV (light, oxygen, or voltage sensing) domain that exhibits fluorescence under aerobic and anaerobic conditions. Interestingly, we have conducted some new simulations that indicated that the accumulation of molecules is increased by several orders of magnitude when using tilted thermophoretic chambers with a gradient in thickness (Supplementary Figure 4). However, with the current version of the Teflon-based thermophoretic chamber, it will be difficult to implement this design, because Teflon foils have a constant thickness.

Although we have yet to achieve our goal of building a robust, cell-like, membrane-less system that generates an active transcription and translation network from dilute solutions, we have built a foundation from which further studies can and will be pursued. We are hopeful that our system will help us gain a deeper understanding of the fundamental processes needed to sustain cellular life and the physico-chemical

role of cellular membranes. Ultimately, we may be able to say whether cellular membranes are dispensable or not.

CONCLUSIONS

Without an agreed upon definition of life, efforts in building living cells from component parts have relied on subjective evaluations of progress. The lack of well-defined criteria to recognize and distinguish living from nonliving systems has slowed progress in building cellular mimics (also called artificial cells) that fully display the properties of natural living cells. Thus far, there were no methods to quantify the performance of the artificial life-like systems in an objective way. In Chapter 1 we proposed a solution to the problem that did not rely upon a definition of the term life. We built cellular mimics that were able to chemically communicate with *V. fischeri* by sensing and synthesizing information in the form of quorum sensing molecules. In this way we could implement a cellular version of the Imitation game or Turing test that was originally meant to evaluate the intelligence of machines. Here we took the same concept whereby the natural cell directly evaluated the performance of the artificial system by assessing how well the artificial system was able to communicate. Since chemical communication leads to changes in gene expression, we decided to exploit RNAseq technology to observe genome wide the response of natural cells when communicating with *V. fischeri* like cells. By comparing the total number of genes that resulted differently expressed from chemical communication between artificial cells and *V. fischeri* we came up with a way to more objectively quantify the performance of the artificial system. With this approach the evaluation is directly taken by the natural cells and not by an observer, therefore for the first time, the field has a less biased metric to quantify progress towards the construction of cellular mimics that possess the properties of living cells. Importantly, with such technology we succeed in building life-like technologies that were capable of quenching the chemical communication of *P. aeruginosa*. With further advancement, this technology could be potentially used for therapeutic purposes.

The focus of the second chapter instead was to build cellular mimics without any direct physical barrier or compartment. We took advantage of thermal gradients to generate disequilibrium conditions. Thermal gradients have been reported to effectively accumulate biomolecules and indeed preliminary experiments suggested that thermal gradients might confer upon a thermally trapped artificial system some of the

functionalities of cell membranes. i.e. we have observed RNA and protein synthesis at the air-water interphase inside microcontainers that were subjected to a temperature gradient, indicating that the complex mixture of components of an *E. coli* cell extract were accumulating and still interacting to function in the absence of membrane compartments. By building a system that possess the functions of a membrane without the need of compartmentalization we expect to gain a deeper understanding on the role and functions of cell membranes and the required processes needed to originate and sustain life as we know it.

APPENDIX

Metal ions are indispensable for extant living cells, and many cellular processes are carried out by metalloproteins that depend on metal ions to fold and function properly. Therefore, extant metalloproteins may be an evolutionary outcome of chemistry that was mediated by metal ions and short peptide-metal ion complexes on the prebiotic Earth.

Modern-day Zn^{2+} and iron-sulfur proteins have been proposed to originate from duplications of short CX_2CG and CX_2CX_2C peptides motifs, respectively (80). This hypothesis has been recently supported by experimental data showing that a short cysteine containing tripeptide γ -ECG (L-glutathione) was capable of coordinating iron sulfur clusters in aqueous solutions and that longer peptides resulting from the synthesis of multiple γ -ECG sequence units containing the CX_2CX_2C motif were better able to stabilizing iron-sulfur clusters (81). Furthermore, γ -ECG coordinating Fe^{3+} was recently shown to lead to the formation of iron-sulfur clusters upon UV-light irradiation that induced cysteine desulfurization by breaking the carbon-sulfur bond (82).

Our interest is now focus in assessing the stability of the sulfhydryl groups of short cysteine containing peptide motifs sequences under UV-light irradiation and high temperature conditions in the presence of different metal ions. Shown in the following section are the experiments I conducted under high temperature conditions while Daniele Rossetto, a new PhD student of the Mansy laboratory is currently conducting experiments under UV-light irradiation.

Preliminary data indicate that a short cysteine containing peptide does not undergo desulfurization when exposed to high temperature conditions in the presence of Zn^{2+} .

RESULTS

The tripeptide (L)-glycyl-cysteinyl-glycine was heated at 150 °C for 4 min in the presence or absence of Zn²⁺. Glycyl-glycine was used as a buffer to keep the pH of the solution near the pK_a value of the sulfhydryl group of cysteine to favor the coordination between the tripeptide and Zn²⁺. Samples were subjected to high performance liquid chromatography (HPLC). The analysis revealed the detection of the intact tripeptide in the metal containing sample as in the non-heated sample control while in the absence of metal the chromatogram peak corresponding to the tripeptide was considerably lower in intensity (Figure 1). The mass of the tripeptide was also assessed and confirmed by mass spectrometry (Figure 2) as well as for glycyl-glycine (Figure 3) and the oxidized version of the tripeptide (Figure 4). This observation indicated that Zn²⁺ protected the integrity of the tripeptide avoiding desulfurization. Glycyl-alanyl-glycine was not detected upon heating in any of the samples indicating that apart from cysteine desulfurization other chemical rearrangements could have occurred that will be further investigated.

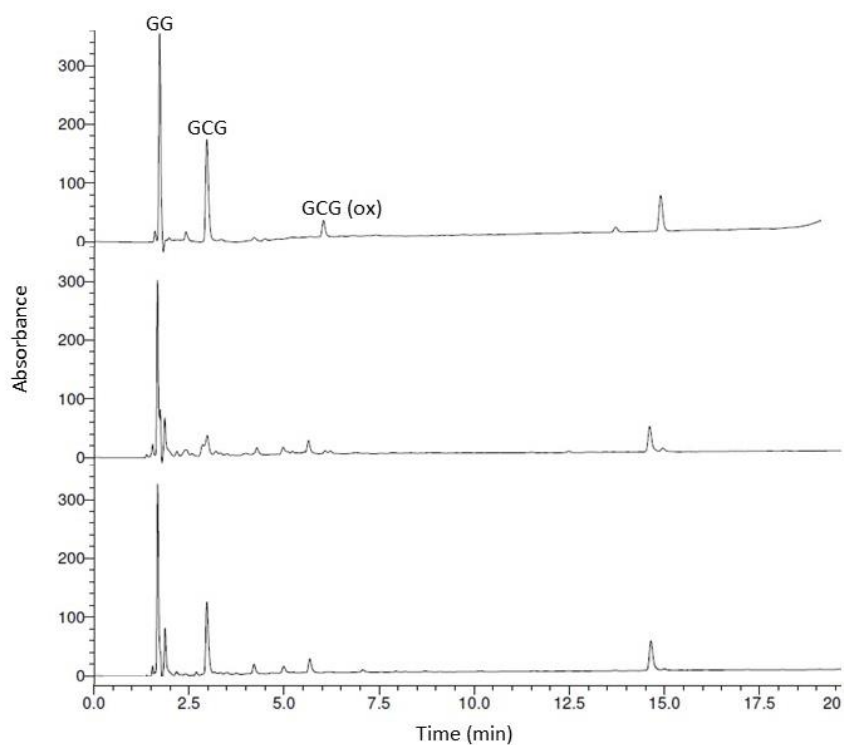


Figure 1. Zn^{2+} protects the integrity of a cysteine containing tripeptide at high temperature. Shown are representative UV-chromatograms acquired at 210 nm of an aqueous solution containing 5 mM glycyl-cysteinyglycine (GCG) and 20 mM glycyl-glycine (GG) at room temperature (top chromatogram) or heated for 4 min at 150 °C in the absence (mid chromatogram) or presence of 5 mM Zinc (bottom chromatogram). (GCGox) corresponds to the oxidized form of Glycyl-cysteinyglycine. (GG) corresponds to glycyl-glycine that was used as buffer. The chromatogram peak at retention time 15 min is not yet characterized. The experiment was conducted in triplicate.

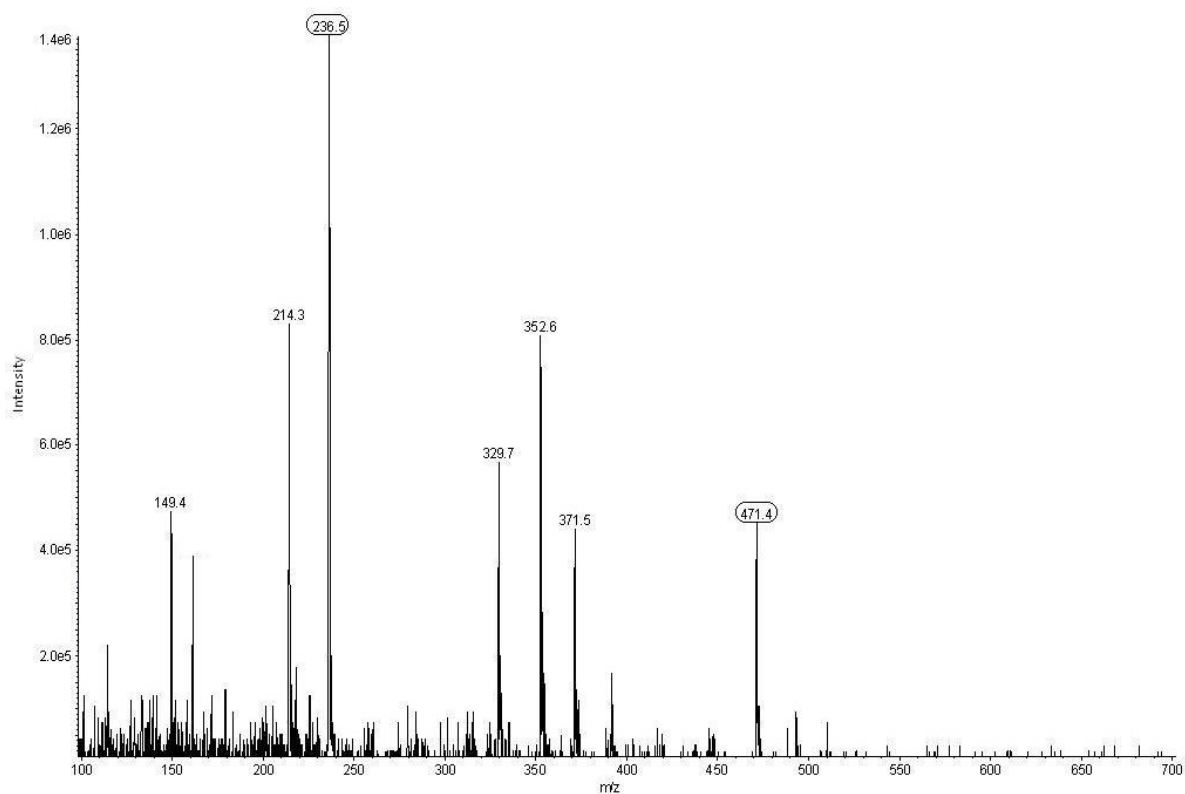


Figure 2. Mass spectrum of the chromatogram peak detected at 3.1 min for the Zn^{2+} containing sample.

The observed $[M+H]^+ = 236.5$ m/z indicates the presence of the intact (L)-glycyl-cysteinyl-glycine tripeptide with a theoretical $[M+H]^+ = 236.0699$ m/z. The observed $[2M+H]^+ = 471.4$ m/z corresponds to the mass of the dimeric tripeptide ion cluster.

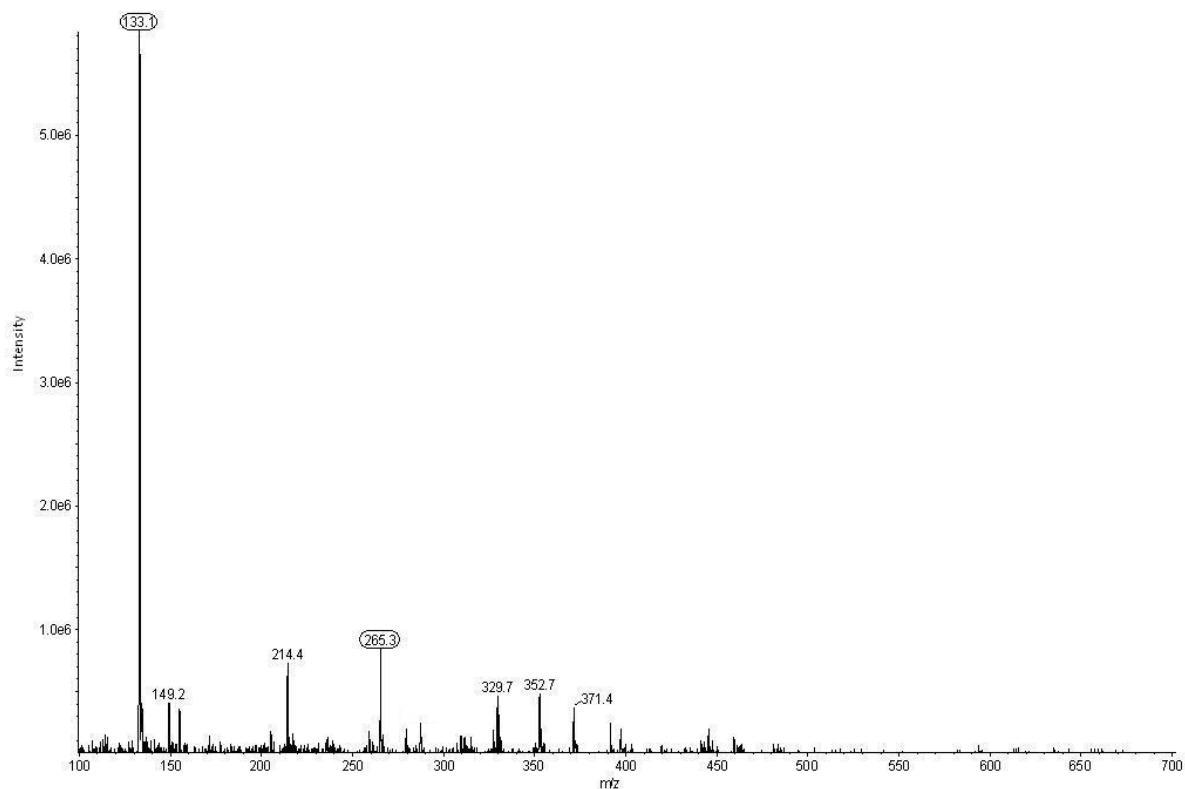


Figure 3. Mass spectrum of the chromatogram peak detected at 1.7 min for the Zn^{2+} containing sample.

The observed $[M+H]^+ = 133.2$ m/z indicates the presence of intact glycyl-glycine dipeptide with a theoretical $[M+H]^+ = 133.0607$ m/z. The observed $[2M+H]^+ = 265.3$ m/z corresponds to the mass of the glycyl-glycine dimeric ion cluster.

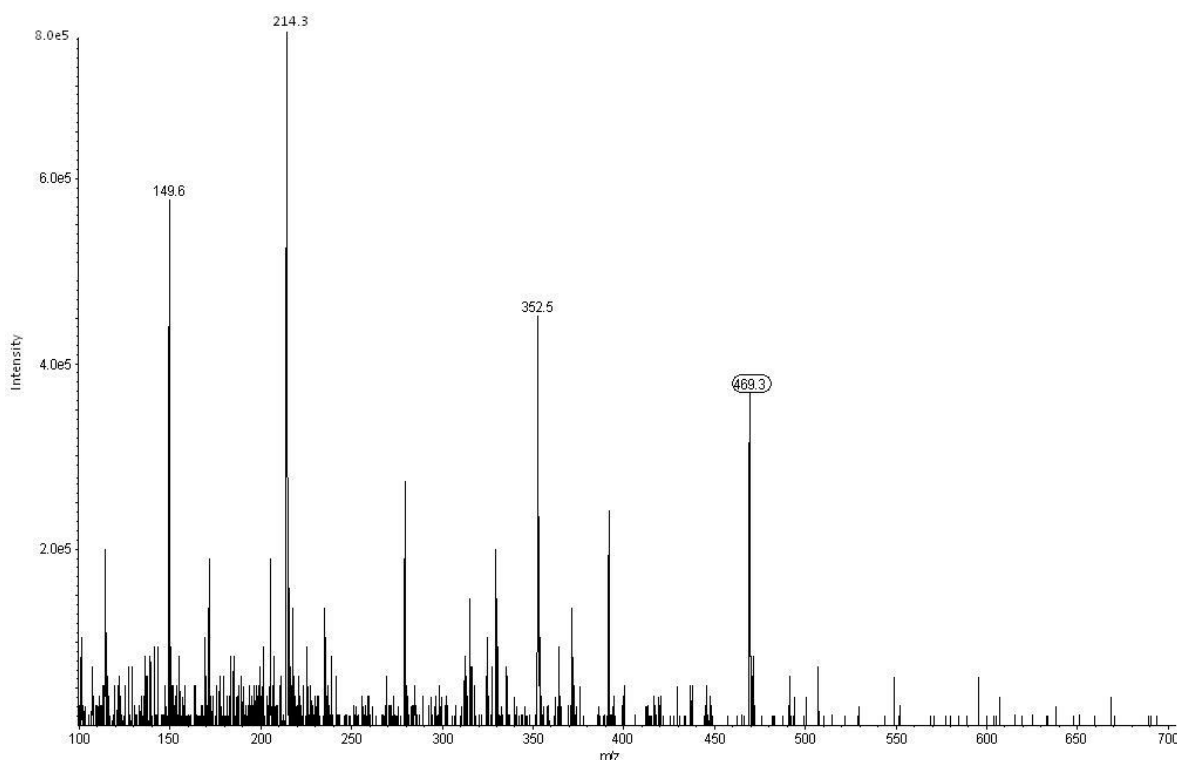


Figure 4. Mass spectrum of the chromatogram peak detected at 5.8 min for the Zn^{2+} containing sample.

The observed $[M+H]^+ = 469.3$ m/z indicates the presence of the intact oxidized version of the (L)-glycyl-cysteinyl-glycine tripeptide with a theoretical $[M+H]^+ = 469.1170$ m/z.

MATERIAL AND METHODS

Sample preparation and heating experiments

A 10 mL stock solution of 5 mM (L)-glycyl-cysteinyl-glycine in 20 mM glycyl-glycine was prepared under controlled N_2 atmosphere using a Schlenk line and Schlenk glassware. Milli-Q (Millipore) water was distilled under N_2 flow and was used as anoxygenic solvent. To keep the pH near the pK_a value of the sulfhydryl group of cysteine to allow for coordination with Zn^{2+} , the pH of the solution was adjusted to 8.7 with NaOH and 20 mM glycyl-glycine was used as a buffer. 100 μ L of peptide solution without or supplemented with 5 mM zinc sulfate were heated at 150 $^\circ$ C for 4 min in a dry bath (FB15101 Fisher Scientific) inside 2 mL glass vials (12x32 mm CLR TARGET DP I-D-Thermo Scientific). Prior LC-MS analysis, 100 μ L anoxygenic water was used to resuspend the peptide-metal solid precipitate.

Solid phase peptide synthesis

The synthesis of (L)-glycyl-cysteinyl-glycine tripeptide was performed by solid phase peptide synthesis as described earlier (81, 82). Dichloromethane (DCM) and N,N-dimethyl formamide (DMF) were used as solvents for washing and coupling steps. Preloaded fluorenylmethyloxycarbonyl-glycyl Wang resin (Fmoc-Gly Wang) was coupled to trityl-protected Fmoc-L-cysteine (Fmoc-L-Cys(Trt)-OH) and subsequently to Fmoc-glycine (Fmoc-Gly-OH). The peptide chain elongation resulted from the sequential Fmoc deprotection of the last amino acid attached to the resin and Fmoc-X-OH (X= Cys,Gly) coupling. For Fmoc deprotection, a solution consisting of 20% (v/v) piperidine in DMF was used. For each coupling step, a 3:1 excess of the Fmoc-amino acid-OH derivative respect to the peptide-anchored resin was used. Fmoc-L-Cys(Trt)-OH was activated with a HOBt/N,N'-diisopropylcarbodiimide (DIC) mixture for 10 min at room temperature prior to the addition to the Fmoc-Gly wang resin. Fmoc-Gly-OH was instead activated for 10 min at room temperature with hydroxyl-benzotriazole (HOBt), O-(Benzotriazol-1-yl)-N,N,N',N'- tetramethyluronium hexafluorophosphate (HBTU), and N,N-diisopropylethylamine (DIPEA). Coupling reactions were carried out at room temperature in a tube revolver rotator for 1 hour. After each coupling step, the peptide-anchored resin was washed with DMF and DCM to remove the coupling reagents leftover. After the elongation step, the tripeptide was Fmoc-deprotected and cleaved from the resin with trifluoroacetic acid (TFA) using 1,2-ethanedithiol (EDT), water, and triisopropyl silane (TIS) as scavengers (volume ratio 92.5:2.5:2.5:2.5). The solution was then precipitated with cold diethyl ether/petroleum ether (70:30 (v/v)) and dried under nitrogen atmosphere to avoid the oxidation of the sulfhydryl group of cysteine. The tripeptide was stored at -20 ° C until use.

High Performance Liquid Chromatography-Mass spectrometry

Mass spectra were acquired with a triple quadrupole API 3000 Sciex/Applied Biosystem mass spectrometer in positive mode. The instrument was equipped with an electrospray ion source and coupled to a Prominence modular HPLC instrument (Shimadzu) with a LC-20AB binary pump and a SPD-M20A detector. 2.5 µL of peptide

samples were injected in an Agilent Eclipse XDB_C18 column (4.6 x 150 mm; 3.5 μm). The solvent system used was 0.1 % (v/v) trifluoroacetic acid (TFA) in mQ water (solvent A) and 0.1 % (v/v) TFA in acetonitrile HPLC grade (solvent B). The peptides were eluted from the column at a constant flow rate of 1 mL/min with a gradient starting with 1 % B to 20% B in 20 min. UV-chromatograms were acquired at 210 nm.

SUMMARY AND FUTURE PERSPECTIVES

The stability of (L)-glycyl-cysteinyl-glycine was investigated under high temperature (150 °C) in the presence or absence of Zn^{2+} . Upon heating, the level of intact tripeptide was considerably higher when Zn^{2+} was present in the sample than in the absence of Zn^{2+} . This observation indicates that Zn^{2+} protected the integrity of the tripeptide under high temperature.

In light of the preliminary results obtained, we will further investigate whether the protection effect can be also observed in the presence of other short peptide sequences carrying similar glycine cysteine motifs. In this regard, other metal ions will be tested for the same purpose. Affinity studies between the different peptides-metal complexes will be assessed as well. We would like to investigate the mechanism by which the protection effect takes place. Whether it depends on peptide-metal coordination or the protection occurs by other means. We next plan to conduct survival competition experiments. Starting from a pool of peptides with different cysteine glycine containing peptide motifs we expect that only the peptide sequence that coordinate the metal with higher affinity will better withstand the high thermal or UV-light irradiation conditions. Furthermore, we would like to test whether metal ions could have templated the polymerization of coordinating peptides, facilitating peptide bond formation among the peptides brought to close proximity and in the right conformation that might have led to peptide sequences motifs found in modern-day proteins. Samples will be then sent to Earth Life Science Institute (ELSI) in Tokyo and will be analyzed by Dr. Yayoi Hongo by High Performance Liquid Chromatography in tandem with high precision mass spectrometry.

These results open a new prebiotic scenario where metal ions could have provided a selective advantage for specific short cysteine containing peptide sequences by conferring protection from desulfurization under various prebiotic conditions.

REFERENCES

1. C. E. Cleland, C. F. Chyba, Defining 'Life.' *Orig. Life Evol. Biosph.* **32**, 387–393 (2002).
2. C. M. Fraser *et al.*, The minimal gene complement of *Mycoplasma genitalium*. *Sci.* **270**, 397–403 (1995).
3. J. I. Glass *et al.*, Essential genes of a minimal bacterium (2006) (available at www.pnas.org/cgi/doi/10.1073/pnas.0510013103).
4. D. G. Gibson *et al.*, Complete chemical synthesis, assembly, and cloning of a *Mycoplasma genitalium* genome. *Sci.* **319**, 1215–20 (2008).
5. D. G. Gibson *et al.*, Creation of a Bacterial Cell Controlled by a Chemically Synthesized Genome. *Science*. **329**, 52–56 (2010).
6. C. A. Hutchison *et al.*, Design and synthesis of a minimal bacterial genome. *Science*. **351**, aad6253-aad6253 (2016).
7. W. Yu *et al.*, Synthesis of functional protein in liposome. *J. Biosci. Bioeng.* **92**, 590–593 (2001).
8. V. Noireaux, A. Libchaber, A vesicle bioreactor as a step toward an artificial cell assembly. *Proc. Natl. Acad. Sci.* **101**, 17669–17674 (2004).
9. A. C. Forster, G. M. Church, Towards synthesis of a minimal cell. *Mol. Syst. Biol.*, 45 (2006).
10. G. Murtas, Y. Kuruma, P. Bianchini, A. Diaspro, P. L. Luisi, Protein synthesis in liposomes with a minimal set of enzymes. *Biochem. Biophys. Res. Commun.* **363**, 12–17 (2007).
11. Y. Shimizu *et al.*, Cell-free translation reconstituted with purified components. *Nat. Biotechnol.* **19**, 751–755 (2001).
12. J. Garamella, R. Marshall, M. Rustad, V. Noireaux, The All E. coli TX-TL Toolbox 2.0: A Platform for Cell-Free Synthetic Biology. *ACS Synth. Biol.* **5**, 344–355 (2016).
13. M. Rustad, A. Eastlund, P. Jardine, V. Noireaux, Cell-free TXTL synthesis of infectious bacteriophage T4 in a single test tube reaction. *Synth. Biol.* **3** (2018), doi:10.1093/synbio/ysy002.

14. M. Li, X. Huang, T.-Y. D. Tang, S. Mann, Synthetic cellularity based on non-lipid micro-compartments and protocell models. *Curr. Opin. Chem. Biol.* **22**, 1–11 (2014).
15. R. J. R. W. Peters *et al.*, Cascade Reactions in Multicompartmentalized Polymersomes. *Angew. Chemie Int. Ed.* **53**, 146–150 (2014).
16. Y. Elani, R. V. Law, O. Ces, Vesicle-based artificial cells as chemical microreactors with spatially segregated reaction pathways. *Nat. Commun.* **5**, 5305 (2014).
17. M. Osawa, H. P. Erickson, Liposome division by a simple bacterial division machinery. *Proc. Natl. Acad. Sci.* **110**, 11000–11004 (2013).
18. A. Martos, M. Jiménez, G. Rivas, P. Schwille, Towards a bottom-up reconstitution of bacterial cell division. *Trends Cell Biol.* **22**, 634–643 (2012).
19. K. Kurihara *et al.*, Self-reproduction of supramolecular giant vesicles combined with the amplification of encapsulated DNA. *Nat. Chem.* **3**, 775–781 (2011).
20. T. F. Zhu, J. W. Szostak, Coupled Growth and Division of Model Protocell Membranes (2009), doi:10.1021/JA900919C.
21. T. A. Lincoln, G. F. Joyce, Self-sustained replication of an RNA enzyme. *Sci.* **323**, 1229–32 (2009).
22. M. P. Robertson, G. F. Joyce, Highly Efficient Self-Replicating RNA Enzymes. *Chem. Biol.* **21**, 238–245 (2014).
23. J. W. Szostak, The eightfold path to non-enzymatic RNA replication. *J. Syst. Chem.* **3**, 2 (2012).
24. T.-Y. D. Tang *et al.*, Gene-Mediated Chemical Communication in Synthetic Protocell Communities. *ACS Synth. Biol.* **7**, 339–346 (2018).
25. Y. Qiao, M. Li, R. Booth, S. Mann, Predatory behaviour in synthetic protocell communities. *Nat. Chem.* (2016), doi:10.1038/nchem.2617.
26. Y. Elani *et al.*, Constructing vesicle-based artificial cells with embedded living cells as organelle-like modules. *Sci. Rep.* **8**, 4564 (2018).
27. P. M. Gardner, K. Winzer, B. G. Davis, Sugar synthesis in a protocellular model leads to a cell signalling response in bacteria. *Nat. Chem.*, 377–383 (2009).
28. G. Rampioni *et al.*, Synthetic cells produce a quorum sensing chemical signal perceived by *Pseudomonas aeruginosa*. *Chem. Commun.* **54**, 2090–2093 (2018).
29. R. Lentini *et al.*, Integrating artificial with natural cells to translate chemical

- messages that direct *E. coli* behaviour. *Nat. Commun.* **5**, 4012 (2014).
30. A. M. Turing, Computing Machinery and Intelligence. *Mind.* **59**, 433–460 (1950).
 31. L. Cronin *et al.*, The imitation game--a computational chemical approach to recognizing life. *Nat. Biotechnol.* **24**, 1203–6 (2006).
 32. M. Schwarz-Schilling, L. Aufinger, A. Mückl, F. C. Simmel, Chemical communication between bacteria and cell-free gene expression systems within linear chains of emulsion droplets. *Integr. Biol. (Camb)*. (2016), doi:10.1039/c5ib00301f.
 33. K. Pappenfort, B. L. Bassler, Quorum sensing signal–response systems in Gram-negative bacteria. *Nat. Rev. Microbiol.* **14**, 576–588 (2016).
 34. T. Miyashiro, E. G. Ruby, Shedding light on bioluminescence regulation in *Vibrio fischeri*. *Mol. Microbiol.* **84**, 795–806 (2012).
 35. A. L. Schaefer, D. L. Valt, B. L. Hanzelka, J. E. Cronan, E. P. Greenberg, “Generation of cell-to-cell signals in quorum sensing: Acyl homoserine lactone synthase activity of a purified *Vibrio fischeri* LuxI protein (autoinduction/lux genes/cell density-dependent gene expression)” (1996), (available at <http://europepmc.org/backend/ptpmcrender.fcgi?accid=PMC38458&blobtype=pdf>).
 36. A. L. Schaefer, B. L. Hanzelka, A. Eberhard, E. P. Greenberg, Quorum Sensing in *Vibrio fischeri*: Probing Autoinducer-LuxR Interactions with Autoinducer Analogs. *J. Bacteriol.* **178**, 2897–2901 (1996).
 37. C. H. Collins, F. H. Arnold, J. R. Leadbetter, Directed evolution of *Vibrio fischeri* LuxR for increased sensitivity to a broad spectrum of acyl-homoserine lactones. *Mol. Microbiol.* **55**, 712–23 (2005).
 38. P. Kumar *et al.*, Directed evolution of LuxI for enhanced OHHL production. *Biotechnol. Bioeng.* (2008), doi:10.1002/bit.21901.
 39. S. T. Rutherford, B. L. Bassler, Bacterial Quorum Sensing: Its Role in Virulence and Possibilities for Its Control. *Cold Spring Harb. Perspect. Med.* **2**, a012427–a012427 (2012).
 40. A. B. Alayande, M. M. Aung, I. S. Kim, Correlation Between Quorum Sensing Signal Molecules and *Pseudomonas aeruginosa*’s Biofilm Development and Virulency. *Curr. Microbiol.* **75**, 787–793 (2018).
 41. K. M. Gray, L. Passador, B. H. Iglewski, E. P. Greenberg, Interchangeability

- and specificity of components from the quorum-sensing regulatory systems of *Vibrio fischeri* and *Pseudomonas aeruginosa*. *J. Bacteriol.* **176**, 3076–3080 (1994).
42. M. L. Vasil, in *Pseudomonas* (Springer US, 2006; http://link.springer.com/10.1007/0-387-28881-3_3), pp. 69–97.
 43. J. Pan *et al.*, Expression and characterization of *aiiA* gene from *Bacillus subtilis* BS-1. *Microbiol. Res.* **163**, 711–6 (2008).
 44. G. A. O’Toole, Microtiter dish biofilm formation assay. *J. Vis. Exp.* (2011), doi:10.3791/2437.
 45. B. D. Jett, K. L. Hatter, M. M. Huycke, M. S. Gilmore, Simplified agar plate method for quantifying viable bacteria. *Biotechniques.* **23**, 648–50 (1997).
 46. M. J. Mandel, M. S. Wollenberg, E. V Stabb, K. L. Visick, E. G. Ruby, A single regulatory gene is sufficient to alter bacterial host range. *Nature.* **458**, 215–8 (2009).
 47. P. Cosson *et al.*, *Pseudomonas aeruginosa* Virulence Analyzed in a *Dictyostelium discoideum* Host System. *J. Bacteriol.* **184**, 3027–3033 (2002).
 48. A. S., FastQC: a quality control tool for high throughput sequence data. Available online at: <http://www.bioinformatics.babraham.ac.uk/projects/fastqc> (2010).
 49. B. Langmead, S. L. Salzberg, Fast gapped-read alignment with Bowtie 2. *Nat. Methods.* **9**, 357–9 (2012).
 50. C. Trapnell *et al.*, Differential gene and transcript expression analysis of RNA-seq experiments with TopHat and Cufflinks. *Nat. Protoc.* **7**, 562–78 (2012).
 51. A. Roberts, H. Pimentel, C. Trapnell, L. Pachter, Identification of novel transcripts in annotated genomes using RNA-Seq. *Bioinformatics.* **27**, 2325–9 (2011).
 52. C. Trapnell *et al.*, Differential analysis of gene regulation at transcript resolution with RNA-seq. *Nat. Biotechnol.* **31**, 46–53 (2013).
 53. L. C. M. Antunes *et al.*, Transcriptome Analysis of the *Vibrio fischeri* LuxR-LuxI Regulon. *J. Bacteriol.* **189**, 8387–8391 (2007).
 54. T. M. Allen, L. G. Cleland, Serum-induced leakage of liposome contents. *Biochim. Biophys. Acta - Biomembr.* **597**, 418–426 (1980).
 55. S. Deshpande, C. Dekker, On-chip microfluidic production of cell-sized liposomes. *Nat. Protoc.* **13**, 856–874 (2018).

56. A. Reece *et al.*, Microfluidic techniques for high throughput single cell analysis. *Curr. Opin. Biotechnol.* **40**, 90–96 (2016).
57. J. Wang, L. Chen, Z. Chen, W. Zhang, RNA-seq based transcriptomic analysis of single bacterial cells. *Integr. Biol.* **7**, 1466–1476 (2015).
58. L. R. Thompson *et al.*, Transcriptional characterization of *Vibrio fischeri* during colonization of juvenile *Euprymna scolopes*. *Environ. Microbiol.* **19**, 1845–1856 (2017).
59. S. Duhr, D. Braun, Why molecules move along a temperature gradient. *Proc. Natl. Acad. Sci.* **103**, 19678–19682 (2006).
60. M. Reichl, M. Herzog, A. Götz, D. Braun, Why Charged Molecules Move Across a Temperature Gradient: The Role of Electric Fields. *Phys. Rev. Lett.* **112**, 198101 (2014).
61. A. Majee, A. Würger, Collective thermoelectrophoresis of charged colloids. *Phys. Rev. E.* **83**, 061403 (2011).
62. C. B. Mast, D. Braun, Thermal Trap for DNA Replication. *Phys. Rev. Lett.* **104**, 188102 (2010).
63. I. Budin, R. J. Bruckner, J. W. Szostak, Formation of protocell-like vesicles in a thermal diffusion column. *J. Am. Chem. Soc.* **131**, 9628–9 (2009).
64. L. M. R. Keil, F. M. Möller, M. Kieß, P. W. Kudella, C. B. Mast, Proton gradients and pH oscillations emerge from heat flow at the microscale. *Nat. Commun.* **8**, 1897 (2017).
65. M. Jerabek-Willemsen *et al.*, MicroScale Thermophoresis: Interaction analysis and beyond. *J. Mol. Struct.* **1077**, 101–113 (2014).
66. N. C. Shaner, P. A. Steinbach, R. Y. Tsien, A guide to choosing fluorescent proteins. *Nat. Methods.* **2**, 905–909 (2005).
67. R. Lentini *et al.*, Fluorescent Proteins and *in Vitro* Genetic Organization for Cell-Free Synthetic Biology. *ACS Synth. Biol.* **2**, 482–489 (2013).
68. D. Shu, E. F. Khisamutdinov, L. Zhang, P. Guo, Programmable folding of fusion RNA in vivo and in vitro driven by pRNA 3WJ motif of phi29 DNA packaging motor. *Nucleic Acids Res.* **42**, e10–e10 (2014).
69. T. D. Craggs, Green fluorescent protein: structure, folding and chromophore maturation. *Chem. Soc. Rev.* **38**, 2865 (2009).
70. M. C. Jewett, K. A. Calhoun, A. Voloshin, J. J. Wu, J. R. Swartz, An integrated cell-free metabolic platform for protein production and synthetic biology. *Mol.*

- Syst. Biol.* **4**, 220 (2008).
71. F. Caschera, V. Noireaux, Synthesis of 2.3 mg/ml of protein with an all Escherichia coli cell-free transcription–translation system. *Biochimie.* **99**, 162–168 (2014).
 72. Z. Z. Sun *et al.*, Protocols for Implementing an Escherichia coli& Based TX-TL Cell-Free Expression System for Synthetic Biology. *J. Vis. Exp.*, e50762–e50762 (2013).
 73. F. Caschera, V. Noireaux, Preparation of amino acid mixtures for cell-free expression systems. *Biotechniques.* **58**, 40–3 (2015).
 74. V. Svetlov, E. Nudler, Basic mechanism of transcription by RNA polymerase II. *Biochim. Biophys. Acta.* **1829**, 20–8 (2013).
 75. W. Zag *et al.*, “The Effect of Magnesium-Ion Concentration on the Translation of Phage-f 2 RNA in a Cell-Free System of Escherichia coli” (1972), (available at <https://febs.onlinelibrary.wiley.com/doi/pdf/10.1111/j.1432-1033.1972.tb01699.x>).
 76. D. J. Klein, P. B. Moore, T. A. Steitz, The contribution of metal ions to the structural stability of the large ribosomal subunit. *RNA.* **10**, 1366–79 (2004).
 77. T. Dora Tang, D. van Swaay, A. DeMello, J. L. Ross Anderson, S. Mann, In vitro gene expression within membrane-free coacervate protocells. *Chem. Commun.* **51**, 11429 (2015).
 78. A. C. Spencer, P. Torre, S. S. Mansy, The Encapsulation of Cell-free Transcription and Translation Machinery in Vesicles for the Construction of Cellular Mimics. *J. Vis. Exp.*, e51304–e51304 (2013).
 79. E. Karzbrun, A. M. Tayar, V. Noireaux, R. H. Bar-Ziv, Synthetic biology. Programmable on-chip DNA compartments as artificial cells. *Science.* **345**, 829–32 (2014).
 80. A. N. Lupas, C. P. Ponting, R. B. Russell, On the Evolution of Protein Folds: Are Similar Motifs in Different Protein Folds the Result of Convergence, Insertion, or Relics of an Ancient Peptide World? *J. Struct. Biol.* **134**, 191–203 (2001).
 81. S. Scintilla *et al.*, Duplications of an iron-sulphur tripeptide leads to the formation of a protoferredoxin. *Chem. Commun.* **52**, 13456 (1345).
 82. C. Bonfio *et al.*, UV-light-driven prebiotic synthesis of iron–sulfur clusters. *Nat. Chem.* **9**, 1229–1234 (2017).

